

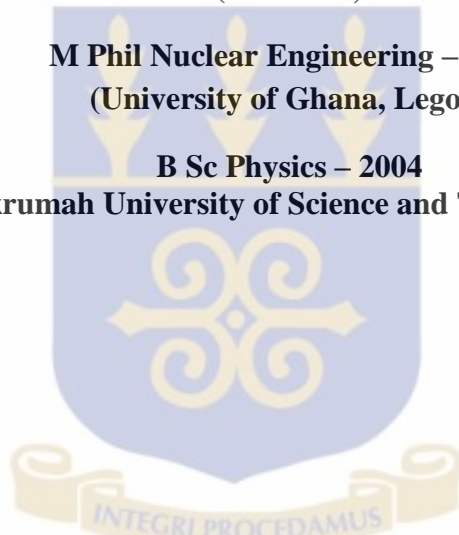
**REACTOR CORE CONVERSION STUDIES OF GHANA
RESEARCH REACTOR – 1 AND PROPOSAL FOR ADDITION OF
SAFETY ROD**

BY

**HENRY CECIL ODOI
(10235606)**

**M Phil Nuclear Engineering – 2008
(University of Ghana, Legon)**

**B Sc Physics – 2004
(Kwame Nkrumah University of Science and Technology, Kumasi)**



**This Dissertation Submitted to University Of Ghana, Graduate School of
Nuclear and Allied Sciences, Department of Nuclear Engineering, in Partial
Fulfillment of the Requirement for the Award of PhD Nuclear Engineering**

June 2014

Declaration

“This dissertation is the result of research work undertaken by **Henry Cecil Odoi** in the Department of Nuclear Engineering, School of Nuclear and Allied Sciences (SNAS) of University of Ghana (UG), under the supervision of **Prof. Emeritus Edward H. K. Akaho** and **Prof. Sunday A. Jonah**”

Sign:

Date:

Henry Cecil Odoi
(Student)

Sign:

Sign:

Date:

Date:

Prof. Emeritus Edward H. K. Akaho
(Supervisor)

Prof. Sunday A. Jonah
(Supervisor)

Dedication

To the trio: my mother, my wife and my son.

To the Lord Almighty, and mother Ghana.

With Love.



ACKNOWLEDGEMENTS

I am grateful to the Almighty God for his protection and guidance.

I do thank all the lecturers of School of Nuclear and Allied Sciences for their selfless gestures.

Further appreciation goes to my entire family for their invaluable support; spiritually, mentally and financially.

I greatly appreciate the advice and encouragement of my supervisors; Prof. Emeritus E. H. K. Akaho and Prof. S. A. Jonah during the undertaking of this project.

I do acknowledge with gratitude the financial support of IAEA for the award of Research Contract Number 13946 and also the Fellowship in Nigeria – GHA/09003.

I also appreciate the fellowships sponsored by US Department of Energy in 2010 and 2011, and I am thankful to the staff of Nuclear Engineering Division of Argonne National Laboratory, especially, J. Roglans-Ribas, J.E. Matos, J.R. Liaw, M. Kalimullah, J. Morman and S.C. Mo for hosting fellowships, and the importance they assigned to this project.

Table of Contents

Title page	i
Declaration	ii
Dedication	iii
Acknowledgements	iv
Table of contents	v
List of tables	viii
List of figures	x
Nomenclature	xiii
Abstract	xvii
1. INTRODUCTION	1
1.1 Reactor Facility Changes	7
1.2 Operation License and Procedural Changes.....	7
1.3 Characteristics of Reference GHARR-1 LEU Core.....	8
1.4 Outline of Thesis	11
2 LITERATURE REVIEW	13
2.1 General	13
2.1.1 Similarity with Other Converted Facilities	13
2.1.2 Advocates of Core Conversion.....	14
2.2 GHARR-1 Reactivity Management	18
2.2.1 Reactivity worth of top beryllium reflector plates	20
2.2.2 Comparison of the HEU and LEU fuel characteristics	21
2.2.3 Xenon poisoning calculations	21
2.3 Central control rod of GHARR-1	23
2.3.1 Control rod drive mechanism.....	24
2.3.2 Measurement of the central control rod worth	27
3 THEORETICAL ANALYSIS	28
3.1 NUCLEAR REACTOR THEORY	28
3.2 Solution of the Neutron Transport Equation	30
3.2.1 Diffusion Theory Approximation.....	31

3.2.2	Multigroup Calculations.....	34
3.3	Generation of Group Constants.....	36
3.4	Few Group (Macro-group) Constants	38
3.5	Monte Carlo Techniques	39
3.5.1	General Overview.....	39
3.5.2	Criticality Calculations.....	42
3.5.3	Neutron Cross section Data Libraries	44
3.5.4	Thermal Scattering Matrix $S(\alpha, \beta)$	45
3.5.5	Mathematical Basis for Monte Carlo Simulation.....	46
3.5.6	Generation of Random Variable.....	49
3.5.7	Variance Reduction	57
3.5.8	Variance Reduction Techniques in Monte Carlo	59
3.5.9	Monte Carlo Simulations.....	61
3.5.10	Monte Carlo Estimates	67
3.6	Burnup.....	71
3.6.1	BURNUP ANALYSIS	75
3.6.2	DESCRIPTION OF REBUS	76
3.7	Analyses of MNSR Thermal Hydraulics	78
3.7.1	Heat transfer process of MNSR.....	78
3.7.2	Thermal – Hydraulic Characteristics of MNSR.....	84
3.7.3	Heat Transfer Calculations of the Steady State.....	85
3.7.4	Transient Thermal hydraulic calculation.....	91
4	METHODOLOGY	102
4.1	Monte Carlo Model for GHARR-1	103
4.1.1	Auxiliary shutdown system.....	106
4.2	REBUS Model for GHARR-1.....	112
4.3	Thermal Hydraulic Analyses.....	114
4.3.1	Steady State	115
4.3.2	Transients Analysis	118
5	Results and Discussion	122
5.1	Criticality Results.....	122

5.1.1	Integral and Differential Control Rod Worth.....	124
5.1.2	Flux Distributions.....	126
5.1.3	Reactivity Coefficients.....	131
5.1.4	Worth of the top beryllium reflector.....	134
5.2	ANALYSIS FOR AUXILIARY CONTROL ROD.....	135
5.3	CORE LIFETIME ANALYSIS.....	137
5.4	THERMAL HYDRAULICS ANALYSES.....	138
5.4.1	Steady State.....	138
5.4.2	Transient.....	141
6	CONCLUSION AND RECOMMENDATION.....	146
6.1	Conclusion.....	146
6.2	Recommendation.....	148
	References.....	149

List of Tables

Table 1.1 Control Rod and Guide Tube Design Parameters in MNSR Models	9
Table 1.2 Comparison of Reference GHARR-1 HEU and LEU Fuel Uranium Isotopes.	9
Table 1.3 Comparison of Key Parameters for Reference GHARR-1 HEU and LEU Cores	10
Table 2.1 Lattice positions for the fuel cage	19
Table 2.2 Characteristics of the GHARR-1 fuel element & dummy	21
Table 2.3 Equilibrium xenon reactivity as a function of core average flux	22
Table 4.1 Dimension of cadmium in capsule (average along each side)	108
Table 4.2 Uncertainties Included in the Six Hot Channel Factors	117
Table 5.1 Comparison of Reactivities for various cores.	122
Table 5.2: Comparison of Criticality Results for HEU and LEU	123
Table 5.3: Differential Reactivity, mk	125
Table 5.4: Peak Flux in the Inner Irradiation Channels (n/cm^2s).....	130
Table 5.5: Fuel Temperature Coefficient	132
Table 5.6: Moderator temperature coefficient (partial).....	133
Table 5.7: Moderator void coefficient	133
Table 5.8: Moderator Temperature coefficient	134
Table 5.9. Auxiliary rod worth, mk for unmodified irradiation site (inner)	136
Table 5.10. Auxiliary rod worth, mk for modified irradiation site (inner)	136
Table 5.11: Xenon Worth and Reactivity Change Rates	137
Table 5.12: Comparison of HEU and LEU steady-state parameters using PLTEMP/ANL	139

Table 5.13: Comparison of computed coolant outlet temperatures at various powers and inlet temperatures	140
Table 5.14: Effect of Inlet Temperature on Temperature Difference at Nominal Operating Power for the HEU and LEU Cores	141
Table 5.15: Peak power, peak fuel temperature and peak clad temperature for various reactivity insertions	145

List of Figures

Figure 2.1 Schematic of Reactor Pool (Cross sectional plane through centres of reactor pool and reactor vessel).....	23
Figure 3.1 : Partial distribution of neutron energies into G groups	35
Figure 3.2 Monte Carlo random works for single particle	63
Figure 3.3 Power iteration for Monte Carlo criticality calculation of the mean value of k_{eff}	63
Figure 3.4 Decision points in generating the history of a single neutron in a Monte Carlo calculation	67
Figure 3.5 The most important actinide nuclides and their relations, via α -decay, β -decay and neutron capture reactions.....	73
Figure 3.6: Schematics of Reactor Core [55].....	79
Figure 3.7: Heat transfer and transport process	83
Figure 3.8: Fuel element	85
Figure 3.9: Temperature distribution in fuel and coolant	90
Figure 3.10: Water temperature variation at core inlet (T_1).....	99
Figure 3.11: Variation of temperature difference between core inlet and outlet.	100
Figure 3.12: Variation of coolant velocity in reactor core.	100
Figure 4.1: MCNP plot of the core configuration and associated experimental channels	105
Figure 4.2: MCNP plot of vertical cross-section of GHARR-1 reactor (in full power mode).....	106
Figure 4.3: Cadmium Capsule.....	107

Figure 4.4: Cadmium foil.....	107
Figure 4.5: Measurement of Cadmium (Side).....	107
Figure 4.6: Measurement of Thickness (a)	108
Figure 4.7: Measurement of Thickness (b)	108
Figure 4.8: Cadmium foil in irradiation channel (Visual editor of MCNP).....	109
Figure 4.9 Three concentric foils in unmodified irradiation site (CFU).....	110
Figure 4.10. Solid auxiliary rod (SR).....	110
Figure 4.11 Foil with a similar arrangement to the cadmium capsule (F2)	111
Figure 4.12 Three concentric foils in modified irradiation site (CFM)	111
Figure 4.13 Solid auxiliary rod (SR2).....	111
Figure 4.14 RZ model of the reactor core (figure is not drawn to scale);.....	114
Figure 5.1: The Integral Control Rod Curve.....	125
Figure 5.2: Comparison of average flux distribution in inner irradiation channel at 30 kW.....	127
Figure 5.3: Comparison of Flux Distribution in Fission Chamber at 30 kW.....	127
Figure 5.4: Comparison of average flux distribution in outer irradiation channel at 30 kW.....	128
Figure 5.5: Comparison of average flux distribution in inner irradiation channel at nominal powers.	128
Figure 5.6: Comparison of average flux distribution in fission chamber at nominal powers.	129
Figure 5.7: Comparison of average flux distribution in outer irradiation channel at nominal powers.	130
Figure 5.8: Peak Power Pin Axial Profile (21 Segments).....	131

Figure 5.9: Reactivity worths of top Be shims for HEU and LEU cores.....	135
Figure 5.10: Differential Reactivity worths of top Be shims for HEU and LEU cores .	135
Figure 5.11:Time vs. Power for a 3.8 mk Reactivity Insertion with HEU and LEU Fuel	142
Figure 5.12: Fuel Temperature comparison of HEU and LEU cores for 3.8 mk reactivity transient.	142
Figure 5.13: Clap Surface Temperature comparison of HEU and LEU cores for 3.8 mk reactivity transient.	143
Figure 5.14: Reactor power for reactivity insertions of 3.8 mk, 6 mk and 8 mk for LEU.	143
Figure 5.15: Fuel Temperature for reactivity insertions of 3.8 mk, 6 mk and 8 mk for LEU.....	144
Figure 5.16: Clad Temperature for reactivity insertions of 3.8 mk, 6 mk and 8 mk for LEU.....	144

NOMENCLATURE

Roman Letters

A_f	Cross sectional area of flow channel (m^2)
C	Specific heat capacity of fuel meat ($J/kg^\circ C$)
D	Diffusion constant
D_e	Equivalent diameter of channel (m)
E	Energy of particle
f	Friction factor
h	Heat transfer coefficient ($w/m^2^\circ C$)
J	Neutron current density
k_{eff}	Multiplication factor
N	Atomic density
p	Probability of the outcome of a particular event
P	Pressure (Pa)
Q	Heat
r	Particle (quantity) distribution in space
R	Sequence of numbers
S	Number of particles emitted from a Source term
t	Time in seconds
U	Coolant velocity (m/s)
x, y, z	General variables

Greek Letters

Ω	Direction in plane, spherical or cylindrical geometry
Σ	Macroscopic cross-section
∇	Spatial gradient
ϕ	Particle Flux (n/cm^2s)
θ	Angle ($^\circ$)
ν	Average number of fission neutrons released
λ	Track trajectory length, (cm)
χ	fraction of fission neutrons
$S(\alpha, \beta)$	Scattering matrix

Abbreviations

ANL	Argonne National Laboratory
BNCT	Boron Neutron Capture Therapy
CANDU	Canadian Deuterium Uranium Reactor
CDF	Cumulative Distribution Function
CHF	Critical Heat Flux
CHFR	Critical Heat Flux Ratio
CIAE	China Institute of Atomic Energy
DNBR	Departure from nucleate boiling ration
ENDF	Evaluated Nuclear Data File

FOM	Figure of Merit
GAEC	Ghana Atomic Energy Commission
GHARR-1	Ghana Research Reactor–1
GTRI	Global Threat Reduction Initiative
HEU	Highly Enriched Uranium
IAEA	International Atomic Energy Agency
IHNI	In-Hospital Neutron Irradiator
INL	Idaho National Laboratory
INSARR	Integrated Safety Assessment for Research Reactors
LEU	Low Enriched Uranium
MCNP	Monte Carlo N- Particle Code
MNSR	Miniature Neutron Source Reactor
NNRI	National Nuclear Research Institute
NNSA	National Nuclear Security Administration
ONBR	Onset of Nuclear Boiling Ratio
PARET	Programme for Analyses of Reactor Transients
PDF	Probability Density Function
PLTEMP	Plate Temperature Analysis

PSA	Project Supply Agreement
RERTR	Reduced Enrichment for Research and Test Reactors
RRDB	Research Reactors Database
SAR	Safety Analysis Report
SLOWPOKE	Safe Low Power Critical (K) Experiments
REBUS	Reactor Burn-up Systems
U-Al₄	Uranium-Aluminium
UO₂	Uranium Oxide
XSDIR	Cross-Section Directorate
Zirc-4	Zircaloy-4

ABSTRACT

The inclusion of an additional safety rod in conjunction with a core conversion study of Ghana Research Reactor-1 (GHARR-1) was carried out using neutronics, thermal hydraulics and burnup codes. The study is based on a recommendation by Integrated Safety Assessment for Research Reactors (INSARR) mission to incorporate a safety rod to the reactor safety system as well as the need to replace the reactor fuel with LEU. Conversion from one fuel type to another requires a complete re-evaluation of the safety analysis. Changes to the reactivity worth, shutdown margin, power density and material properties must be taken into account, and appropriate modifications made. Neutronics analysis including burnup was studied followed by thermal hydraulics analyses which comprise steady state and transients. Four computer codes were used for the analysis; MCNP, REBUS, PLTEMP and PARET. The neutronics analysis revealed that the LEU core must be operated at 34 kW in order to attain the flux of $1.0E12 \text{ n/cm}^2\cdot\text{s}$ as the nominal flux of the HEU core. The auxiliary safety rod placed at a modified irradiation site gives a better worth than the cadmium capsules. For core excess reactivity of 4 mk, 348 fuel pins would be appropriate for the GHARR-1 LEU core. Results indicate that flux level of $1.0E12 \text{ n/cm}^2\cdot\text{s}$ in the inner irradiation channels will not be compromised, if the power of the LEU core is increased to 34 kW. The GHARR-1 core using LEU-UO₂-12.5% fuel can be operated for 23 shim cycles, with cycle length 2.5 years, for over 57 years at the 17 kW power level. All 23 LEU cycles meet the ~ 4.0 mk excess reactivity required at the beginning of cycle. For comparison, the MNSR HEU reference core can also be operated for 23 shim cycles, but with a cycle length of 2.0 years for just over 46 years at the 15.0 kW power

level. It is observed that the GHARR-1 core with LEU UO_2 fuel enriched to 12.5% and a power level of 34 kW can be operated ~25% longer than the current HEU core operated at 30 kW. Based on the results presented in this report, it is concluded that the conversion of the GHARR-1 to LEU core is not likely to compromise safety nor increase the frequency/severity of any of the postulated design basis accidents identified in the current approved SAR.

CHAPTER ONE

1. INTRODUCTION

The purpose of this introduction is to present the historical background of Ghana's first and only research reactor, justify the need for core conversion from HEU to LEU and highlight improved safety due to addition of an auxiliary safety rod.

The Ghana Research Reactor-1 (GHARR-1) is a commercial version of the Miniature Neutron Source Reactor (MNSR) and belongs to the class of tank-in-pool type reactors [1]. It is under-moderated with an H/U atom ratio of 197. Thermal power is rated at 30 kW with a corresponding peak thermal neutron flux is 1.0×10^{12} n/cm².s. For fresh core, its cold clean excess reactivity is about 4mk. Cooling is achieved by natural convection using light water. Presently, the GHARR-1 core consists HEU (U-Al₄ alloyed) fuel elements arranged in ten concentric rings about a central control rod guide tube which houses the reactor's only control rod. The reactor is fuelled with uranium aluminium alloy with an enrichment of 90.2 %. The control rod's reactivity worth is about -7mk, providing a core shutdown margin of -3mk of reactivity. The small core has a U-235 content of about 1 kg. However, its relatively large negative temperature coefficient of reactivity is capable of boosting its inherent safety properties [2]. The small size of the core facilitates neutron leakage and escape in both axial and radial directions. To minimize such losses and thereby conserve neutron economy, the core is heavily reflected respectively on the side and underneath the fuel cage by a thick annulus and slab of beryllium material. Adding regulated thickness of beryllium shims to the top tray can compensate loss of reactivity due to axial neutron leakage.

GHARR-1 was obtained under a Project Supply Agreement (PSA) between the International Atomic Energy Agency (IAEA), the China Institute of Atomic Energy (CIAE) and the Government of Ghana in 1994 [3]. The reactor was assembled between October and December 1994 and it went critical in 17th December, 1994 [4]. Subsequently, it was commissioned on 15th March 1995. Since then it has been used for neutron activation analysis, experiments and training of human resource in nuclear science and technology.

According to the IAEA Research Reactor Database (RRDB), 735 research reactors have been constructed around the world for civilian applications. On the basis of the RRDB, 244 research reactors are currently in operation, 148 are shut down and 306 have been decommissioned, while others are under temporary shutdown [5]. One type of such research reactors in operation is the Miniature Neutron Source Reactors (MNSR).

MNSR can be classified as low power research reactor. It is a tank-in-pool type reactor, water-moderated and cooled. The general principles of design and operation are similar to other low power research reactors as SLOWPOKE 1, SLOWPOKE II. SLOWPOKE, acronym for Safe LOW POWER Critical (K) Experiments, is a nuclear reactor developed by the Atomic Energy of Canada Limited (AECL). SLOWPOKE-2, the commercial version of this reactor, is similar to GHARR-1 and is installed in 8 institutes. The reactors have a combined operating record of over 80 reactor years.

SLOWPOKE-2 is a small, light-water moderated, tank-in-pool type reactor, which has an inherent safety feature based on a large negative temperature coefficient of

reactivity. It contains a small critical mass with HEU fuel. All these characteristics are associated with GHARR-1. To maintain a steady neutron flux in the reactor for experimental purposes, the reactor also employs a cadmium control rod that responds to a self-powered neutron flux detector that is located in the beryllium annulus surrounding the core. These features provide a safe and cost-effective reactor as it is with GHARR-1.

All the features described briefly before are inherent to all the 8 SLOWPOKE-2 installations except the facility at the Royal Military College of Canada. This particular SLOWPOKE-2 facility uses low enriched uranium fuel (LEU) of 19.89 % U-235 in the core [6]. A heavy water column is installed in the reactor vessel from which a vertical neutron beam is installed for neutron radiography studies.

Several transient experiments were performed for the insertion of large reactivities to demonstrate the self-limiting power excursion features of SLOWPOKE type reactors. The results of these investigations have been applied to GHARR-1 to show that it exhibits similar safety features [2].

All MNSR facilities are equipped with a single control rod, which serves to compensate for the excess reactivity necessary for long term core operation and also to adjust the power level of the reactor in order to bring the core to power, follow load demands and shutdown the reactor. Because the movement of the single control rod is controlled by mechanical clutches, it is possible for the mechanical systems to malfunction and therefore jeopardize its safety function. In the case of malfunction of the single control rod such as rod stuck situation, emergency shutdown of the reactor is achieved by pumping Cd rabbits and strings into irradiation channels [2]. Pumping of

cadmium rabbits may not also be achieved in case of pressure failure. There is a possibility of single point failure which could lead to excessive power excursion and ultimately to radiation exposure of personnel in the process of inserting cadmium strings. Even though the MNSR is inherently safe due to high negative temperature coefficient of reactivity, which provides self limiting power excursion characteristics, reactor safety experts have recommended for redundancies in design for reliability of systems important to safety.

One of such recommendations was made during an Integrated Safety Assessment for Research Reactors (INSARR) Mission in May, 2009 [7]. It was stated in section 3.11 of the INSARR report that, “The design of the GHARR-1 has been carried out in accordance with Chinese standards with some attention being focussed on relevant IAEA standards. However, this design is not fully in conformance with the IAEA Safety Standards. In particular, the lack of redundancies of safety rods, and neutronic, temperature, and water level channels does not provide for protection against single failure”.

INSARR Mission is provided upon request to all Member States of IAEA. It is a peer review of the safety of research reactors against IAEA Safety Standards and provides recommendations for safety improvements [8]. To date, over 70 INSARR missions were implemented in research reactors in different regions of the world. INSARR missions cover all safety areas of research reactors. Key review areas include design, safety analysis, operational limits and conditions, regulatory supervision, reactor operation and maintenance, ageing management, radiation protection and waste management, and experiments and modifications. The host organization may request a

full-scope INSARR or a review of a specific area(s). INSARR missions are in three stages, namely, PRE-INSARR, INSARR and FOLLOW-UP.

The single control rod does not satisfy the safety requirements of the IAEA Standards which are stated below:

1. At least one automatic shutdown system shall be incorporated into the design. The provision of a second independent shutdown system may be necessary, depending on the characteristics of the reactor, and this shall be given due consideration.
2. The effectiveness, speed of action and shutdown margin of the reactor shutdown system shall be such that the specified limits and conditions are met.
3. No single failure in the shutdown system shall be capable of preventing the system from fulfilling its safety function when required (e.g. with the most reactive shutdown rod stuck in the out position).
4. One or more manual initiations suitable for emergency shutdown may be necessary and this shall be given due consideration.

Several activities related to normal research reactor operation involve safety evaluation. In principle, any activity that may influence neutronic, thermal-hydraulic and mechanical properties of the reactor should be supported by safety evaluation. Typical activities involving safety evaluation are as follows:

1. Modifications of reactor components, power upgrading, new experimental setups, aging, etc.

2. Complete safety evaluation related to major changes in reactor system and resulting in safety analysis report modifications is normally performed by competent institutions (e.g. reactor manufacturer, national institutions, consultant companies and the like).

The Nuclear Reactors Research Centre (NRRC) of National Nuclear Research Institute (NNRI) which operates GHARR-1 is undertaking steps to convert the reactor core. This is in response to the global trend in converting research and test reactors from the use of High Enriched Uranium (HEU) to Low Enriched Uranium (LEU) in civil nuclear application. As part of the Core Conversion of the GHARR-1 to LEU Core, the National Nuclear Research Institute (NNRI) – the Operating Organization of the reactor – is considering the introduction of a safety rod to augment the safety features of the GHARR-1.

The first objective of this study is to design an LEU core with similar operational capabilities as the original HEU core and with acceptable safety margins under both normal and anticipated or design basis accident conditions. In order to provide comparisons between the proposed LEU core and the initial HEU core, thorough analyses must be performed for both cores. It was decided that the proposed LEU core consists of UO_2 fuel elements clad in Zircaloy-4 alloy, the control element of the control rod material will remain unchanged but the diameter of the absorber material would increase, leaving the diameter of the control rod guide tube unchanged.

The second objective is to design an auxiliary shut down rod for emergency shutdown of the reactor core thereby augmenting the safety of the GHARR-1 facility.

The auxiliary shutdown rod will replace the cadmium capsules in emergency situations. As earlier stated, this is in response to the recommendation made by experts during an Integrated Safety Assessment for Research Reactors (INSARR) Mission in 2009.

Two changes that are required for the conversion are Reactor Facility changes and Operation License and Procedural Changes.

1.1 Reactor Facility Changes

For the Reactor Facility Changes, there is the need

- i. To replace the current UAl_4 HEU fuel elements with UO_2 LEU fuel elements enriched to 12.5 % in U-235. The dimensions of the LEU fuel elements are identical to the HEU fuel. In addition, the proposed LEU fuel has obtained approval from the China Institute of Atomic Energy, the manufacturers of the facility for use in non-power reactors such as the Miniature Neutron Source Reactors (MNSR). Section 1.3 provides a detailed description of the proposed LEU fuel.
- ii. To improve on the shutdown margin of the control rod by increasing the cadmium component.
- iii. To design means of emergency shutdown in case of control rod failure; either by an auxiliary safety rod placed in an irradiation channel or displacing part of annular beryllium reflector to accommodate the safety rod.

1.2 Operation License and Procedural Changes

For the operational license and procedural changes, the GHARR-1 operating license shall have to be amended to allow possession of both the LEU and HEU fuel

inventories during conversion as stated in Section 17.3 of the facility's Safety Analysis Report (SAR). Changes to the technical specifications that are significant include:

1. Changing all references to fuel type from UAl_4 in Al matrix to UO_2 fuel.
2. Review of the characteristics of the central control rod.
3. Review of provision on amount of reactor fuel to be held by NNRI during the conversion exercise.
4. Addition of auxiliary safety rod or displacement of part of the annular beryllium reflector.

1.3 Characteristics of Proposed GHARR-1 LEU Core

The GHARR-1 LEU core base model was established from the reference HEU core base model. The core layout was kept the same. Only the components within the fuel cage (fuel pins, dummy pins, tie rods, and top and bottom grid plates) and the control rod design were different between these two reference models. All other core and reactor structure components are kept the same. A control rod design with a larger outer diameter for the cadmium absorber was also implemented for the LEU core as shown in Table 1.1.

Uranium isotopes used in the GHARR-1 models are compared in Table 1.2. Comparison of key core parameters between the HEU and LEU models are shown in Table 1.3. In an actual LEU core, adjustments to the excess reactivity are likely to be needed to compensate for differences between the reactor design data and the manufacturer's as-built materials and geometry data.

Table 1.1 Control Rod and Guide Tube Design Parameters in MNSR Models

Parameter (Dimension in mm)	HEU	LEU
Outer diameter of cadmium	3.9	4.5
Thickness of SS cladding	0.5	0.5
Thickness of water gap	2.0	1.7
Thickness of guide tube	1.5	1.5
Material of guide tube	LT-21	Zirc-4

Table 1.2 Comparison of Reference GHARR-1 HEU and LEU Fuel Uranium Isotopes

Uranium Isotopic, wt%	HEU	LEU
U-235	90.2	12.5
U-238	8.3	87.65
U-234	1.0	0.2
U-236	0.5	0.25
Total	100.0	100.0

Some of the most important of these differences are in the as-built U-235, U-234 and U-236 loadings, and the as-built impurity levels in the fuel meat. The adjuster rods would be made available to make these adjustments, depending on the results of the low power experiments that are planned at the CIAE before the LEU core is shipped to the customer's site.

Table 1.3 Comparison of Key Parameters for Reference GHARR-1 HEU and LEU Cores

Key Parameters	HEU	LEU
Fuel Meat	U-Al ₄	UO ₂
U-235 Total Core Loading, g	~ 998	~ 1358
U-235 Enrichment, wt %	90.2	12.5
U-234 content, wt%	1.0	0.2
U-236 content, wt%	0.5	0.25
Density of Meat, g/cm ³	3.456	10.6
Meat Diameter, mm	4.3	4.3
Cladding Diameter, mm	5.5	5.5
Thickness of He Gap, mm	None	0.05
Cladding Material	Al-303-1	Zirc-4
Number of Fuel Rods	344	348
Material for Grid Plates	LT-21	Zirc-4
Top Shim Tray (not modeled)	LT-21	LT-21
Number of Dummy Elements	6	2

Material for Dummy Elements	Al-303-1	Zirc-4
Number of Tie Rods	4	4
Material for Tie Rods	Al-303-1	Zirc-4
Adjuster Guide Tubes	4	4

Ghana, a member of the IAEA and a signatory to various conventions, is to use nuclear science and technology for peaceful applications. The Ghana Atomic Energy Commission (GAEC), and for that matter NNRI, is poised to support any advocate or initiative that intends to minimize the likelihood of proliferation of nuclear materials. Hence the Commission is putting in all efforts to make the reactor core conversion a success.

1.4 Outline of Thesis

The literature review is presented in Chapter Two with reference made to the paradigm shift of research reactors from HEU cores to LEU cores.

In Chapter Three, nuclear theory and the required reactor physics as well as thermal hydraulics analyses are highlighted.

In Chapter Four, the 3-D Monte Carlo methodology developed for GHARR-1 reactors using the versatile MCNP transport code and upon which this work is based is described. Three other codes used are also reviewed.

The results of the neutronics and thermal hydraulics analyses performed for the

conversion of GHARR-1 from the use of HEU to LEU has been highlighted in Chapter Five of this thesis.

CHAPTER TWO

2 LITERATURE REVIEW

2.1 General

The conversion of MNSRs is being performed as part of the Global Threat Reduction Initiative (GTRI) – Conversion Program of the United States Government at Argonne National Laboratory and the IAEA's Coordinated Research Project on Conversion of Miniature Neutron Source Research Reactors to Low Enriched Uranium [9]. The project started in 2006 and various neutronics, thermal hydraulic and numerical computations have been performed.

The Reduced Enrichment for Research and Test Reactors (RERTR) Program develops technology necessary to enable the conversion of civilian facilities using high enriched uranium (HEU) to low enriched uranium (LEU) fuels and targets. The RERTR Program was initiated by the U.S. Department of Energy in 1978. During the Program's existence, over 40 research reactors have been converted from HEU (= or >20% U-235) to LEU (< 20% U-235) fuels, and processes have been developed for producing radioisotopes with LEU targets. The RERTR Program is managed by the Office of Nuclear Material Threat Reduction in the National Nuclear Security Administration (NNSA). The main technology components of the program includes the development of advanced LEU fuels and design and safety analysis for research reactor conversion.

2.1.1 Similarity with Other Converted Facilities

In the framework of the IAEA Coordinated Research Project entitled

“Conversion of MNSRs to LEU”, it has been established that it is possible to convert GHARR -1 to UO_2 LEU fuel [10]. The CIAE has successfully commissioned a variant of the MNSR with LEU core, called the In-Hospital Neutron Irradiator (IHNI) designed exclusively for the treatment of cancer based on the boron neutron capture therapy (BNCT) technique [11].

Over 60 research reactor facilities worldwide have been converted to LEU since the 1980s due to international concerns on nuclear proliferation. In 1985, the first LEU-fuelled SLOWPOKE-2 reactor was commissioned at the Royal Military College of Canada (RMC) in Ontario [12]. The reactor at Ecole Polytechnique, Montreal was installed in 1976 and operated with HEU fuel for 21 years [13]. In 1997 the tray of beryllium shim-plates was full and there was no remaining excess reactivity. The exhausted fuel was removed and replaced with LEU fuel in the same beryllium reflector, making it essentially identical to the reactor at RMC. Other conversions include the RPI reactor in Lisbon, Portugal in 2007 [14], Kyoto University Research Reactor in 2010 [15] and the HFETR near Chengdu around 2008 [16].

In the U.S., research reactors at Washington State and Oregon State Universities were recently converted to use LEU fuel rather than HEU. Research reactor conversions were also completed at Purdue University in September 2007 and at Texas A&M and the University of Florida in September 2006.

2.1.2 Advocates of Core Conversion

The Department of Energy's National Nuclear Security Administration (NNSA) has successfully converted a research reactor at the University of Florida from the use of

highly enriched uranium to low enriched uranium [17]. This conversion comes on the heels of a reactor conversion at Texas A&M University. The NNSA had converted over six U.S. and international research reactors.

As a part of its nonproliferation mission, NNSA converts research reactors in the U.S. and around the world from operating on highly enriched uranium (HEU) to low enriched uranium (LEU) fuel. The LEU is not suitable for use in a nuclear weapon and is not sought by terrorists or criminals. The conversion is part of the Bush administration's efforts to minimize the use of highly enriched uranium in civil applications around the world.

HEU is primarily used in research reactors to produce isotopes for medical applications, and early reactor technology used HEU fuel because it was more difficult to achieve comparable power levels using LEU. However, modern reactor designs can use newer high-density LEU fuels while maintaining comparable power levels, making conversion an attractive option for limiting the availability of HEU nuclear material.

The NNSA worked closely with the Department of Energy's Office of Nuclear Energy, the U.S. Nuclear Regulatory Commission, and the University of Florida to complete this reactor conversion. On October 20, 2006 Senior Officials from NNSA joined others in Gainesville to commemorate the successful fuel conversion of the reactor.

Under the 2005 North American Security and Prosperity Partnership, the United States, Mexico, and Canada agreed to convert civil HEU reactors on the North American continent to LEU fuel by 2011, where such LEU fuel is available. The University of

Florida research reactor is the second of six domestic research reactors the United States will convert. Mexico will convert its one research reactor in Mexico City, and Canada will convert three research reactors.

This reactor conversion also supports the 2005 Bratislava Joint Statement on Nuclear Security Cooperation issued by President Bush and Russian President Vladimir Putin. Under the statement, the United States and Russia agreed to work together to convert more than 30 U.S. and Russian-supplied research reactors around the world from the use of HEU to LEU.

GTRI mission includes returning and securing nuclear fuel and radiological sources, protecting radiological and nuclear material and converting research reactors around the world. Currently, GTRI is working to convert 59 more reactors around the world from HEU to LEU by 2014.

Established by Congress in 2000, NNSA is a semi-autonomous agency within the U.S. Department of Energy responsible for enhancing national security through the military application of nuclear science. NNSA maintains and enhances the safety, security, reliability, and performance of the U.S. nuclear weapons stockpile without nuclear testing; works to reduce global danger from weapons of mass destruction; provides the U.S. Navy with safe and effective nuclear propulsion; and responds to nuclear and radiological emergencies in the United States and abroad.

One of the most practical ways to prevent nuclear terrorism is to secure the materials necessary for making a weapon of mass destruction [18]. That was the call to

action outlined in Prague in 2009, and again at the Nuclear Security Summit in 2010. Today, the message is resonating.

Worldwide, nuclear materials that could be stolen and fashioned into a nuclear weapon exist in dozens of nations. However, ongoing efforts led by the National Nuclear Security Administration (NNSA) and supported by U.S. national laboratories are working to minimize the use of HEU.

At Idaho National Laboratory (INL), engineers support the NNSA Global Threat Reduction Initiative's (GTRI) Reactor Conversion Program, which converts domestic research reactors from operating with highly enriched uranium fuel to using LEU fuel. The LEU fuel is less than 20 percent enriched, and cannot be used to make a nuclear weapon.

Engineers at INL integrate conversion activities including performing conversion analyses, fuel fabrication, and fuel replacement. During conversions, three parameters are considered, including (1) the new fuel will not significantly impact the reactor's performance, (2) no major modification to the reactor is required, and (3) there is no significant increase in operational costs. The laboratory is also developing a high-density, low-enriched uranium fuel that can be used in global high-power reactors.

The INL collaborates with the Nuclear Regulatory Commission, national laboratories, universities, international partners, and commercial entities for both reactor conversions and fuel development.

Other interesting information includes:

- To date, reactors at the University of Florida, Texas A&M, Purdue University, Oregon State University, Washington State University, University of Wisconsin, and INL have been converted.

- INL researchers are developing a high-density LEU fuel by leading the design, fabrication technology development, irradiation testing, and fuel performance modeling.

- More than 300 fuel plates have been irradiated at INL to support development of a uranium-molybdenum-based alloy fuel design that can be qualified for the high-power reactors.

2.2 GHARR-1 Reactivity Management

The core consists of 344 cylindrical fuel elements, which form a fuel cage. The cage is located inside an annular beryllium reflector and rests on a lower beryllium reflector plate [2]. The volume of the vessel which accommodates the core is 1.5 m³. The fuel elements are all enriched uranium-aluminium (U-Al₄) alloy extrusion clad with aluminium. They are arranged in 10 multi-concentric circle layers at a pitch distance of 10.95 mm. The fuel cage consists of 2 grid plates, 4 tie rods and a guide tube for the control rod. Screws connect the 2 grid plates and 4 tie rods. The total number of lattice positions is 354 and the number of fuel elements is 344. The remaining positions are occupied with 6 dummy aluminium elements.

Ten circles of holes are concentrically arranged in the upper and lower grid plates to form a lattice.

Table 2.1 contains the characteristics of the arrangement for the lattice.

The annulus and lower reflectors are spaced to form the lower orifice, which controls water flow through the core. The top plate of the core and annulus are spaced to form the upper orifice. An aluminium tray holds the upper reflector, which contains semicircular beryllium shims which are added approximately once a year to compensate for fuel burn-up and samarium (Sm) poisoning.

The top reflector is of variable thickness and assembled by stacking semi-circular plates within an aluminium tray. It is composed of a group of semi-circular beryllium shims with internal diameter of 243 mm. Four different thickness sizes are available, namely 10 pieces of 1.5 mm, 20 pieces of 3.0 mm, 8 pieces of 6.0 mm and 8 pieces of 12.0 mm.

Table 2.1 Lattice positions for the fuel cage

Circle no.	Lattice no.	Circle diameter (mm)	Rod pitch (mm)
0	1	0.00	0.00
1	6	21.90	11.47
2	12	43.80	11.47
3	19	67.70	10.86
4	26	87.60	10.98
5	32	109.60	10.78
6	39	131.40	10.58
7	45	153.30	10.70
8	52	175.20	10.58
9	58	197.10	10.68
10	65	219.00	10.58

Long-term reactivity control is exercised by periodically increasing the thickness of this reflector to compensate for reactivity loss caused by fuel burn-up and samarium poison. Under normal operating conditions of the reactor, the top shims need to be added less frequently than once every one and half years. The maximum thickness of top shims is 109.5 mm for a cold, clean reactor, which is equivalent to 18 mk. In addition to the initial excess reactivity of the core, the presence of the shims ensures that the core life of the reactor fuel elements shall be longer than 10 years.

2.2.1 Reactivity worth of top beryllium reflector plates

The core excess reactivity gradually decreases as ^{235}U is consumed and poisons build up in the fuel. Compensation for this decrease is accomplished by increasing periodically the thickness of the top reflector. This is accomplished by adding small beryllium shim plates of known reactivity worth. Specially authorized persons using appropriate procedures will perform this operation [19]. The typical plot of measured top reflector reactivity worth against thickness of reflector plates is shown in the results given in Chapter 5 of this thesis. As can be observed from the plot when the core burn-up proceeds, the top reflector thickness increases correspondingly and the specific worth of additional beryllium decreases. The graph is used to select the correct thickness to be added to the aluminium tray when the core excess reactivity drops just below 3 mk.

2.2.2 Comparison of the HEU and LEU fuel characteristics

For better fuel characteristics, UO_2 is the preferred option for the conversion.

Comparison of some characteristics of the two fuels in question is shown in the Table 2.2.

Table 2.2 Characteristics of the GHARR-1 fuel element & dummy

Item	HEU	LEU
Fuel/Cladding material	U-Al alloy/Al alloy (LT-21)	UO_2 / Zirc-4
Uranium wt. (%) / U-235 Enrichment (%)	27.5/90.2	12.5
Density (g/cm^3)	3.456	10.6
Diameter (mm)/Length (mm)	4.3/230.0	4.3/230.0
Uranium loading of each rod (g)	2.88	
No. of fuel rod positions/fuel rod loading	350/344	350/348
No. of dummy elements/thickness (mm)	6/0.6	2/0.6
Dummy element material	Al	Zirc-4

2.2.3 Xenon poisoning calculations

Xenon poisoning is small for low power reactors such as GHARR-1. The equilibrium xenon poisoning has been determined to be 5.2 mk [20]. Since the core excess reactivity is only 4 mk, the operation of the reactor is strongly influenced by xenon. This means that the reactor can only be operated intermittently. After operating

the reactor for a period of 2.5 hours at the rated power, the reactor will be shut down because of the xenon poisoning and can re-start only after xenon decay. Under the conditions of maximum flux of 1×10^{12} n/cm².s in the inner experimental tube, a cold excess reactivity of 4 mk and initial core temperature of 15.8 °C, the maximum operable time is about 7.25 hours per day [21]. By lowering the operating power, the maximum operating time can be increased. The variation in the equilibrium xenon poisoning as the average core flux changes can be seen in Table 2.3.

Table 2.3 Equilibrium xenon reactivity as a function of core average flux

Core average flux, 10^{12} n/cm ² .s	1.0	4.0	5.0	6.0	7.0	8.0	9.0	10.0
Equilibrium xenon, mk	0.6	2.2	2.7	3.25	3.8	4.2	4.7	5.0

The trend of fuel management for seventeen years of successful operations: 3 mm thick of beryllium shim have been added to the shim tray on three different occasions. These were added in February, 2002; April, 2009 and January, 2011. All three were added when the reactivity had fallen below 2.5 mk. Regulatory rods are sometimes used to fine-tune the reactivity.

Wet Storage of Spent Fuel could be done in the pool. For this reason, the reactor vessel is not placed at the centre of the pool but rather placed in order to make room for the spent fuel as show in Figure 2.1. In the figure shown, the cross sectional plane cuts through the centre of the reactor pool as well as the centre of the reactor vessel. The code used for the burnup analyses is described in Section 3.7.2 of this thesis.

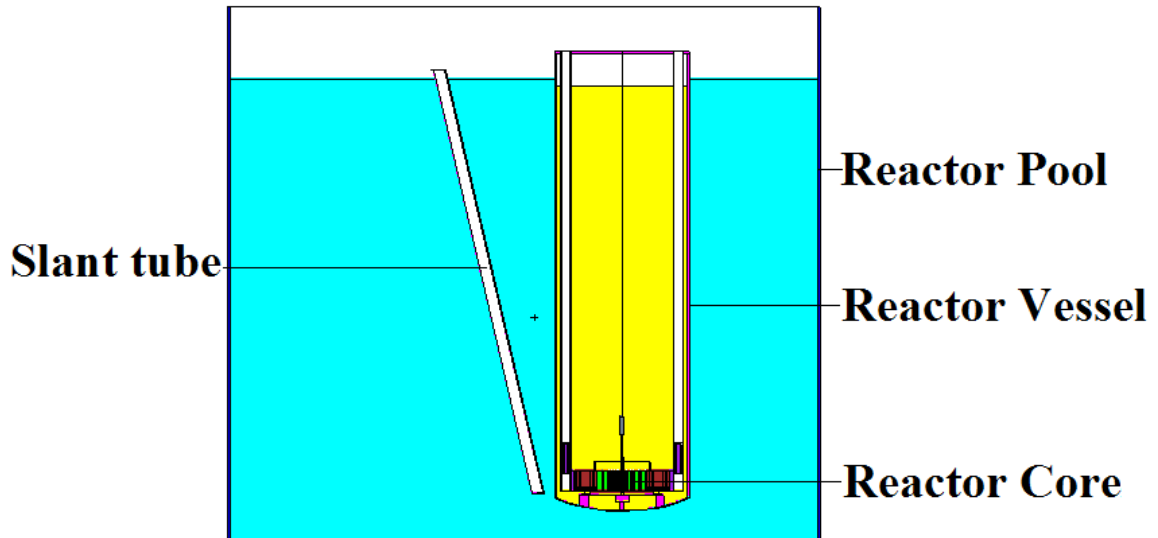


Figure 2.1 Schematic of Reactor Pool (Cross sectional plane through centres of reactor pool and reactor vessel)

2.3 Central control rod of GHARR-1

The reactor assembly consists of the reactor core, beryllium (Be) reflector, small fission chambers for detecting neutron fluxes, one central control rod made of cadmium (Cd) and its drive mechanism

The reactor is designed to have self-limiting power excursion characteristics. Only 1 control rod is at the centre of the reactor core. A fail-safe principle is adopted in the design of the reactor control system. A single cadmium rod is used for regulating the power level, compensating for fuel consumption, startup and shutdown of the reactor. The control rod drive mechanism is mounted on the top plate of the container.

The control range of the automatic control system is designed to cover $108 - 1012 \text{ n/cm}^2 \cdot \text{s}$. The control accuracy is $\pm 1\%$ of the maximum value of the range. The design control rod worth of the reactor is 6.8 mk and the shutdown margin is 3.0 mk for

maintaining the reactor in safe shutdown conditions. The total cold excess reactivity to be compensated is about 4.0 mk by the control rod.

As stated earlier, there is only one central rod for GHARR-1 serving as shim, regulation as well as safety rod. The rod is installed to the control rod mechanism. The total cold excess reactivity to be compensated is about 3.5 - 4.0 mk. The central control rod has a worth of at least 6.8 mk. The shutdown margin is 3 mk. Thus, it can be used to maintain the reactor in a safe shutdown condition.

The control rod has a total length of 440 mm and its diameter is 5 mm. The length of the control rod absorber is 226 mm and its diameter is 3.9 mm. The thickness of the stainless steel cladding is 0.5 mm. Results of zero-power critical experiments have indicated that the movement of the central control rod will have no effect on the flux distribution at the positions of both inner and outer irradiation sites. This characteristic is very beneficial for neutron activation analysis and production of short-lived radioisotopes.

2.3.1 Control rod drive mechanism

The control rod drive mechanism is mounted on the top cover plate of the reactor vessel. It consists of a small AC servomotor, an electromagnetic clutch, a gearbox, a winch drum linked with the steel rope and an autosyn.

The servomotor and electromagnet are energized when the power is applied to the motor and to the 'Protection Ready' on the control console. For this case the electromagnetic clutch is closed. When receiving the signal for control rod withdrawal

or insertion, the motor will rotate clockwise or anti-clockwise; this rotation drives the gear and this operates the winch drum. The drive mechanism moves the control rod up or down at a speed of 8.7 mm/s. For off-normal conditions when the power supply to the clutch is cut off, the clutch immediately opens and the control rod, weighing 1 kg, will fall rapidly into the core. By so doing, fast reactor shutdown is achieved. There are limit switches provided in the control rod drive mechanism to limit movement of the control rod. The switches are connected to a circuit on the main control console, which indicates the rod position either on the top or bottom of the core through the display lights. The autosyn of the drive mechanism is connected to the rod position indicator on the main control console to show the exact position of the control rod in the core. Procedures for the maintenance of the control rod drive mechanism are given in reference [22].

The control for the GHARR-1 reactor is achieved mainly by the withdrawal and insertion of the control rod located in the centre of the reactor core. This control rod is used both as safety and regulating rod. The main parameters are:

- i. The control rod with its balance weight is 1 kg,
- ii. Working distance of the rod is 230 mm,
- iii. Manual rod up and down speed ~9 mm/s,
- iv. Quick rod dropping time for the whole distance <11 s,
- v. Position indicating error ± 1 mm.

The drive mechanism consists of three parts:

- i. Drive mechanism - It consists of AC servo-motor, electromagnetic clutch, compact gearbox, multi-turn potentiometer, water seal tube, guide tube cover, etc.
- ii. Control Rod Position Indicator - The remote indication is achieved owing to the characteristics of the synchronisation between the sending autosyn and the receiving autosyn. The position indicator is installed in the central part of the vertical panel on the control console.
- iii. Control Rod - The control rod consists of a 3.9 mm diameter cadmium rod with stainless steel cladding. Its weight, including the balance is 1 kg. It is installed in the central lattice hole in the active area and hanged by a wire rope. It is connected to a winch of the drive mechanism through the water seal tube, the position limit tube and the guide tube. Its worth is $\leq 7\text{mk}$.

If the drive mechanism of the control rod is out of order and the control rod cannot be inserted into the core for reactor shutdown, the irradiation system described in Section 10.3.1 may be used to shut down the reactor. To do this, 4 cadmium rabbits are inserted into the inner irradiation sites to provide negative reactivity worth greater than 4 mk. If the transfer system is operating, the rabbits can be inserted pneumatically. If the transfer system is inoperable, the sample rabbits can be inserted manually by opening the plastic cover of the reactor, disconnecting the plastic tubing from the top of the aluminium rabbit tube, and inserting a rabbit or a string of rabbits into the tube.

2.3.2 Measurement of the central control rod worth

In order to determine the shutdown margin of GHARR-1, the worth of the central control rod of the reactor was measured by means of the in-hour method [23]. The overall travel length of the control rod in the reactor core is 230 mm and its total worth is at least 6.8 mk. When the central control rod is totally inserted into the core, the reactor shutdown margin is therefore at least 2.8 mk.

In conclusion, the Operating Organization of the Ghana first research reactor has decided to undertake the necessary studies, first by characterizing the HEU Core and subsequently, seek the optimum LEU Core characteristics that can replace the current HEU core.

The theoretical analysis of this thesis is presented next in Chapter Three.

CHAPTER THREE

3 THEORETICAL ANALYSIS

The technical and the design specification of reactor core determine the behaviour of the neutrons in the reactor and hence the associated criticality conditions [24]. This is an essential requirement of reactor design. In particular, the design of a nuclear reactor is based on the interaction of several variables including fuel type, the moderator and reflector, core geometry and composition, radiation shielding, thermal hydraulics, criticality and reactor safety.

In the next and subsequent sections, a brief review is made of the basic nuclear theory and the required reactor physics as well as thermal hydraulics analyses.

3.1 NUCLEAR REACTOR THEORY

In a steady state radiation field, the net rate at which particles are lost in an element must exactly be balanced by the rate of secondary or source particles which are introduced into the volume. The linear particle transport equation or linearized Boltzmann transport equation is used to determine the particle distribution in space, r direction Ω and energy, E in plane, spherical or cylindrical geometry. The equation is the basic physical model to describe the transport of uncharged particles such as neutrons and photons (γ - rays, light, etc.)

The transport equation can be derived by simple balancing of the various mechanisms by which particles can be gained or lost from an element in a phase-space, (r, Ω, t) i.e.

$$\begin{bmatrix} \text{time rate of} \\ \text{particle density} \\ \text{change} \end{bmatrix} = \begin{bmatrix} \text{change due to} \\ \text{physical leakages} \end{bmatrix} + \begin{bmatrix} \text{change due} \\ \text{to collision} \end{bmatrix} + \begin{bmatrix} \text{sources} \end{bmatrix} \quad (3.1)$$

which can be expressed mathematically as:

$$\frac{1}{v} \frac{\partial}{\partial t} \phi(r, \Omega, E, t) = -\Omega \cdot \nabla \phi(r, \Omega, E, t) + S(r, \Omega, E, t) - \Sigma_t(r, E, t) \phi(r, \Omega, E, t) + \int_0^{\infty} dE' \int_{4\pi} d\Omega' \Sigma_s(r, E' \rightarrow E, \Omega' \rightarrow \Omega, t) \phi(r, \Omega', E', t) \quad (3.2)$$

where

$\phi(r, \Omega', E', t) =$ the expected number of particles per unit time at r with energies in unit energy about E and moving in a unit angle about Ω ,

$S(r, \Omega, E, t) =$ the number of source particles emitted in a volume dV travelling in a cone of direction $d\Omega$ about Ω with energies between E and dE

$\Sigma_s(r, E' \rightarrow E, \Omega' \rightarrow \Omega) =$ macroscopic scattering cross-section which is the probability that the particles at position r with energy E' travelling in the direction Ω' scatter into dE about E and into the cone of direction $d\Omega$ about Ω .

The corresponding steady state equation is

$$[\Omega \cdot \nabla + \Sigma_t] \phi(r, \Omega, E) = \int dE' \Sigma_s(r, \Omega' \rightarrow \Omega, E' \rightarrow E) \phi(r, \Omega', E') d\Omega' dE' + S(r, \Omega, E) \quad (3.3)$$

The equation is solved for shielding problems, including deep penetration and neutron-gamma coupled problems as well as multiplying media problems in the reactor theory,

including criticality search and others.

For neutrons besides a scattering reaction, a collision of neutrons with a host medium can generate other neutrons by fission (multiplying medium). Equation 3.3 is written to describe the system containing fissile nuclides which can be regarded as sub-critical, critical or supercritical. The criticality problem is approached by introducing the effective multiplication factor to balance the fission source with other terms in the transport equation such that neglecting external source of Equation 3.3 becomes:

$$\Omega \cdot \nabla \phi + \Sigma_t \phi = \int_0^\infty \int_{4\pi} \Sigma_s(r, \Omega' \rightarrow \Omega, E \rightarrow E') d\Omega' dE' \phi(r, \Omega', E') d\Omega' dE + \frac{1}{k} \int_0^\infty \int_{4\pi} \frac{\chi(E)}{4\pi} \nu(E') \Sigma_f(r, E') \phi(r, \Omega', E') d\Omega' dE \quad (3.4)$$

The neutron transport equation is a linearized version of the Boltzmann equation based on neutron conservation and vector calculus. The “integro-differential” transport equation is linear with seven independent variables [25].

3.2 Solution of the Neutron Transport Equation

Generally, the particle transport equation is difficult to solve analytically except in simple cases with numerical methods. The transport equation is thus solved analytically for limited cases only. For estimation of particle flux it is approximated by solving it numerically using various techniques [25].

Most reactor studies assume that neutrons diffuse from regions of high to low density, akin to the diffusion of heat from high to low temperature, or as gas molecules diffuse to reduce spatial variations in concentration. However, while diffusion of heat

and gases is quite accurately modeled, the treatment of neutron transport as a diffusion process is quite limited. In conventional diffusion, particle trajectories are irregular, random, and zigzag-like; yet, in neutron transport, low reaction cross-sections (~ 1 barn, 10^{-24} cm²), lead to long mean free paths, with dimensions characteristic to the transport medium (inhomogenities). Thus, a more accurate description of neutron transport is required.

Neutron diffusion equation follows from integrating out the angular dependence of the neutron flux, among other approximations. Recent advances in computational power and methods provide an enormous opportunity for improved and more accurate computational solutions to the neutron transport/diffusion equations and problems.

The two general approaches to solving the neutron particle transport include - **Deterministic methods** (Finite Difference, Finite Element, Discrete Ordinates): These methods include discretization of variables, replacement of the mathematical equation with coupled linearized algebraic equations and solution of the system of equations with numerical methods.

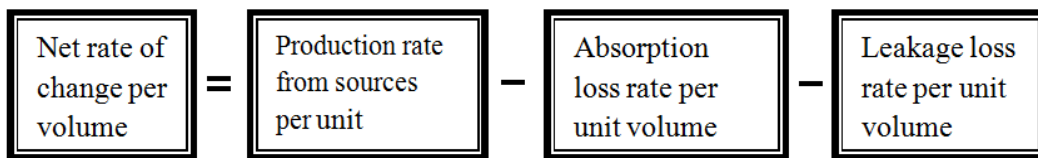
- **Stochastic methods (Monte Carlo)**: Stochastic methods are statistical and describe a physical system by its corresponding probability density functions and also utilize numerical methodologies to simulate the probability density functions.

3.2.1 Diffusion Theory Approximation

As per the previous discussion, diffusion theory approximation and Monte Carlo approaches of the neutron transport theory are used in reactor analysis and design. In

particular, diffusion theory approximates the transport theory and provides an exact solution and analysis. In this section, the diffusion equation for describing the behaviour of neutrons in a reactor system is presented.

The neutron conservation equation indicates that the net rate of change of the neutron density, n , with time t in a given nuclear system is balanced by the rate of neutron production from sources, loss rates by absorption and leakage per unit volume, i.e.,



$$\text{i.e., } \frac{\partial n}{\partial t} = \text{Sources} - \text{Absorption} - \text{Leakage}$$

Mathematically, the above can be expressed as

$$\frac{\partial n}{\partial t} = S - \Sigma_a \phi - \text{Leakage} \quad (3.5)$$

where $\Sigma_a \phi$ is the absorption term and Σ_a is the macroscopic cross-section for neutron absorption.

Calculation of the neutron leakage term is based on the use of a physics parameter called the neutron current density, J . In particular, the neutron current density is defined as the defined as the net number of neutrons crossing a unit surface area in a given direction per unit time. In a system defined in a 3-D configuration in x , y , and z -directions, the neutron current density will have corresponding J_x , J_y , and J_z components. Then the rate of loss of neutrons per unit volume in the system in the x , y and z -directions can be expressed as

$$\text{x-direction} = \frac{\partial J_x}{\partial x}, \quad \text{y-direction} = \frac{\partial J_y}{\partial y} \quad \text{and} \quad \text{z-direction} = \frac{\partial J_z}{\partial z}$$

Thus, the net rate of loss (or leakage) of neutron per unit volume

$$= \frac{\partial J_x}{\partial x} + \frac{\partial J_y}{\partial y} + \frac{\partial J_z}{\partial z} = \text{div}J = \nabla \cdot J \quad (3.6)$$

Using the above definition, Equation 3.5 reduces to

$$\frac{\partial n(r,t)}{\partial t} = S(r,t) - \Sigma_a \phi(r,t) - \nabla \cdot J(r,t) \quad (3.7)$$

The diffusion equation is derived via Fick's Law of Diffusion. Accordingly, the net rate of neutron flow in a given direction is proportional to the (negative) spatial gradient of the neutron flux. Mathematically,

$$J = -D\nabla \phi \quad (3.8)$$

where D is the diffusion constant

Equation 3.7 can then be re-written, using Equation 3.8 as

$$\begin{aligned} \frac{\partial n(r,t)}{\partial t} &= S(r,t) - \Sigma_a \phi(r,t) - \nabla \cdot [-D\nabla \phi(r,t)] \\ &= \nabla \cdot [D\nabla \phi(r,t)] - \Sigma_a \phi(r,t) + S(r,t) \end{aligned} \quad (3.9)$$

$$\nabla \cdot [D\nabla \phi(r,t)] = D\nabla^2 \phi(r,t) \quad (3.10)$$

where ∇^2 represents the Laplacian Operator and

$$\nabla^2 \phi = \frac{\partial^2 \phi}{\partial x^2} + \frac{\partial^2 \phi}{\partial y^2} + \frac{\partial^2 \phi}{\partial z^2}$$

The diffusion equation, (Equation 3.9) can then be commonly written in the form

$$\frac{\partial n(r,t)}{\partial t} = D\nabla^2 \phi(r,t) - \sum_a \phi(r,t) + S(r,t) \quad (3.11)$$

For steady state conditions, $\frac{\partial n}{\partial t} = 0$

The diffusion equation in steady state condition becomes

$$D\nabla^2 \phi(r) - \sum_a \phi(r) + S(r) = 0 \quad (3.12)$$

In the absence of a primary (or independent) source, the external source, S, is given by

$$S = k_\infty \sum_a \phi \quad (3.13)$$

where k_∞ is the infinite neutron multiplication factor.

3.2.2 Multigroup Calculations

The energy of neutrons produced in nuclear fission range up to about 10 MeV. In a nuclear reactor, these neutrons are slowed down by scattering collisions with atomic nuclei until they are thermalized. In the thermal energy region (below about 1 eV), the neutrons exchange energy with the moderator atoms, so that up-scattering as well as down-scattering can occur. Consequently, the neutron energies in a reactor core range from about 10 MeV to 0.001 eV or less.

Reactor analysis is performed in favour of reactor design, neutronics calculations and other important particle transport activities in nuclear reactors. Since the neutron energy varies, it is impractical in reactor analysis to treat the neutron energy as a

continuous variable. Consequently, the energy range of interest is divided into a finite number of discrete energy groups as shown below in Figure 3.1.

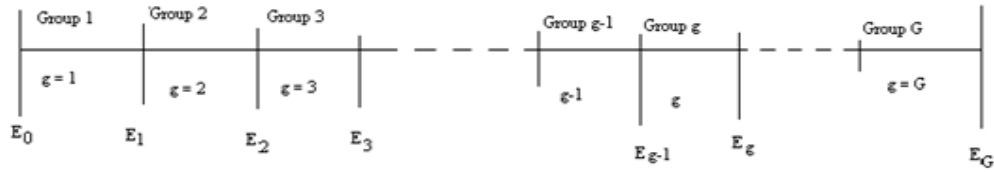


Figure 3.1 : Partial distribution of neutron energies into G groups

where $E_0 > E_1 > E_2 > \dots > E_{g-1} > E_g > \dots > E_G$.

The larger the number of energy groups, the more closely will the group energy distribution approach the actual neutron energy spectrum. However, increasing the number of groups also increases the complexity of the computation. Hence, the number of energy groups selected depends on circumstances and represents a compromise between accuracy on one hand, and the complexity of the calculations on the other hand [26].

To set up the multigroup equations for a critical reactor, three group constants are first be defined. These are

Σ_{fg} = group-average macroscopic fission cross-section for group g

ν_g = average number of fission neutrons released as the result of nuclear fissions induced by neutrons in the gth group: and

χ_g = fraction of fission neutrons that are emitted with energies in the gth group.

The number of fissions per cm³/s in the hth group can now be written as $\sum_{fh}\varphi_h$ where φ_h the flux in the hth group. As a result of these fissions, $\nu_h \sum_{fh}\varphi_h$ neutrons are released. The total number of neutrons emitted as the result of fissions in all groups is then

$$n = \sum \nu_h \sum_{fh} \varphi_h \quad (3.14)$$

where the sum is carried over all groups. If the fraction χ_g of these neutrons appears in the gth group, it follows that the source term for the gth multigroup equation is

$$S_g = \chi_g \sum_{k=1}^N \nu_k \sum_{fk} \varphi_k \quad (3.15)$$

and the gth group equation in a set of N multigroup equations is

$$D_g \nabla^2 \varphi_g - \Sigma_{ag} \varphi_g - \sum_{h=g+1}^N \Sigma_{g \rightarrow h} \varphi_g + \sum_{h=1}^{g-1} \Sigma_{h \rightarrow g} \varphi_h + \chi_g \sum_{h=1}^N \nu_h \sum_{fh} \varphi_h = 0 \quad (3.16)$$

For a typical reactor, which has several regions of differing material properties, there is a set of equations like those represented by Equation 3.16 for each region. In this case, it is necessary to solve the equations in each region and satisfy boundary conditions at every interface as well as at the reactor surface.

3.3 Generation of Group Constants

Before an attempt is made to solve Equation 3.16, the flux weighted quantities, D_g , Σ_{tg} , $\Sigma_{g' \rightarrow g}$ and $\nu_g \Sigma_{fg}$ known as group constants must be determined. The group macroscopic cross-section is expressed as

$$\Sigma_g \phi_g = \int \Sigma(E) \phi(E) dE \quad (3.17)a$$

or

$$\Sigma_g = \frac{1}{\phi_g} \int \Sigma(E)\phi(E)dE \quad (3.17)b$$

where ϕ_g is the group flux and defined by

$$\phi_g = \int \phi(E)dE \quad (3.18)$$

and $\phi(E)$ is the neutron flux per unit energy interval at energy E within the group and the integration is carried over the energy range of the group g, i.e. from E_{g-1} to E_g . The evaluation of the group cross-sections requires knowledge of Σ and of ϕ as functions of the neutron energy for all nuclides present.

A simpler procedure is based on the assumption that, even though the number of microgroups is large over a small range, $\phi(E)$ may be taken as constant and Equation 3.18 then reduces to

$$E \approx (\text{constant}) \Delta E_g \quad (3.19)$$

where $\Delta E_g = E_{g-1} - E_g$ and Equation 3.18 becomes

$$E_g \approx \frac{1}{\Delta E_g} \int \Sigma(E)\phi(E)dE \quad (3.20)$$

thus Σ_g can be evaluated. In general, the group constants that Equation 3.20 is applicable are for absorption, scattering and fission.

The group diffusion coefficient reduces to the form

$$D_g \approx \frac{1}{\phi_g} \int D(E)dE \approx \frac{1}{\Delta E_g} \int D(E)dE \quad (3.21)$$

assuming $\phi(E)$ is taken as constant over the group energy range.

In calculating D_g , the quantity $D = \frac{1}{3}E_t - \mu_o \Sigma_s$ is invoked to express $D(E)$ in terms of cross-sections as functions of the neutron energy. The transfer (scattering) cross-section, $\Sigma_{sg \rightarrow g1}$ is defined by

$$\Sigma_{sg^1 \rightarrow g} = \frac{1}{\phi_g} \int_{g^1} \int_g \Sigma_s(E^1 \rightarrow E) \phi(E^1) dE dE^1 \quad (3.22)$$

where

$\Sigma_s(E^1 \rightarrow E)$ is the differential scattering cross-section from energy E^1 to E .

The group fission constant $\nu_g \Sigma_{fg}$ is defined by

$$\nu_g \Sigma_{fg} = \frac{1}{\phi_g} \int_{g^1} \nu(E) \Sigma_f(E) \phi(E) dE \quad (3.23)$$

$$\approx \frac{1}{\Delta E_g} \int_{g^1} \nu(E) \Sigma_f(E) \phi(E) dE \quad (3.24)$$

3.4 Few Group (Macro-group) Constants

Many group constants are collapsed into few group (macro-group) constants for determining the spatial distribution of the neutron flux. For water-moderated reactors, four groups are commonly used. These are:

1. Fast region – from 10 MeV to 0.05 MeV. The fission neutrons possess energies in this group and both elastic and inelastic scattering occur.
2. Slowing-down region – from 50 keV to 500 eV. In this range slowing down is by elastic scattering and there may be absorption in unresolved resonance.
3. Resonance region – from 500 eV to 0.625 eV. Slowing down occurs by elastic scattering and there is absorption in resolved resonances.

4. Thermal region – below 0.625 eV. Both down-scattering and up-scattering can occur in addition to absorption.

For some reactor analysis, 3 or 2 neutron energy groups are sufficient. For graphite-moderated reactors, more than four groups may be needed. For Ghana MNSR which is both water and beryllium reflected, four groups are adequate [25]. For the MNSR MCNP model, three groups are considered for the neutronic analysis.

3.5 Monte Carlo Techniques

Stochastic Monte Carlo methods are extensively used in nuclear applications such as radiation shielding, radiation transport, neutronics, reactor physics, design and analysis. Monte Carlo methods refer to statistical methodology wherein the expected characteristics of particles (e.g. particle flux) are estimated by sampling a large number of individual particle histories whose trajectories are simulated by a digital computer. In some cases, there are equations that adequately describe the behaviour of such systems and that can be solved either analytically or numerically.

3.5.1 General Overview

The basic advantage of Monte Carlo techniques over the deterministic techniques (e.g., numerical solution of the Boltzmann transport equation) is that Monte Carlo methods more accurately represent the geometry and nuclear data than do deterministic techniques. Deterministic methods require reasonably simple geometries for the numerical techniques to work and use multigroup group approximations to continuous energy neutron cross-section data [27].

Additionally, Monte Carlo techniques can handle complex geometries and continuous cross-section data, as well as the simple geometries and multigroup data. In many cases, the geometry of a system is more complex than a cylinder or a stack of cubes; it often includes both cylindrical and planar surfaces. For these situations, Monte Carlo is a better technique as it statistically evaluates the system with few approximations rather than trying for a numerical approximation to the analytic description.

The disadvantages of the Monte Carlo approach are that it is statistical in nature and does not provide an exact solution to the problem. All results represent estimates with associated uncertainties. Also, Monte Carlo techniques can be quite time consuming on a computer if very small uncertainties are required. The relationship between Monte Carlo and deterministic techniques can best be summarized as: deterministic techniques provide an exact solution to an approximation of the problem while Monte Carlo techniques provide an approximate solution to an exact representation of the problem.

Monte Carlo methods can be used to duplicate theoretically a statistical process and is particularly useful for complicated geometries and complex problems that cannot be modeled with deterministic codes. The individual probabilistic events constitute processes and are simulated sequentially. The probability distributions governing these events are statistically sampled to describe the total phenomenon.

In particle transport, the Monte Carlo technique is pre-eminently realistic and consists of actually following each of many particles from a source throughout its life to

its death in some terminal category such as absorption and leakage. Probability distributions are randomly sampled using transport data to determine the outcome at each step of its life.

In a neutron field such as in the core of a nuclear reactor, when a neutron traverses a material, it interacts with the constituent atoms of that material. The neutron gets scattered or absorbed depending on the cross-sections of the material. These processes occur statistically in nature with the probability of occurrence determined by its cross-section. Whereas the distance of travel by one neutron particle cannot be predicted exactly in the material before interacting; the distribution of flight distances that a large number of those particles will have prior to the first interaction, can however, be predicted via the Monte Carlo approach.

Using “random” numbers, a statistical history for the life of each particle (a random walk analysis) can be generated by a computer. That is, an individual particle may experience many scattering interactions before finally being absorbed or leaked from the system. Random numbers (a set of numbers which have no pattern and are sampled uniformly between zero and one) are used at each interaction to determine which process (absorption, fission, elastic scattering, etc.) occurs, how much energy is lost, what is the new direction of the particle (for scattering), or how many neutrons are released in a fission event.

The life of a particle begins at birth, either from an external neutron source or from a fission event, and ends with absorption or with a scattering event that moves the neutron outside the assembly. The events that occur during a particle’s life are tabulated

as the particle's histories. Because a single particle is usually not representative of the total system, a number of histories must be evaluated to accurately describe what occurs.

3.5.2 Criticality Calculations

Nuclear criticality is an important activity required in reactor analysis, reactor design, reactor operation and safety. Hence, the effective multiplication factor in Monte Carlo criticality applications is of primary interest. In these calculations, a group of neutron histories is often referred to as a k_{eff} cycle with the multiplication factor of the assembly defined by the ratio of the number of neutrons generated at the end of the k_{eff} cycle to the number of neutrons whose histories are evaluated in this cycle. The expected value of the multiplication factor is then estimated by averaging over the events in the k_{eff} cycle.

The relative error in the estimate of the effective multiplication factor will usually decrease as the number of k_{eff} cycles increases. Thus, numerous criticality cycles are necessary to arrive at a good estimate. In addition, the first few cycles are inaccurate because the spatial neutron source has not converged. Because the distribution of source (fission) neutrons in a system is dependent on the Eigen-value of the system and on its geometry, it takes a number of inactive cycles for the Monte Carlo spatial neutron distribution to approach the converged distribution. For this reason, the first few cycles are ignored in the final estimate of k_{eff} . The estimates of k_{eff} from the remaining cycles are averaged to obtain a mean value for the effective multiplication factor.

In the MCNP Monte Carlo, if G criticality generations are evaluated and the first D cycles are discarded, then the estimated effective multiplication factor of the system is

given by

$$\bar{k} = \frac{1}{(G-D)} \sum_{i=D+1}^G k_i \quad (3.25)$$

where \bar{k} is the estimated system multiplication factor and k_i is the multiplication factor determined from the i th cycle. The repeatability of the estimate (i.e., if the same calculation is performed with different random numbers, how much different will the estimate of \bar{k} be) is determined from the estimated standard deviation of the mean. The standard deviation of the mean is calculated using the standard deviation, σ , of the distribution of k -values.

$$\sigma = \sqrt{\frac{1}{(G-D-1)} \sum_{i=D+1}^G (k_i - \bar{k})^2} \quad (3.26)$$

For a valid Monte Carlo calculation, the range $\bar{k} - \sigma$ to $\bar{k} + \sigma$ should include the precise k_{eff} .

The literature review on the associated nuclear reactor physics has been briefly limited to particle transport theory and the approximated diffusion theory as well as a discussion on the differences between deterministic and Monte Carlo approaches to the transport theory. As mentioned earlier, the MCNP Monte Carlo code was utilized in this work and the review is thus somewhat skewed towards Monte Carlo techniques. For purposes of brevity, the presentation made in this thesis about the MCNP code is however limited. Details of the physics, theory and mathematical models upon which the MCNP code is built can be obtained in the literature [27].

3.5.3 Neutron Cross section Data Libraries

The basis for the simulation of all fundamental process in MCNP, are the cross section and other nuclear data for neutrons and correlated secondary particles, which are organized in data libraries. Neutron-induced cross sections depend primarily on the nucleus with which the neutron is interacting, incident neutron energy and temperature of the medium. Cross section values are derived from experimental data and theoretical models if experimental measurement is not possible. Cross sections are summarized and organized in the Evaluated Nuclear Data Files (ENDF) [28]. To utilize the evaluated data libraries with neutronics codes such as the MCNP, the data is adequately formatted to suit the requirement of the code and the problem to be solved. For MCNP this task is done by processing code NJOY [29]. The processed nuclear data libraries retain as much detail from the original evaluations as is feasible to faithfully reproduce the evaluator's intent.

MCNP uses continuous-energy nuclear and atomic data libraries. Nuclear data tables exist for neutron interactions, neutron-induced photons, photon interactions, neutron dosimetry or activation, thermal particle scattering $S(\alpha, \beta)$ etc. In the case of neutron interaction, continuous-energy and discrete reaction data are available, the latter based on multi-group cross section. In addition to cross section data, the MCNP libraries also include angular distributions for scattering, fission yields, Q-values, etc.

The calculations performed in this work are based on the cross section data distributed with the code and thermal particle treatment for hydrogen in light water. Each data table available to MCNP is listed on a directory file, XSDIR. Specific data

tables may be selected through unique identifiers for each table, called ZAIDs. These identifiers generally contain the atomic number Z , mass number A , and library indicator ID.

Since GHARR-1 is operated at relatively low pressure and temperature, nuclear data evaluated for a temperature of 300K are used in all simulations. Cross sections are required for all materials used in the model of the reactor. The materials include: structural materials, the coolant and the moderator and nuclides built-up in the fuel.

Other sources of nuclear data apart from the Evaluated Nuclear Data File are Advanced Computational Technology Initiative (ACTI) [30], the Evaluated Nuclear Data Library (ENDL) [31], Evaluated Photon Data Library (EPDL) [32], the Activation Library (ACTL) [33] compilations from Livermore, and evaluations from the Nuclear Physics (T-16) Group [34] [35] [36] at Los Alamos.

3.5.4 Thermal Scattering Matrix $S(\alpha, \beta)$

For low energies, the scattering behavior of neutrons depends on binding effects in the material and the possibility to excite vibrational modes, if the target nucleus is a low mass number (A) material embedded in a molecule or lattice. In this case, incoherent inelastic scattering strongly contributes to the thermal scattering cross sections of neutrons described as [29]:

$$\sigma(E, E', \mu) = \frac{\sigma}{2kT} \sqrt{\frac{E'}{E}} \exp\left(-\frac{\beta}{2}\right) S(\alpha, \beta) \quad (3.27)$$

where E and E' are the energies of the incident and the scattered neutron respectively, μ is the cosine of the scattering angle in the laboratory system, and σ is the integral cross

section of the bound nucleus for the limit of low neutron energies at $T = 0$. The scattering matrix $S(\alpha, \beta)$ is a function of the momentum transfer α and energy transfer β , which are both defined as dimensionless quantities.

$$\alpha = \frac{E' + E - 2\mu\sqrt{E'E}}{AkT} \quad \text{and} \quad \beta = \frac{E' - E}{kT} \quad (3.28)$$

For gaseous and unbound nuclei, MCNP explicitly calculates the scattering matrix $S(\alpha, \beta)$ with the analytical expression.

$$S(\alpha, \beta) = \frac{1}{\sqrt{4\pi\alpha}} \exp\left(-\frac{\alpha^2 + \beta^2}{4\alpha}\right) \quad (3.29)$$

In all other occasions, i.e. for specified material compositions, the values of $S(\alpha, \beta)$ are tabulated in additional libraries and can be requested by the code. Since incoherent inelastic scattering is most relevant for materials with low mass number nuclei, MCNP provides tabulated data for hydrogen in light water, deuterium in heavy water, beryllium or graphite [37].

3.5.5 Mathematical Basis for Monte Carlo Simulation

3.5.5.1 Generation of Random Numbers

A computer is a precise and deterministic machine, and hence, the output of a computer is predictable and not truly “random”. The word “random” represents the output of a truly random physical process such as the decay of radioactive nuclei. In radioactive decay process, we cannot predict which nucleus is going to decay and when. However, we can say that after time t , how many nuclei would have decayed using probabilistic models. Computer generated sequences are “pseudo-random” number [38]. It is preferable to have a random number sequence that is reproducible. This way it is

possible to reproduce a calculation. If every calculation uses different numbers, it is hard to make a distinction between a new result of the calculation and a change in result due to the new set of random numbers.

A random number with a uniform probability distribution in the unit interval (0,1) is generated and any number in the unit interval generated is equally likely to be picked. Most commonly used methods for generating sequences R of numbers from a uniform distribution are based upon a mixed congruential relationship [39] [40] given by Halton [41] and Marseguerra [42]:

$$\mathbf{R}_{k+1} = (\mathbf{aR}_k + \mathbf{c})\mathbf{mod} \mathbf{m} \quad (3.30)$$

The new number R_{k+1} is the remainder, modulo a positive integer m , of an affine transform of the old R_k , with a non-negative integer coefficient a and c . The sequence obtained is made up of numbers $R_k < m$ and is periodic with period $p < m$. The sequences generated with Equation 3.30 are called pseudorandom numbers and are reproducible. The constants a , c and m may be selected so that (Bart, 2009):

- i. The sequence pass statistical test for randomness
- ii. The period p is very large.

In MCNP the period is typically 2^{46} [43] [44]. In other words, 2^{46} , random numbers can be generated before the numbers start to repeat themselves.

The numbers generated in Equation 3.30 is smaller than m so that when divided by m ($R_k = R_{k+1}/m$), they must all lie in the interval (0,1), i.e Uniform PDF on (0,1).

3.5.5.2 Probability Density Function

A Probability Density Function (PDF) is the mathematical expression of a stochastic physical law. In Monte Carlo, PDF is the input in which the underlying physical process is described [42].

Let x be a random variable (a variable that takes on a particular values with a frequency that is determined by some underlying probability distribution) that takes the value in the interval $x_{min} \leq x \leq x_{max}$. The likely hood of obtaining x in the interval is the ratio n/N of the number n of values x that fall within the interval and the total number N of generated x values, in the limit as $N \rightarrow \infty$. A PDF, $p(x)$ is the probability that the outcome of a particular event will occur in dx about x for continuous and discrete distribution.

For continuous distribution, we can define

$$p(x)dx = P\{x \leq x' \leq x + dx\} \quad (3.31)$$

On physical grounds, $p(x)$ must be everywhere non-negative and be normalized to a total probability of 1, i.e.,

$$p(x) \geq 0 \text{ and } \int_{-\infty}^{\infty} p(x)dx = 1 \quad (3.32)$$

A function that satisfies Equation 3.32 is interpreted as PDF. The likely hood of obtaining x in the interval (a, b) is

$$Prob\{a \leq x \leq b\} = \int_a^b p(x)dx \quad (3.33)$$

The Cumulative Distribution Function (CDF) for the continuous distribution is defined by

$$P(x) = \int_{-\infty}^x p(x') dx' = P\{x' \leq x\} \quad (3.34)$$

where $P(x)$ is non-negative and monotonically increasing from $\mathbf{0}$ to $\mathbf{1}$ and it is continuous and differentiable at will

$$\mathbf{0} \leq P(x) \leq \mathbf{1}; p(x) = \frac{dP(x)}{dx} \geq \mathbf{0} \quad (3.35)$$

The probability of having x in the interval (a, b) is

$$\int_a^b p(x') dx' = P\{a \leq x \leq b\} = P(b) - P(a) \quad (3.36)$$

For discrete distribution, the PDF of a random variable x is

$$p(x_i) = p_i \delta(x - x_i) \quad (3.37)$$

Where $\delta(x - x_i)$ is the Dirac Delta function $p(x_i)$ must be everywhere non-negative and be normalized to 1.

$$p(x_i) \geq \mathbf{0}; \sum_i p(x_i) (\Delta x_i) = \mathbf{1} \text{ or } \sum_i p_i = \mathbf{1} \quad (3.38)$$

The discrete CDF is

$$P(x) = \sum_{x_i < x} p_i = \sum_{x_i < x} p(x_i) (\Delta x_i) \quad (3.39)$$

The uniform distribution is frequently used in Monte Carlo simulation since sampling from the distribution allows obtaining random variable obeying any other distribution.

3.5.6 Generation of Random Variable

In this section we discuss various methods for generating non-uniform random variables from a prescribed distribution. We will consider the inverse-transform method and the acceptance-rejection method which are of great importance to this work.

3.5.6.1 Sampling by Inversion of CDFs from Continuous Distribution

Let $X \in (-\infty, \infty)$ be a random variable with CDF $P_X(x)$ and PDF $p_X(x)$ namely [42]:

$$P_X(x) = \int_{-\infty}^x p_X(x) dx = \text{prob}\{X \leq x\} \quad (3.40)$$

Where,

$$0 \leq P_X(x) \leq 1, p_X(x) \geq 0, \int_{-\infty}^{\infty} p_X(x) dx = 1 \quad (3.41)$$

Since $P_X(x)$ is a non-decreasing function, for any $y \in (0,1)$ its inverse is defined as

$$P_X^{-1}(y) = \text{Inf}\{x: P_X(x) \geq y\}, \quad 0 \leq y \leq 1 \quad (3.42)$$

We can obtain values $X \sim P_X(x)$ starting from values R sampled from the uniform distribution $U_R(0,1)$. Since both $U_R(r)$ and $P_X(x)$ are increasing function of $(0,1)$, for each $R \sim U_R(r)$ there exists only one value

$$X = P_X^{-1}(R) \quad (3.43)$$

The X values computed are actually sampled from $P_X(x)$ i.e. $X \sim P_X(x)$: for any $r \in (0,1)$ there is one x value such that $P_X(x) = r$. We then have

$$\text{Prob}\{X \leq x\} = \text{Prob}\{P_X^{-1}(R) \leq x\} \quad (3.44)$$

Applying the function $P_X(\cdot)$ to the right hand side of 2.74, we get

$$\text{Prob}\{X \leq x\} = \text{Prob}\{R \leq r\} \quad (3.45)$$

Also applying the function $P_X(\cdot)$ to both sides of 2.75 we have

$$R = \int_{-\infty}^X p_X(x) dx \quad (3.46)$$

Equation 3.46 gives the fundamental relationship of the inverse transform method since

for any R value sampled from the uniform distribution $U_R(0, 1)$ it gives the corresponding X value, which is sampled from the $P_X(x)$ distribution.

A random variable X is said to be uniformly distributed in the interval (a, b) if the PDF and CDF is respectively given by

$$\begin{aligned}
 p_X &= \frac{1}{b-a} \text{ for } a \leq x \leq b & p_X &= \frac{x-a}{b-a} \text{ for } a \leq x \leq b \\
 &= 0 \text{ for } x < a & \text{and } &= 0 \text{ for } x < a \\
 &= 0 \text{ for } x > b & &= 1 \text{ for } x > b
 \end{aligned} \tag{3.47}$$

Substituting into Equation 3.46 and solving with respect to X gives

$$X = a + R(b - a) \tag{3.48}$$

Thus, to generate a random variable X with cumulative distribution function P , draw $R \sim U(0,1)$ and set $X = P_X^{-1}(R)$. In practical terms, X is generated from the cumulative distribution in the the following steps:

- i) Generate R from $U(0,1)$
- ii) Return $X = P_X^{-1}(R)$

3.5.6.2 Sampling by Direct Inversion of CDFs from Discrete Distribution

Let X be a random variable that can only have discrete values x_k ,

where $k = 0, 1, \dots$ with probability [42]

$$p_k = \text{prob}\{X = x_k\} \geq 0, \quad k = 0, 1, \dots \tag{3.49}$$

Ordering the $\{x\}$ sequence so that $x_{k-1} < x_k$ the cumulative distribution is

$$P_k = \mathbf{prob}\{X \leq x_k\} = \sum_{i=0}^k p_i = P_{k-1} + p_k, \quad k = 0, 1 \quad (3.50)$$

where, $P_{-1} = \mathbf{0}$. The normalization condition of the cumulative distribution now is

$$\lim_{k \rightarrow \infty} P_k = \mathbf{1} \quad (3.51)$$

Following the scheme of the inversion method, in the discrete case, given a value R sampled from the uniform distribution, the probability that R falls within the interval (P_{k-1}, P_k) is

$$\mathbf{prob}\{P_{k-1} < R \leq P_k\} = \int_{P_{k-1}}^{P_k} dr = P_k - P_{k-1} = p_k = \mathbf{prob}\{X = x_k\} \quad (3.52)$$

that is, for any $R \sim U(0,1)$, we get the random variable $X = x_k$ where k is the index for which $P_{k-1} < R \leq P_k$.

Practically, X is sampled from the cumulative distribution P_k in the following steps:

- i) sampling an $R \sim U(0,1)$
- ii) find the smallest positive integer, k , such that $R \leq P_k$
- iii) return to (the required value) $X = x_k$

3.5.6.3 Sampling of a Direction Ω from an Isotropic Distribution

Consider sampling of a direction Ω from an isotropic distribution in 3-dimension. In polar co-ordinates the direction Ω is identified by $\theta \in (0, \pi)$ between Ω and the z axis and by the angle $\phi \in (-\pi, \pi)$ between the projection of Ω on the xy plane and the x axis. We can now write [42]

$$d\Omega = \sin\theta d\theta d\phi = -d\mu d\phi \quad (3.53)$$

where, $\mu = \cos\theta$. The probability distribution function of the isotropic distribution is given by

$$p(\Omega) d\Omega \equiv p(\mu, \phi) d\mu d\phi = \frac{|d\Omega|}{4\pi} = p_1(\mu) d\mu p_2(\phi) d\phi \quad (3.54)$$

where,

$$p_1(\mu) = \frac{1}{2} \quad \text{and} \quad p_2(\phi) = \frac{1}{2\pi} \quad (3.55)$$

The probability distribution function is the product of the two uniform probability distribution functions $p_1(\mu)$ and $p_2(\phi)$. If R_μ and R_ϕ are two random variable $U(0,1)$ we have

$$R_\mu = \int_{-1}^{\mu} p_1(\mu') d\mu' = \frac{\mu+1}{2} \quad \text{and} \quad R_\phi = \int_{-\pi}^{\phi} p_2(\phi) d\phi = \frac{\phi+\pi}{2\pi} \quad (3.56)$$

and solving Equation 3.56 we have

$$\mu = -1 + 2R_\mu \quad \text{and} \quad \Phi = -\pi + 2\pi R_\phi \quad (3.57)$$

Practically, the direction cosines l, m , of Ω are obtained in the following steps:

- i) sampling of two random variables $R_\mu, R_\phi \sim U(0,1)$
- ii) computation of $\mu = -1 + 2R_\mu, \Phi = -\pi + 2\pi R_\phi$
- iii) direction cosines:

$$l = \Omega \cdot i = \sin\theta \cos\Phi = \sqrt{1 - \mu^2} \cos\Phi,$$

$$m = \Omega \cdot j = \sin\theta \sin\Phi = \sqrt{1 - \mu^2} \sin\Phi = \sqrt{1 - \mu^2 - l^2},$$

$$n = \Omega \cdot k = \mu$$

3.5.6.4 Acceptance-Rejection Method

The inverse-transform and composition methods are direct methods in the sense that they deal directly with the CDF of the random variable to be generated. The acceptance-rejection method is an indirect method due to Stan Ulam and John von Neumann [45]. It can be applied when the Inverse transform method fail or turn out to be computationally inefficient. The rejection technique [46] [47] has the advantage that the sampling procedure can be carried out using only the PDF of the random variable. In the simplest form, a constant $c \geq 1$ and another density function $g(x)$ are assigned to $p(x)$ in such a way that:

$$p(x) \leq g(x) \quad (3.58)$$

for all values of x . First, a value for x is sampled from the distribution $g(x)$. Another random variable R , is then sampled on the unit interval and the value of x is accepted as a sample from $p(x)$ if:

$$R < \frac{p(x)}{cg(x)} \quad (3.59)$$

If the inequality does not hold, the value is discarded and the procedure is repeated from the beginning. There are certain properties that are desired from $g(x)$. The function should be chosen in such a way that the sampling can be performed using the inversion method (or some other efficient technique). Another important aspect is that the difference between the functions $cg(x)$ and $p(x)$ should be small, or more precisely, the ratio of the integrals:

$$\rho = \frac{\int_{-\infty}^{\infty} p(x) dx}{\int_{-\infty}^{\infty} cg(x) dx} \quad (3.60)$$

should be close to unity as possible. The ratio is called the efficiency of the algorithm. If the efficiency is low, computing time is wasted as the re-sampling loop has to be repeated over and over again before finding an acceptable value for the variable.

Sampling procedure:

- i) Sample X from $g(x)$: $X = G^{-1}(R_1)$
- ii) Test: $R_2 \cdot cg(X) \leq p(x)$

If true accept X .

If false reject X and try again.

3.5.6.5 Exponential Distribution

A system for which the probability of future events in time or space depends only on the present state of the system and not on the way this state was reached i.e. the future of the system does not depend on its past history is called Markovian system. A Markovian system is homogeneous when the events occur with constant probability density $1/\lambda$. Starting from a given point - in time or space – the interval distribution for the occurrence of the next event is exponential with decay constant $1/\lambda$.

A random variable $X \in (0, \infty)$ is said to be exponentially distributed if its cumulative distribution function and its probability distribution function are respectively [42]

$$P_X(X) = 1 - e^{-x/\lambda} \quad \text{and} \quad p_X(X) = \frac{1}{\lambda} e^{-x/\lambda} \quad \text{for} \quad x \geq 0$$

$$= 0 \qquad = 0 \qquad \textit{otherwise} \qquad (3.61)$$

Substituting into Equation 3.46 and solving for X gives

$$X = -\lambda \ln(1 - R)$$

Since the random variable $1 - R$ is distributed as R we can write

$$X = -\lambda \ln R \qquad (3.62)$$

The algorithm for the generation of an exponential random variable is

- i) Generate $R \sim U(0,1)$
- ii) Return $X \leftarrow -\lambda \ln R$ as a random variable from $\text{exp}(1/\lambda)$

3.5.6.6 Multinomial Distribution

Consider a random game such as throwing a dice and neutron nucleus interaction (scattering, absorption, fission, etc) once it is known that the interaction has occurred. Such a random game can have only n possible values, the probability of $k - th$ one being p_k . The game is simulated by first dividing the interval $(0,1)$ in n successive subintervals of amplitudes p_1, p_2, \dots, p_n and then performing a large number of trials in each of which a random variable $R \sim U(0,1)$ is thrown on the interval $(0,1)$. Each time a point falls on the $k - th$ subinterval, we say $ak - th$ event out of the n possible ones has occurred. The probability of such event obeys the multinomial distribution.

3.5.7 Variance Reduction

3.5.7.1 Tally Variance

Two basic principles of statistics are used to determine the accuracy of calculation. They are the laws of large numbers and central limit theory [48]. When we run a random-walk simulation, the i th history contributes a score x_i to the tally. If the particle (or its daughters) never reaches the tally region, then $x_i=0$, whereas, if reaches tally without interaction, the score x_i generally is very large. The probability any history will contribute a score between x and $x + dx$ is denoted by a probability distribution function $p(x)dx$. In MCNP simulation, we seek the mean score (or expected value) of x , given by

$$\langle x \rangle = \int x p(x) dx \quad (3.63)$$

Unfortunately, we do not know $p(x)$. Instead, we estimate $\langle x \rangle$ by the mean \bar{x} of the scores of N particles, i.e.

$$\bar{x} = \frac{1}{N} \sum_{i=1}^N x_i \quad (3.64)$$

As $N \rightarrow \infty$, the law of large numbers guarantees that $\bar{x} \rightarrow \langle x \rangle$, provided $\langle x \rangle$ is finite.

The variation in the different scores x_i is measured by the standard deviation of the population (histories), which for large N

$$S^2 = \frac{1}{N} \sum_{i=1}^N (x_i - \bar{x})^2 \approx \overline{x^2} - \bar{x}^2 \quad (3.65)$$

where

$$\overline{x^2} = \frac{1}{N} \sum_{i=1}^N x_i^2 \quad (3.66)$$

The estimated variance of the mean \bar{X} is then

$$S_{\bar{x}}^2 = \frac{1}{N} S^2 \quad (3.67)$$

The central limit theory states that if we repeated the simulation a large number of times (each with N histories) the variation of the means \bar{x} from each simulation will be distributed normally about the true mean $\langle x \rangle$ and have a variance $S_{\bar{x}}^2$. It is this uncertainty or variance we are trying to reduce in MCNP simulations, i.e. for a fixed number of particles, we seek an estimate \bar{x} which has the least uncertainty or minimum $S_{\bar{x}}$.

3.5.7.2 Relative Error and Figure of Merit

In any variance reduction method, we change the simulation and hence change the underlying distribution $p(x)$ so that it produces fewer zero-score histories and becomes more concentrated about its mean $\langle x \rangle$. By making $p(x)$ more concentrated about its mean (which remains the same as the analog PDF), the variance of the mean $S_{\bar{x}}^2$ will be less than that of the analog PDF, i.e., the estimate of the mean will be more precise.

For each tally, the MCNP calculates several other statistics apart from sample mean \bar{x} . One of such statistics and the most important is the relative error R (tells us the fraction of the error compared to the value) defined as

$$R = S_{\bar{x}}/\bar{x} \quad (3.68)$$

It can be seen that we want to make R as small as possible. For a reliable tally confidence interval, R should be less than 0.1. Combining Equations 3.67 and 3.68, we have

$$R \sim 1/\sqrt{N} \quad (3.69)$$

Another important statistics generated by MCNP is the figure of merit (FOM) defined as

$$FOM = \frac{1}{R^2 T} \quad (3.70)$$

where T is the simulation time or CPU time, which is proportional to N the number of histories run. We can see in Equation 3.70 that FOM is independent of N . For different simulations of the same problem, the simulation with the largest FOM is preferred since it requires the least time or produces the smallest error.

3.5.8 Variance Reduction Techniques in Monte Carlo

Methods for reducing the variance in the estimated solution to reduce the computational time for Monte Carlo simulation is called variance reduction technique. Alternative to large number of particles and long computation is to, reduce the variance S^2 by more efficient random walk designed to reduce the spread of the tally results about the mean. There will be some histories which will not contribute to the tally because of absorption or motion in the wrong direction. The computer time spent on these zero contribution histories can be reduced by implicit capture or population control of low weight and out of range particles.

3.5.8.1 Implicit Capture

Particles which are tracked but are absorbed before they reach the tally surface represent wasted computing effort. This Analog capture is replaced with implicit capture. In Analog simulation the particle is killed at collision site, with a probability σ_a/σ_t . However in Implicit capture, the particle is allowed to continue on its

trajectory as if no interaction had occurred with the particle but the particles weight w_i is reduced by

$$w_i(\text{new}) = w_i(1 - \sigma_a/\sigma_t) \quad (3.71)$$

By so doing, no particles are lost due to absorption, but absorption effects are properly for.

3.5.8.2 Population Control

Population control makes sure that there are enough particles in the interesting region. These are methods used by the MCNP to boost the particle population in the region of interest at the expense of other region. They include:

3.5.8.2.1 Geometry Splitting by Cell Importance

To track neutron in the reactor core, it is divided into several thicknesses of approximately one mean free path and have increasing importance within each thickness. The neutron splits into two at each surface within the material and each new neutron has half the weight of original neutron. The paths of the separate neutrons are followed and their scores are added to that of the original neutron. Here the weight of the neutron is conserved and this way there are more different scores in the interesting region or tally side thereby generating lower variance in the region. However, the calculation time is higher. This technique is used in the region of interest.

3.5.8.2.2 Russian Roulette

In Russian roulette, neutrons with low weight are terminated, below a threshold w_{rr} with a known probability because they will not contribute a lot anymore. There is a probability r that the particle terminates; if the particle survives the weight will become:

$$w_i = \frac{w_i}{r} \quad (3.72)$$

Defining r by a survival weight w_s we have:

$$r = \frac{w_i}{w_s} \quad (3.73)$$

Combining Equations 3.72 and 3.73 the weight of the surviving particle is w_s . By setting the threshold and survival weight different in the different areas, the number of neutrons can be controlled. This way the result is unbiased, the calculation time will decrease, but the variance will increase. This technique is therefore used in less interesting part of the core. Splitting and Russian roulette methods can also used with particle energy.

3.5.9 Monte Carlo Simulations

The nature of Monte Carlo simulation is shown in Figure 3.2. A source particle is introduced. A source particle is introduced with phase space coordinates (\mathbf{r}, \mathbf{v}) which may be sampled randomly according to PDFs representing the spatial, directional and energy distributions of source particles in the specific physical problem considered.

In the transport portion of the analysis, the distance to the particle's next collision is sampled randomly from the PDF which describes the random-walk of particles in a background medium. Geometric information describing the material and region boundaries, usually in the form of first or second degree surface equations, is then

analyzed to determine whether the sampled distance to collision is less than distance to a boundary. If less, the collision did not occur, and the collision analysis proceeds by sampling the particle's exit energy and direction from the appropriate PDFs. Production of secondary particles such as (n, γ) or (n, f) reactions is also determined by sampling from the appropriate PDFs. The Monte Carlo analysis alternates between transport and collision analysis until the particle and its progeny have been killed by absorption or leakage from the system. Another source particle is then introduced and followed throughout its history, and so on. Typical problems can involve the processing of up to several million particle histories to achieve accurate scores.

For reactor calculations, iterative procedure is used to obtain the eigenvalue [49] [50] shown in Figure 3.3. An assumed spatial distribution of fission site is used to perform the initial iteration (generation 0). New fission sites recorded during the random-walk analysis are then used to provide estimates of both the eigenvalue and the source distribution to be used for the next generation. Additional generations are then analyzed as needed to converge the eigen function.

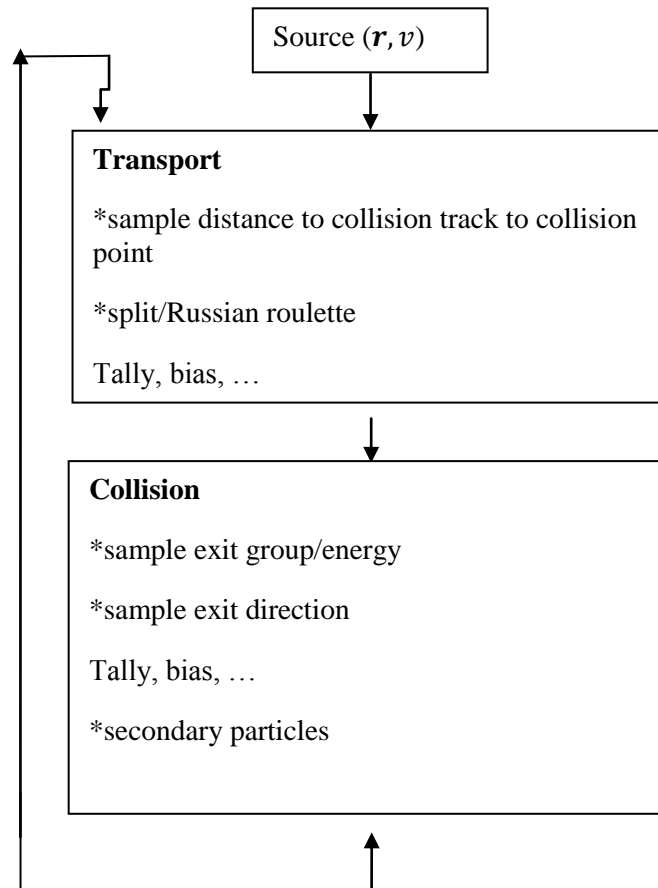


Figure 3.2 Monte Carlo random works for single particle

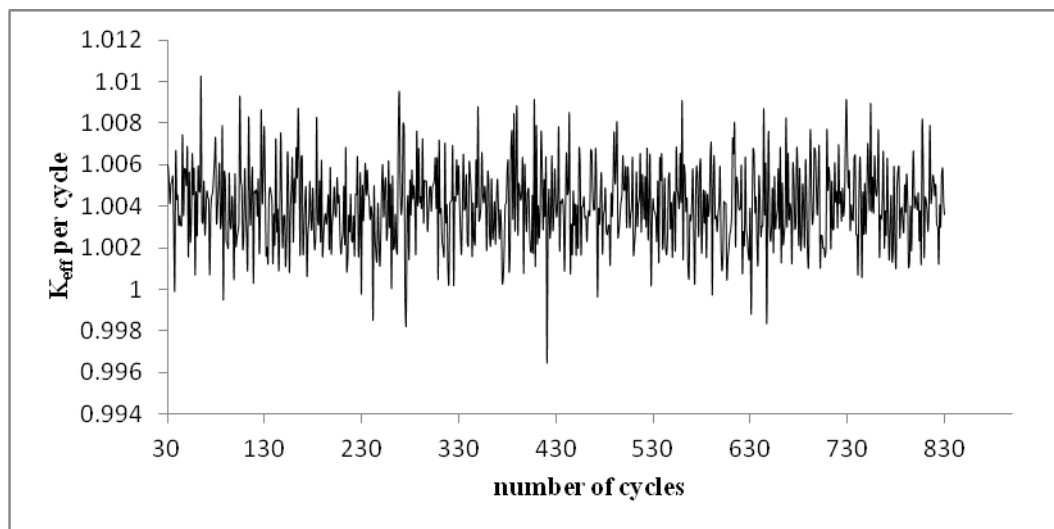


Figure 3.3 Power iteration for Monte Carlo criticality calculation of the mean value of k_{eff}

For each trial, the neutron typically goes through the following steps:

- i) Determination of the source parameters r, Ω, E .

We start with a fission neutron source so that the direction Ω and the energy E may be sampled from an isotropic distribution as in Equation 3.57 and from the Watt spectrum, respectively. For multiplying systems such as nuclear reactors, the iterated fission source methodology which closely follows the k – *eigenvalue* method is adopted. The first iteration starts by assuming a suitably large number l_1 of fission locations distributed throughout the reactor core. A guess of the multiplication factor of the system say k_1 is made and we assume that the mean number of neutron released in fission, instead of having the true value \bar{v} is $\bar{v}_1 = \bar{v}/k_1$. Then the Monte Carlo simulation is carried out: the $\bar{v}_1 l_1$ fission neutrons emitted is followed one after the other and the l_2 locations of the fissions neutrons they induce are recorded. The l_2 locations are better distributed within the core than l_1 since they are due to neutrons which follow real physics processes. In order to proceed to the second iteration we update k_1 and \bar{v}_1 . This is done as the reactor were critical by requiring that at each iteration the number of fission neutrons should remain equal to the initial value $\bar{v}_1 l_1$. Generally, if l_i is the locations at the i – *th* iteration (by following the fates of the neutrons of the preceding generation), then we have

$$\bar{v}_i = \bar{v}/k_i \quad , \bar{v}_i l_i = \bar{v}_1 l_1$$

from which

$$k_i = \frac{l_i}{l_1} \cdot k_1 \quad , \bar{v}_i = \frac{\bar{v}_i}{k_i} = \bar{v}_1 \cdot \frac{l_i}{l_1} \quad (3.74)$$

- ii) Determination of the next collision point.

From the knowledge of the neutron position r and energy E the code looks up in its files the region, say Z_1 , where the neutron is and the total macroscopic cross section Σ_{T1} pertaining to that region. The next collision point is then sampled from the exponential distribution on the straight line starting at r in the direction Ω . If Z_1 were infinite in extent the neutron would travel a distance given by the Equation 3.62 namely,

$$X = -\frac{1}{\Sigma_{T1}} \ln R \quad (3.75)$$

where, $R \sim U(0,1)$ and $\lambda = \frac{1}{\Sigma_T}$. If X is less than the geometric chord X_1 from r to the Z_1 boundary along Ω , the collision actually occurs at the point $r + \lambda\Omega$ which is within Z_1 . If $X > X_1$ the neutron, going along Ω , enters the next region, say Z_2 , whose total cross section at the energy E is E_2 . At the point P_{12} on the boundary between Z_1 and Z_2 the residual way is

$$X = -\frac{1}{\Sigma_{T2}} (X_1 \Sigma_{T1} + \ln R) \quad (3.76)$$

and everything happens as X were the distance to be traveled from the point P_{12} within Z_2 . More formally if Z_1, Z_2, \dots are successive regions along Ω and $\tau_k = \Sigma_k X_k$, $k = 1, 2, \dots$ are the corresponding optical lengths (macroscopic cross section times geometrical chord), the neutron will collide in that region Z_i for which

$$\sum_{k=1}^{i-1} \tau_k < -\ln R \leq \sum_{k=1}^i \tau_k \quad (3.77)$$

where by definition, the first sum vanishes if $i = 1$.

- iii) Determination of the kind of collision:

Assume that the total cross section Σ_i of the i – th region where the collision occurs is made up of n components namely $\Sigma_{i1}, \Sigma_{i2}, \dots, \Sigma_{in}$ relating to the various nuclides in the medium and to the various reactions. Then the particular k – th reaction occurs with discrete probability $p_k = \Sigma_{ik}/\Sigma_i$ and the selection of the collision as mentioned in section 2.10.6

iv) Parameters of the emerging neutron

Assume that at point r in zone Z a neutron of energy E' and direction Ω' has an interaction with a given nucleus of mass A . If the collision is an absorption, the neutron disappears and we start a new trial that is another fission neutron among the $\bar{\nu}_i$ of the present i – th generation, begins to be processed. If the collision is fission the point r is recorded as a fission location for the $(i + 1)$ – th generation to be used as in 1 above and again, another trial is started. Finally if the collision is elastic scattering the code looks up the angular distribution of the involved nucleus at the neutron energy E' in its files and samples a scattering angle ϑ_0 . Knowledge of this angle allows computing the energy of the scattered neutron from the kinematics of the elastic collision. To obtain the new direction we have still to sample the azimuthal angle φ around Ω' from the uniform distribution in $(0, 2\pi)$. By so doing the new direction has been found with respect to the previous direction Ω' so that we have to reorient the axes to get the new direction Ω with respect to the coordinate system.

As illustrated in Figure 3.2, Monte Carlo code is basically a collection of random decision points shown in Figure 3.4, with relatively simple arithmetic in between. The physics of a problem is contained in the PDFs used for the random sampling of the

collision kernel and the transport kernel, problem geometry is involved in the surface equations utilized for particle tracking in the transport kernel and results are obtained by tallying the quantities of interest.

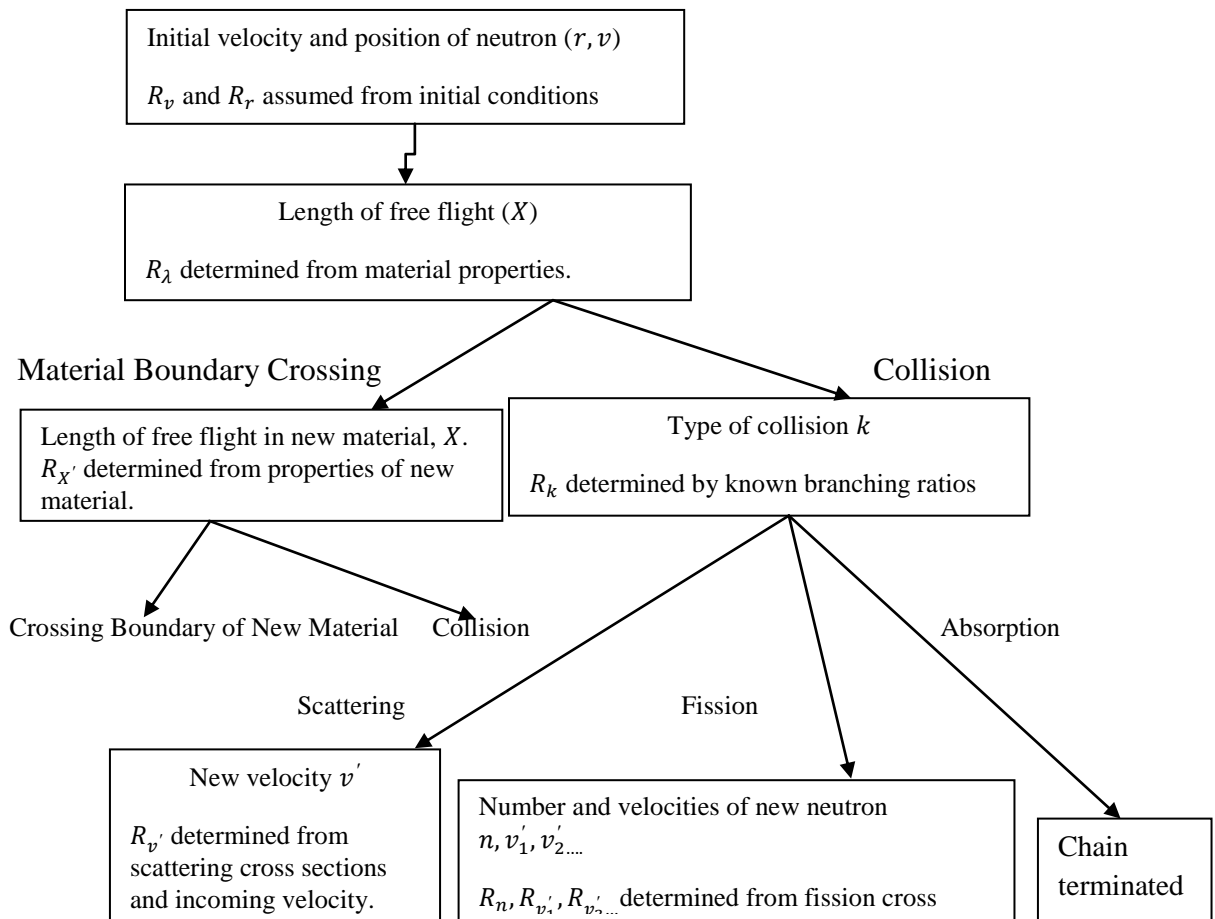


Figure 3.4 Decision points in generating the history of a single neutron in a Monte Carlo calculation

3.5.10 Monte Carlo Estimates

Now the particles are simulated and behave the same as the physical particles and it is time to extract results from the simulation. The quantities that need to be measured have to be estimated by estimators. To estimate the flux, we may need three different

estimators namely [44]: collision estimator, an absorption estimator and a track length estimator.

An estimator is a specific function of the random samples, of a random variable, that statistically represents a true unknown mean. If x is a random variable, with an associated distribution and an unknown mean, then the function $X(x_1, x_2, x_3, \dots, x_N)$ is an estimator of the unknown mean. The set $\{x_1, x_2, x_3, \dots, x_N\}$ consists of N independent random samples selected from the probability density distribution of x . A good estimator should be unbiased, consistent, and efficient. An estimator is unbiased if its expectation value equals the true mean,

$$\langle x \rangle = \bar{x} \quad (3.78)$$

for all X . An estimator is consistent if it approaches, in a statistical sense, the true mean, as N gets larger. An efficient estimator is the one, among a group of unbiased estimators, which produces the minimum variance for a Mathematical expression for each of the three estimators of k_{eff} .

3.5.10.1 Collision Estimator

The collision estimate for k_{eff} for any active cycle is given by:

$$k_{eff}^c = \frac{1}{N} \sum_i w_i \left[\frac{\sum_k f_k \bar{\nu}_k \sigma_{fk}}{\sum_k f_k \sigma_{fk}} \right] \quad (3.79)$$

where i is summed over all collisions in a cycle where fission is possible;

k is summed over all nuclides of the material involved in the i th collision;

σ_{T_k} is the total microscopic fission cross section;

σ_{fk} is the microscopic fission cross section;

$\bar{\nu}_k$ is the average number of prompt or total neutrons produced per fission by the collision nuclide at the incident energy;

f_k is the atomic fraction for nuclide k;

N is the nominal source size for a cycle; and

w_i is the weight of particle entering collision.

Because w_i represents the number of neutrons entering the i th collision:

$$w_i \left[\frac{\sum_k f_k \bar{\nu}_k \sigma_{fk}}{\sum_k f_k \sigma_{fk}} \right] \quad (3.80)$$

is the expected number of neutrons to be produced from all fission processes in the collision. Thus k_{eff} is the mean number of fission neutrons produced per cycle.

3.5.10.2 Absorption Estimator

The absorption estimator for k_{eff} for any active cycle is made when a neutron interacts with a fissionable nuclide. For implicit capture which is a default in MCNP5 it is given by:

$$k_{eff}^a = \frac{1}{N} \sum_i w_i \bar{\nu}_k \frac{\sigma_{fk}}{\sigma_{c_k} + \sigma_{fk}} \quad (3.81)$$

where i is summed over all collisions in which fission is possible and

$$w'_i = w_i (\sigma_{c_k} + \sigma_{fk} / \sigma_{fk}) \quad (3.82)$$

is the weight absorbed in the implicit capture. The difference between the implicit absorption estimator and the collision estimator is that only the nuclide involved in the collision is used for the absorption k_{eff} estimate rather than an average of all nuclides in the material for the collision k_{eff} estimator. The absorption estimate also differs from the collision estimate in that the collision estimate is based upon the expected value at

each collision, whereas the absorption estimate is based upon the events actually sampled at a collision. Thus all collisions will contribute to the collision estimate k_{eff}^c of and by the probability of fission in the material. Contribution to the absorption estimate will only be made for the nuclide sampled.

3.5.10.3 Track Length Estimators

The track length estimator of k_{eff} is accumulated every time the neutron traverses a distance d in a fissionable material cell:

$$k_{eff}^l = \frac{1}{N} \sum_i w_i N \lambda \sum_k f_k \bar{v}_k \sigma_{fk} \quad (3.83)$$

Where i is summed over all neutron trajectories,

N is the atomic density in the cell, and

λ is the trajectory track length from the last event.

Because $N \lambda \sum_k f_k \bar{v}_k \sigma_{fk}$ is the expected number of fission neutrons produced along trajectory d , k_{eff}^l is a third estimate of the mean number of fission neutrons produced in a cycle per nominal fission source neutron. The track length estimator tends to display the lowest variance for optically thin fuel cells (e.g. plates) and fast systems where large cross-section variations because of resonances may cause high variances in the other two estimators.

The methodology adopted for performing this work using the versatile MCNP particle transport code is presented next in Chapter 4.

3.6 Burnup

The initial composition of a fuel element will depend on the source of the fuel. For reactors operating on the uranium cycle, fuel developed directly from natural uranium will contain a mixture of U-234, U-235 and U-238, with the fissile U-235 content varying from 0.72% (for natural uranium) to more than 90%, depending on the enrichment. Recycled fuel from reprocessing plants will also contain the various isotopes produced in the transmutation-decay process of uranium [51]. Presently, a typical MNSR uses enriched uranium fuel of about 90 % of U235.

During the operation of a nuclear reactor a number of changes occur in the composition of the fuel. Various fuel nuclei are transmuted by neutron capture and subsequent decay. For a uranium-fueled reactor, this process produces a variety of transuranic elements in the actinide series of the periodic table. For a thorium fueled reactor, a number of uranium isotopes are produced. The fission event destroys a fissile nucleus, of course, and in the process produces two intermediate mass fission products. The fission products tend to be neutron-rich and subsequently decay by beta or neutron emission (usually accompanied by gamma emission) and undergo neutron capture to be transmuted into a heavier isotope, which itself undergoes radioactive decay and neutron transmutation, and so on. The fissile nuclei also undergo neutron transmutation via radiative capture followed by decay or further transmutation [51]. Figure 3.5 shows a simplified diagram of transmutation of nuclei in the uranium series. Actinides of interest are marked with thick borders.

The buildup of actinides in the U-238 transmutation-decay process introduces a fuel reactivity penalty because some of actinides act primarily as parasitic absorbers. While Pu-239 and Pu-241 are fissionable in a thermal reactor, and Pu-240 transmutes into Pu-241(fissile), Pu-242 transmutes into Pu-243 with a rather small cross section and thus build up in time. Pu-243 decays immediately towards Am-243(non-fissile). Pu-242 is effectively a parasitic absorber. The Am²⁴³ also accumulates and acts primarily as a parasitic absorber. Whereas the Am-243, which is produced by the decay of Pu-243, can be separated readily, it is quite impossible to separate the different plutonium isotopes from each other by chemical means, so the negative Pu-242 reactivity effect is exacerbated if the plutonium is recycled with uranium [51].

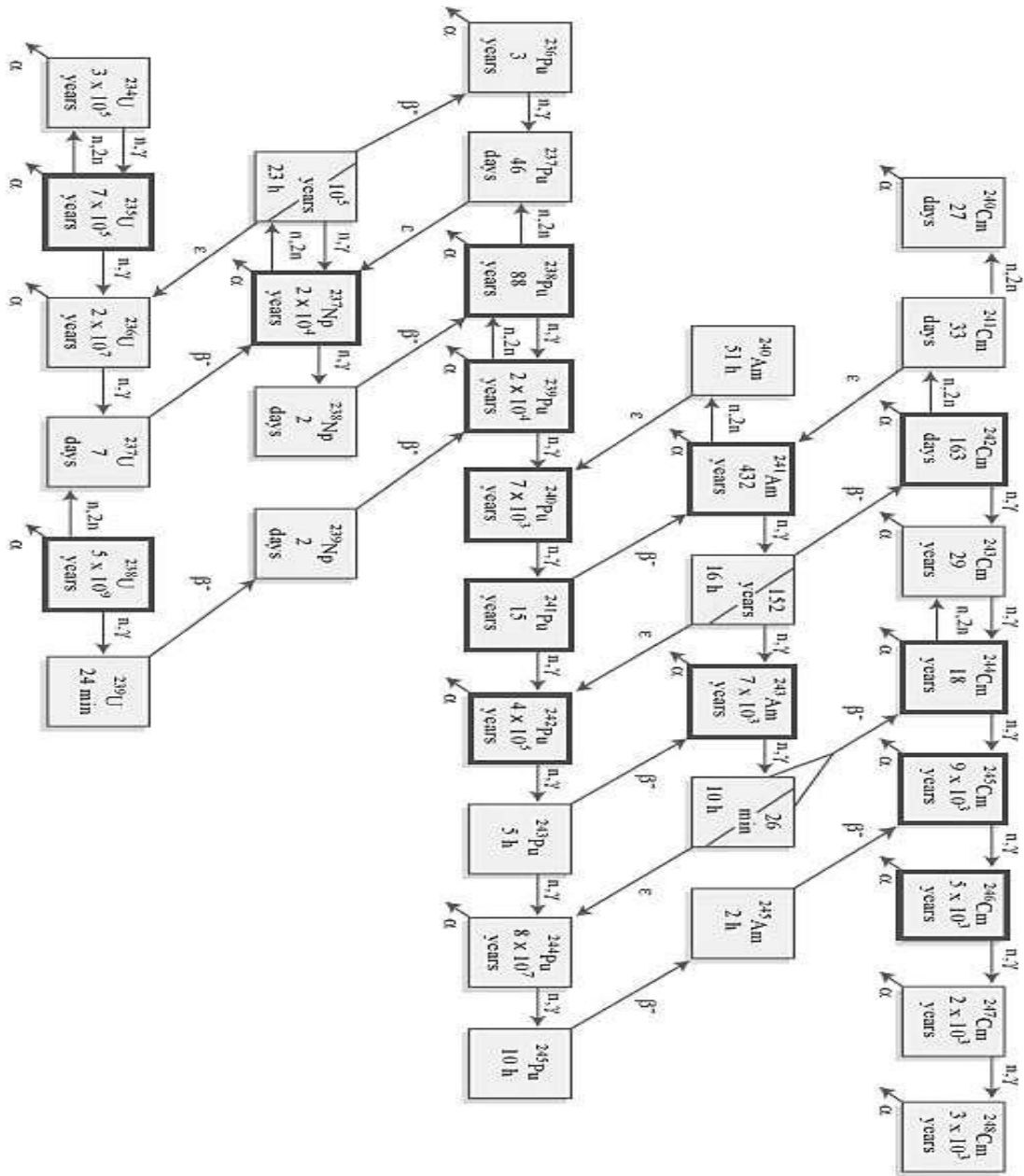


Figure 3.5 The most important actinide nuclides and their relations, via α -decay, β -decay and neutron capture reactions

In nuclear power technology, burn-up is a measure of the number of fuel atoms that underwent fission. It is normally quoted in megawatt–days per metric ton of heavy metal (MWd/THM), or its equivalent gigawatt–days/T (GWd/tHM). The unit GWd/tHM is the (average) thermal output, multiplied by the time of operation, and divided by the mass of heavy involved. This gives a rough measure of the number of nuclear fission events that have taken place within the fuel.

The actual fuel may be uranium, plutonium, or a mixture of these or of either or both of these with thorium. This fuel content is often referred to as the heavy metal (the only nuclei which can fission to produce energy) to distinguish it from other elements present in the fuel, such as oxygen of an oxide fuel or those used for cladding. The heavy metal is typically present as either metal or oxide, but other compounds such as carbides or other salts are possible. In a power station, high fuel burn-up is desirable for:

- ❖ Reducing downtime for refueling
- ❖ Reducing the number of fresh nuclear fuel elements required and spent nuclear fuel elements generated while producing a given amount of energy
- ❖ Reducing the potential for diversion of plutonium from spent fuel for use in nuclear weapons, for short BU, the plutonium produced is essentially Pu-239 which highly fissile. Alpha decay of this isotope also leads to the formation of U 235.

It is also desirable that burn-up should be as uniform as possible both within individual fuel elements and from one element to another within a fuel charge [52]. In reactors with online refueling (as in the case of CANDU reactor), fuel elements can be

repositioned during operation to help achieve this. In reactors without this facility, fine positioning of control rods to balance reactivity within the core, and repositioning of remaining fuel during shutdowns in which only part of the fuel charge is replaced may be used, this type of fuel management is incorporated in this work with four fractionating cycles for the study of mono-recycling of the americium.

3.6.1 BURNUP ANALYSIS

One of the most important and difficult problems in reactor design is the prediction of the properties of a reactor core throughout its life. How these properties change in time must be known to ensure that the reactor will operate safely throughout the lifetime of the core. The changing reactor properties also determine the length of time that a given reactor core will remain critical, producing power at the desired level. This is an important practical consideration also for waste and spent-fuel characterization, as well as natural resource consumption. It obviously makes little sense for a public utility to purchase a reactor that must be shut down every month for refueling, if it can obtain one that needs to be refueled every 2 years, except for power reactors that can be fueled online such as the CANDU system. However, it makes equally little sense to buy a core that has fuel enough to remain critical for 20 years when radiation damage is known to compromise the fuel elements in 3 or 4 years [24].

In a typical UO_x fueled thermal reactor, as energy is removed from a reactor, the fuel composition changes as a result of loss of fissionable material due to fission, buildup and decay of fission products, and transmutation of other reactor materials due to neutron capture. These composition changes occur over a relatively long period of

time [53]. All fission products absorb neutrons to some extent, so they are known as reactor poisons. Most fission product poisons simply build up slowly as the fuel burns up and are accounted for as a long-term reactivity. The neutron absorbing fission products such as Xe-135 have particular operational importance. Their concentrations can change quickly, producing major changes in neutron absorption on a relatively short time scale. Each arises from the decay of a precursor fission product, which controls their production rate, but, because they have large absorption cross-sections, their removal changes quickly with changes in flux [54]. Notwithstanding, U-235 in a UOX fuel fissions into other fission products and minor actinides while the fertile isotopes U-238 undergoes neutron capture to build up fissile isotope Pu-239. All these phenomenon and transmutations tend to modify the core parameters during the core-lifetime of the fuel.

Computations of changing reactor properties are known as burnup calculations or lifetime calculations [24]. Reactor Burnup Systems (REBUS) is a code that is used for such calculations.

3.6.2 DESCRIPTION OF REBUS

The REBUS-PC code has evolved away from its roots as a design tool for fast reactors to encompass the needs of thermal reactor design and analysis. Since its conception in the 1960's, REBUS (the REactor BUrnup System) has always been a general-purpose tool.

REBUS designed for the analysis of research reactor fuel cycles. Optionally, reprocessing may be included in the specification of the external fuel cycle and

discharged fuel may be recycled back into the reactor. For non-equilibrium cases, the initial composition of the reactor core may be explicitly specified or the core may be loaded from external feeds and discharged fuel may be recycled back into the reactor as in equilibrium problems.

Four types of search procedures may be carried out in order to satisfy user-supplied constraints:

- 1) adjustment of the reactor burn cycle time to achieve a specified discharge burnup,
- 2) adjustment of the fresh fuel enrichment to achieve a specified multiplication constant at a specified point during the burn cycle,
- 3) adjustment of the control poison density to maintain a specified value of the multiplication constant throughout the reactor burn cycle, and 4) adjustment of the reactor burn cycle time to achieve a specified value of the multiplication constant at the end of the burn step.

REBUS-PC will handle both equilibrium and non-equilibrium problems using a number of different core geometries including triangular and hexagonal mesh. The neutronics solution may be obtained using finite difference or nodal diffusion-theory methods. Other features include: fully automatic restart capability, no restrictions on number of neutron energy groups, and general external cycle with no restrictions on number of external feeds, reprocessing plants, etc. Fuel management is completely general for non-equilibrium problems.

Microscopic cross sections are permitted to vary as a function of the atom density of various reference isotopes in the problem as appropriate for thermal reactor systems. The previous capability where neutron capture and fission processes were fitted to low-order polynomials as functions of burnup is retained. In addition, the user now may select cubic spline interpolation for (n,gamma), (n,fission), (n,alpha), (n,p), (n,d), and (n,t) reactions as functions of burnup. The user may specify control rod positions at each time node in the problem. Output edits have been extensively revised and better organized for use in a PC environment. A number of ASCII format datasets containing various types of summary results are available for use in tailoring reports with the aid of auxiliary PC software such as spreadsheet or word processor programs.

3.7 Analyses of MNSR Thermal Hydraulics

3.7.1 Heat transfer process of MNSR

The thermal hydraulic design of the reactor is closely related to the neutronic calculations and the structural design [2]. The geometrical dimensions of the fuel element, fuel element temperatures, coolant pressure, temperatures and velocities are analytically shortened to satisfy the requirements of reactor safety during all operational states.

The core of the MNSR is immersed into the lower part of the reactor tank, which is filled with coolant water [55]. The tank is immersed in a quite large water pool. The heat generated from the nuclear fuel is carried out of the core by coolant through heat conduction, heat convection and heat transport.

The heat generated by the nuclear fuel is first transferred to the outer surface of cladding through the heat conduction of fuel pellets and cladding, and then the heat is transferred to the coolant water by the natural convection. The density of the heated water decreases, and the buoyancy force causes coolant water to flow up, thus the heat is carried away from the reactor, which is called the transport process.

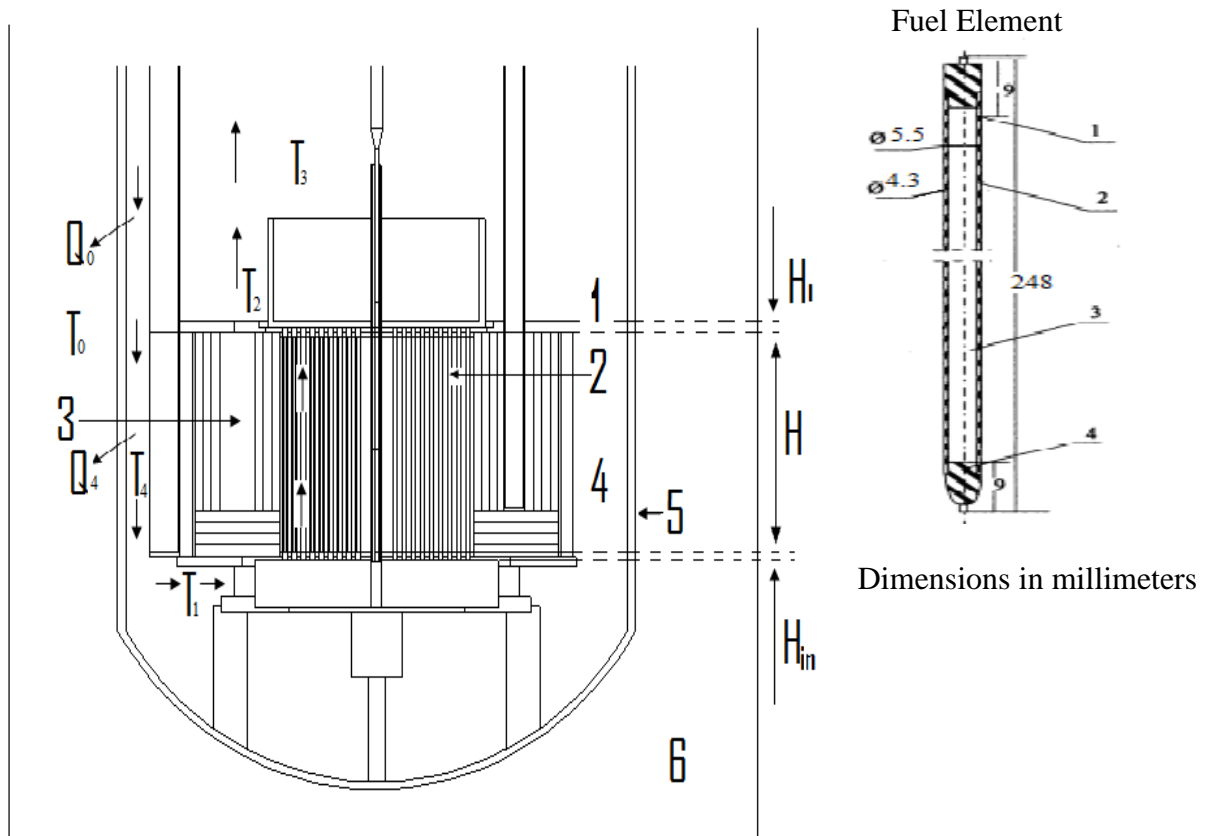


Figure 3.6: Schematics of Reactor Core [56]

Core	Fuel element
1 – Elevation line of core outlet	1. Top end plug
2 – Fuel element	2. Cladding
3 – Beryllium reflector	3. Meat
4 – Downcomer	4. Lower end plug

5 – Reactor vessel

6 – Pool water

T_1 – Inlet temperature

T_2 – Outlet temperature

T_3 – Temperature above Core

T_4 – Temperature at downcomer region

T_o – Pool temperature

The core region of GHARR-1 is located 4.7 m under water close to the bottom of a watertight reactor vessel. The quantity of water is 1.5 m³ in the vessel, which serves the purpose of radiation shielding, moderation and as primary heat transfer medium. In addition, heat can be extracted from the water in the vessel by means of a water-cooling coil located near the top of the vessel. The water-filled reactor vessel is in turn immersed in a water-filled pool of 30 m³. Cold water is drawn through the inlet orifice by natural convection. The water flows past the hot fuel elements and comes out through the core outlet orifice. The hot water rises to mix with the large volume of water in the reactor vessel and to the cooling coil. Heat passes through the walls of the container to the pool water. A diagrammatic representation of the heat transfer mechanism is represented in Figure 3.6.

The core inlet flow orifice impedes the natural circulation of water through the core. Its area is fixed during assembly of the reactor and it is deliberately chosen such that the highest power achieved during the design basis self-limiting power excursion can cause no damage to the core or present any hazard to staff about the reactor.

The GHARR-1 reactor has a small core. It can be shown that the coolant flow in the core is at the transient phase from laminar flow to turbulent flow. The flow transition will occur when there is an increase in power. The closer to the upper part of elements, the stronger the turbulence becomes. The buoyancy force in natural circulation must overcome the friction. Calculations show that the friction resistance is small, about 10% of the total resistance. Meanwhile, the inlet resistance is about 70% of the resistance and thus has a great effect on the state of flow. An appropriate choice for the inlet flow orifice is a very important factor in the thermal-hydraulic design. As inlet orifice gets smaller, the flow velocity and in turn, the turbulence in the core will increase. As a result, the heat transfer from fuel element to coolant will be improved. However, a smaller inlet orifice will cause an increase in resistance and a decrease in flow rate resulting in a rapid increase of temperature. An appropriate temperature rise is an essential condition.

The water in the reactor is not pressurized and it relies upon natural convection. The problems of de-pressurization or coolant flow pump failure are not posed. A water-cooled coil of limited heat removal capacity removes the thermal energy generated in the core eventually. Due to the fact that the reactor possesses limited excess reactivity and reactivity feedback characteristics, any significant deterioration in heat removal capability will eventually result in an automatic decrease in reactor power to match up with the new heat removal capacity.

The temperature in an operating reactor varies from point to point within the system. As a consequence, there is always one fuel rod (usually one near the centre of the reactor) that at some point along its length is hotter than all the rest. This maximum

fuel temperature is determined by the power level of the reactor, the design of the coolant system, and the nature of the fuel [24]. One major design of a reactor coolant system is to provide for the removal of heat produced at the desired power level while ensuring that the maximum fuel temperature is always below this predetermined value. This in turn ensures good safety margin. Under sub-cooled flow boiling conditions, the boiling crisis is often called departure from nucleate boiling (DNB) and the heat flux at which the boiling crisis occurs is named the critical heat flux (CHF) [57]. In general, thermal performance improvements are highly desirable and it is therefore needed to predict CHF accurately at the earliest stages of a new product design. In the case of a nuclear reactor core, CHF margin gain (e.g. using improved fuel assembly design) can allow power uprate and enhanced operating flexibility [58]. Most metal-finishing operation score tiny grooves on the surface, but they also typically involve some chattering or bouncing action, which hammers small holes into the surface. When a surface is wetted, liquid is prevented by surface tension from entering these holes, so small gas or vapour pockets are formed. These little pockets are sites at which bubble nucleation occurs [24]. The ONB is not a limiting criterion in the design of a fuel element. However, it is a heat transfer regime which should be identified for proper hydraulic and heat transfer considerations, i.e., single-phase flow versus two-phase flow.

For reactor design purposes, acceptable data on burnout heat flux are needed since departure from nucleate boiling (DNB) is potentially a limiting design constraint. Optimization of core cooling against other neutronic, economic, and materials constraints can best be accomplished by judicious use of standard, experimentally-deduced DNB correlations [59]. The parameter most used to evaluate margin to failure

by boiling crisis is the critical heat flux ratio (CHFR), or departure from nucleate boiling ratio (DNBR). This is the ratio of critical heat flux calculated by the correlation to the most limiting heat flux condition in the reactor [53]

The heat generated from the nuclear fuel is carried out of the core by coolant through heat conduction, heat convection and heat transport. The heat generated by the nuclear fuel is first transferred to the outer surface of cladding through the heat conduction of fuel pellets and cladding, and then the heat is transferred to the coolant water by the natural convection. The density of the heated water decreases, and the buoyancy force causes coolant water to flow up, thus the heat is carried away from the reactor, which is called the transport process [60]. The progression is depicted in Figure 3.7.

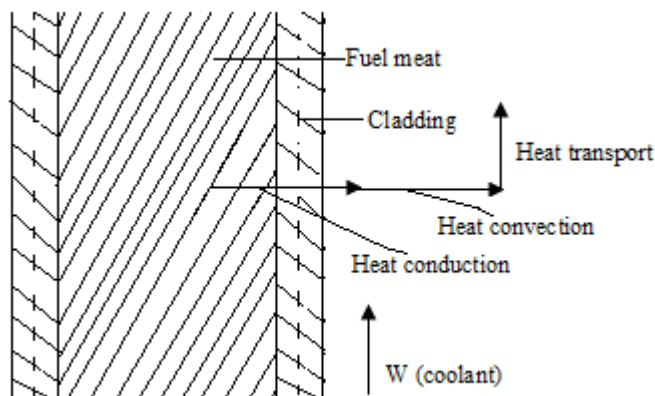


Figure 3.7: Heat transfer and transport process

In the early stages of the reactor start-up, the water temperature difference between the upper part of the tank and the pool is not large; the heat transferred is little, so that the heat released from the fuel elements cannot be all transported out. Therefore the water temperature in the tank increases continuously, the natural circulation is

intensified and the flow velocity of the water in the core increases accordingly. So the heat transferred to the pool water increases continuously. After some time a steady natural circulations can be established to a large extent.

After this, the water flow and heat transport in reactor are steady state conditions. The time of reactor startup is usually several hours, during which the heat transport and flow in reactor are the transient process, and the thermal-hydraulic parameters are under transient variation. The purpose of transient calculation is to predict fuel element temperature variation with time at reactor inlet and outlet, predict fuel element temperature and the relation between reactor power and inlet – outlet temperature difference.

3.7.2 Thermal – Hydraulic Characteristics of MNSR

Characteristics of MNSR considered for thermal-hydraulics [2]:

- i. Low linear power density of fuel element: about 3.8 W/cm, close to that of powers at the period of residual heat removal.
- ii. U-Al alloy is adopted as fuel meat for the highly enriched fuel, but a UO₂ is proposed for the expected low enriched fuel.
- iii. Natural convection is adopted for cooling. The reactor core is immersed in a quite large reactor tank, in which the water possesses a considerable heat capacity. The natural circulation cooling of MNSR possesses a very good inherent safety. It is also economical since there is no pumping device which might in turn need power to operate.

3.7.3 Heat Transfer Calculations of the Steady State

3.7.3.1 Heat conduction in fuel pellets

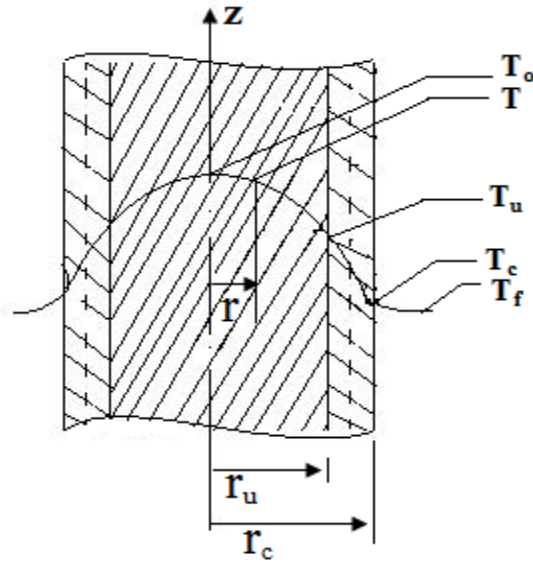


Figure 3.8: Fuel element

$$\frac{d^2T}{dr^2} + \frac{1}{r} \frac{dT}{dr} + \frac{q_v}{K_u} = 0 \quad (3.84)$$

Where q_v – heat production rate, W/m^3

K_u – thermal conductivity of pellets, $W/m \cdot ^\circ C$

When q_v is distributed uniformly, solving Equation 3.83 to get

$$T_o - T_u = \frac{q_v r_u^2}{4K_u} = \frac{q r_u^2}{2K_u} = \frac{q_l}{4\pi K_u} \quad (3.85)$$

Where T_o – temperature at the centre of the pellets,

T_u – temperature at the surface of pellets,

r_u – radius of pellets; see Figure 3.8.

q – Surface heat flux,

q_l – linear power density

$$q_l = 2 \pi r_u q = \pi r_u^2 q_v \quad (3.86)$$

Heat conduction of cladding

$$Q = -K_c F \frac{dT}{dr} \quad \text{Fourier law [61]} \quad (3.87)$$

Solving Equation 3.87, one can obtain

$$T_u - T_c = \frac{Q}{2\pi K_c L} \ln \frac{r_c}{r_u} = \frac{q_l}{2\pi K_c} \ln \frac{r_c}{r_u} \quad (3.88)$$

Where Q – total heat conducted through the cladding (w),

F – area perpendicular to conduction direction

L – length of pellets (m).

3.7.3.2 Heat Convection between cladding outer surface and coolant

The convection heat transfer mode is comprised of two mechanisms. In addition to energy transfer due to random molecular motion, energy is also transferred by the bulk, or macroscopic, motion of the fluid. This fluid motion is associated with the fact that, at any instant, large numbers of molecules are moving collectively or as aggregates. Such motion, in the presence of temperature gradient, contributes to heat transfer [62]. Let us consider the convection heat which occurs between coolant and clad surface when the two are at different temperature.

$$q_l = 2\pi r_c h (T_c - T_f) \quad \text{Newton's Law of Cooling} \quad (3.89)$$

Or

$$T_c - T_f = \frac{q_l(z)}{2\pi r_c h} \quad (3.90)$$

Where T_f – mixed temperature of coolant ($^{\circ}\text{C}$)

h – heat transfer coefficient ($\text{W}/\text{m}^2 \cdot ^{\circ}\text{C}$)

Given q_l , T_f and h , one can get the temperature at the outer surface of cladding by means of Equation 3.90. Here the key problem is how to calculate h , which is related to the velocity of coolant, the thermal properties of coolant and the geometries of flow channel etc.

- i. Forced convection heat transfer in a circular channel

$$Nu = 0.023 Re^{0.8} Pr^{0.4} \quad \text{Dittus – Boelter [61]} \quad (3.91)$$

Where $Nu = \frac{hDe}{K_f}$, $Re = \frac{\rho_f U De}{\mu_f}$ and $Pr = \left(\frac{\mu C_p}{K}\right)_f$

De – equivalent hydraulic diameter (m)

K_f – thermal conductivity of coolant ($\text{W}/\text{m} \cdot ^{\circ}\text{C}$)

ρ_f – density of coolant (Kg/m^3)

U – coolant dynamic viscosity (Pa.S)

μ_f – coolant flow velocity ($\text{J}/\text{Kg} \cdot ^{\circ}\text{C}$)

C_p – specific heat capacity for coolant ($\text{J}/\text{Kg} \cdot ^{\circ}\text{C}$)

- ii. Heat transfer coefficient for rod bundles

Weisman suggested the following

$$Nu = CRe^{0.8}Pr^{1/3} \quad (3.92)$$

Where C – constant determined by lattice arrangement.

For square lattice, when $1.1 \leq P/d \leq 1.3$,

$$C = 0.042(P/d) - 0.024$$

For triangular lattice, when $1.1 \leq P/d \leq 1.5$

$$C = 0.026(P/d) - 0.006$$

P – distance between adjacent fuel rods, (m)

d – diameter of fuel bundle (m)

iii. Natural convection heat transfer

Natural convection refers to the fluid flow which is caused by density gradient within the fluid. The density gradient is usually produced by temperature difference in the fluid. Therefore, the intensity of natural convection depends on temperature difference. The heat transfer coefficient of the natural convection is often expressed in the form of the following correlation:

$$Nu = c(GrPr)_m^n$$

Gr is the Grashof number; $Gr = g\beta De^3(T_c - T_f)/\gamma_f^2$

g – acceleration due to gravity (m/s)

β – volumetric expansion coefficient (1/°C)

De – characteristic dimension (m)

γ_f – kinematic viscosity of coolant (m²/s)

m – means $T_m = 1/2(T_c - T_f)$ as the temperature calculation the physical properties, c and n mainly depend on the geometry and orientation of the solid, heat flux direction, and the range of $Gr.Pr$.

On the full scale simulation facility of the MNSR at China Institute of Atomic Energy, the natural heat transfer coefficient was measured and the following correlations were obtained:

$$Nu = 0.68(GrPr)^{0.25}, \text{ when } (GrPr) < 6E^6$$

$$Nu = 0.174(GrPr)^{1/3}, \text{ when } (GrPr) > 6E^6$$

3.7.3.3 Heat transport in the reactor

When coolant is flowing through reactor core, the heat released from fuel elements is carried away from the reactor core. The process is called heat transport. For steady state conditions, the heat balance equation is

$$Q(z) = WC_p [T_f(z) - T_{fin}] \quad (3.93)$$

Where

$Q(z)$ – heat power transported by coolant from inlet of core to axial position z , (W)

W – mass flow of coolant (Kg/s)

C_p – specific heat of coolant (J/Kg°C)

From Equation 3.93, coolant temperature distribution may be obtained:

$$T_f(z) = T_{fin} + \frac{Q(z)}{WC_p} = T_{fin} + \frac{1}{WC_p} \int_{z_{in}}^z q_l(z) dz \quad (3.94)$$

Where

q_l – linear power density at position z , (W/m),

$T_{f_{in}}$ – inlet temperature of coolant, ($^{\circ}\text{C}$)

Given $T_{f_{in}}$, w , and $q_l(z)$, one can calculate coolant temperature distribution along the axial direction for Equation 3.94, $T_{f_{in}}$, maximum cladding surface temperature $T_{c_{max}}$, position $Z_{c_{max}}$, maximum centre temperature of fuel pellet position $T_{o_{max}}$, position $Z_{o_{max}}$ shown in Figure 3.9.

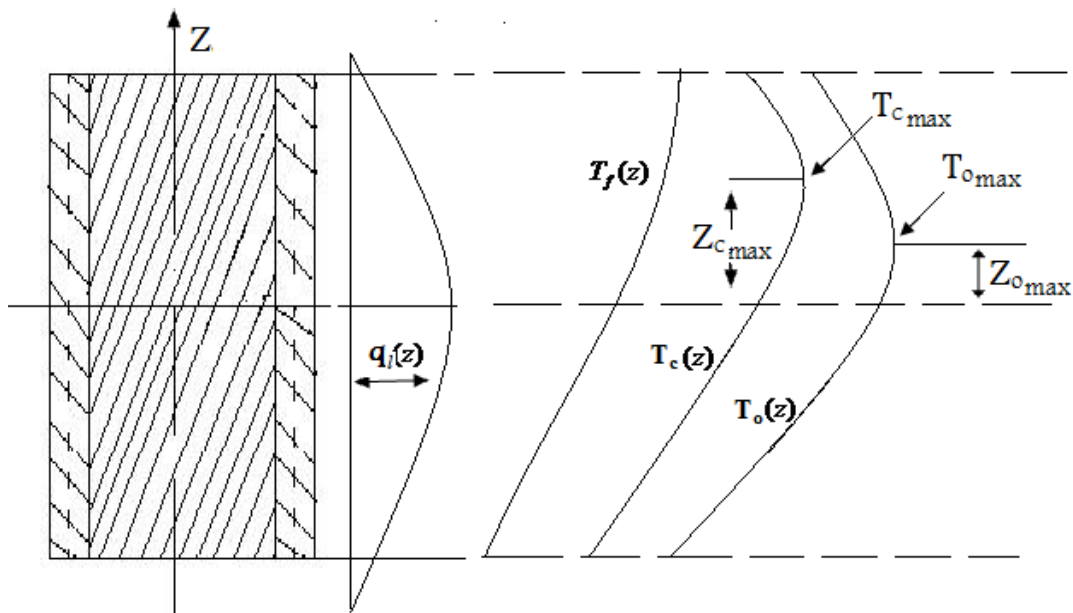


Figure 3.9: Temperature distribution in fuel and coolant

Coolant temperature gains maximum value at the exit, the maximum temperature at the outer surface of cladding and the maximum centre temperature of the pellet occur all between the middle and exit of the flow channel, their values must be less than their limiting values [26].

For the HEU reactor at a power of 30 Kw, the calculated maximum fuel temperature ($T_{0\max}$) is about 70 ° C, much less than the melting point of U-Al alloy which is 640 ° C.

3.7.4 Transient Thermal hydraulic calculation

Under transient conditions, the heat generated by the fuel meat Q_u is not equal to the heat transferred from the outer surface of cladding to the coolant Q_f , as part of Q_u is transferred to the coolant through the cladding, another of Q_u is used to raise the temperature of fuel elements. The temperatures of fuel and coolant and the velocity of coolant all vary with time. Generally speaking, partial differential equations of heat conduction within fuel element and hydro-dynamical partial differential equations are simultaneously solved.

3.7.4.1 The partial differential equations of heat conduction within fuel and cladding under transient conditions

Fuel:

$$C_u \rho_u \frac{\partial}{\partial t} T(r, t) = \frac{1}{r} \frac{\partial}{\partial r} [K_u(T) r \frac{\partial}{\partial r} T(r, t)] + q_v(r, t) \quad (3.95)$$

Cladding:

$$C_c \rho_c \frac{\partial}{\partial t} T(r, t) = \frac{1}{r} \frac{\partial}{\partial r} [K_c(T) r \frac{\partial}{\partial r} T(r, t)] \quad (3.96)$$

Boundary conditions:

$$i) \quad -K_c \frac{\partial}{\partial r} T(r, t) |_{r=r_c} = h(T_c - T_f)$$

$$\begin{aligned}
\text{ii)} \quad & K_u \frac{\partial}{\partial r} T(r, t) |_{r=r_u} = K_c \frac{\partial}{\partial r} T(r, t) |_{r=r_u} \\
\text{iii)} \quad & \frac{\partial}{\partial r} T(r, t) |_{r=r_u} = 0 \\
& \text{i), ii) and iii)} \tag{3.97}
\end{aligned}$$

3.7.4.2 The hydro-dynamical partial differential equations of coolant flowing in reactor core

i) Mass conservation equation;

$$\frac{\partial \rho_f}{\partial t} + \frac{\partial}{\partial z} (\rho_f U) = 0 \tag{3.98}$$

ii) Momentum Conservation equation;

$$-\frac{\partial P}{\partial z} = \rho_f \frac{\partial U}{\partial t} + \rho_f U \frac{\partial U}{\partial z} + \frac{1}{2} \left(\frac{f}{D_e} + \frac{\rho}{\Delta z} \right) \rho_f U^2 + \rho_f g \tag{3.99}$$

iii) Energy conservation equation;

$$C_{pf} \rho_f \frac{\partial T_f}{\partial t} + C_{pf} \rho_f U \frac{\partial T_f}{\partial z} = \frac{P_h}{A_f} h(T_c - T_f) \tag{3.100}$$

iv) State equation of coolant;

$$\rho_f = f(P, T_f) \tag{3.101}$$

where ρ_f – coolant density (kg/m^3),

U – coolant velocity (m/s)

C_{pf} – specific heat capacity of coolant ($\text{J/Kg } ^\circ\text{C}$)

T_f – coolant temperature ($^\circ\text{C}$)

P_h – heated perimeter (m)

A_f – cross sectional area of flow channel (m^2)

h – heat transfer coefficient ($\text{w/m}^2\text{°C}$)

T_c – temperature at outer surface of cladding (°C)

P – coolant pressure (Pa)

f – friction factor

D_e – equivalent diameter of channel (m)

ϕ – form resistance coefficient

The Equations 3.97 to 3.101 stated above include five known variables; T (including T_u and T_c), U , T_f , P and ρ_f . These equations are simultaneously solved by the finite difference to obtain the distributions of these five variables and variations with time.

3.7.4.3 Simplified method of integrated parameters

According to the characteristics of MNSR, a method of integrated parameters is adopted: taking the reactor core as a calculated unit, and assuming that [55]:

- i. Uniform power distribution of fuel element, that is $q_v = f(t)$
- ii. Water temperature T_f varies linearly along axial direction z , and

taking average water temperature at reactor core $\bar{T}_f = \frac{1}{2}(T_1 + T_2)$ as

reference variable, $\bar{T}_f = f(t)$

- iii. Uniform coolant velocity U in the reactor core, that is,

$$\frac{\partial U}{\partial z} = 0, \quad U = f(t);$$

- iv. The fuel meat possesses high thermal conductivity, a small contact resistance between the meat and cladding, low power density of fuel and small diameter of fuel element, hence the temperature difference between the centre and cladding surface approximately the same,

$$T_o \approx T_c \text{ and } T_c = f(t)$$

As a result, the partial differential equations of heat conduction within fuel and cladding as shown in equations 3.95 and 3.96, and boundary condition in equation 3.97i are approximately expressed as in the following equation:

$$(G_u C_u + G_c C_c) \frac{dT_c}{dt} = Q_u(t) - F_s h [T_c(t) - \bar{T}_f(t)] \quad (3.102)$$

Where G_u – total mass of fuel meat in core (kg)

C_u – specific heat capacity of fuel meat (J/kg°C)

G_c – total mass of cladding in the core (kg)

C_c – specific heat capacity of cladding (J/kg°C)

Q_u – reactor power (W)

F_s – total surface area of fuel elements in core (m²)

T_c – average temperature of fuel elements (°C)

\bar{T}_f – average temperature of coolant (°C)

h – heat transfer coefficient (W/m²°C)

According to the assumptions mentioned above, the energy equation of coolant in core can become:

$$C_{pf} \frac{d\bar{T}_f}{dt} \int_0^H \rho_f dz + C_{pf} U \int_0^H \frac{\partial T_f}{\partial z} \rho_f dz = \frac{P_h}{A_f} \int_0^H h(T_c - \bar{T}_f) dz \quad (3.103)$$

The integrated equation, 3.103, may be written as

$$HC_{pf} \bar{\rho}_f \frac{d\bar{T}_f}{dt} = \frac{F_s}{A_f} h(T_c - \bar{T}_f) - C_{pf} U \bar{\rho}_f (T_2 - T_1) \quad (3.104)$$

Where A_f – total cross section area of flow channel in core (m²)

$$\bar{\rho}_f = \frac{1}{H} \int_0^H \rho_f dz \quad (3.105)$$

H – height of core (cm)

T_1 – coolant temperature at the inlet of core (°C)

T_2 – coolant temperature at the outlet of core (°C)

$$T_2 = 2\bar{T}_f - T_1 \quad (3.106)$$

If the flow resistance in the downcomer is neglected and coolant velocity in the downcomer is approximately equal to coolant velocity in the core U , the integrated momentum equation of coolant in the reactor (a cycle path) can be written as [55]

$$\begin{aligned}
0 = & \frac{dU}{dt} \int_0^H \rho_f dz + \frac{1}{2} \left(\frac{f}{D_e} + \frac{\wp}{\Delta z} \right) U^2 \int_0^H \rho_f dz + g \int_0^H \rho_f dz \\
& + \frac{dU}{dt} \int_0^{H_1} \rho_f dz + g \int_0^{H_1} \rho_f dz - \frac{dU}{dt} \int_0^{-H_1} \rho_f dz + \\
& g \int_0^{-H_1} \rho_f dz - \frac{dU}{dt} \int_0^{-H} \rho_f dz + g \int_0^{-H} \rho_f dz
\end{aligned} \tag{3.107}$$

The above equation may be written as

$$\begin{aligned}
(H \bar{\rho}_f + H_1 \rho_{f2} + H_1 \rho_{f3} + H_1 \rho_{f4}) \frac{dU}{dt} = \\
gH(\rho_{f4} - \bar{\rho}_f) + gH_1(\rho_{f3} - \rho_{f2}) - \frac{fH}{2D_e} \bar{\rho}_f U^2 - \frac{1}{2} \wp \bar{\rho}_f U^2
\end{aligned} \tag{3.108}$$

Where H_1 equal temperature height above the core (m)

ρ_{f2} – coolant density at the outlet of core (kg/m³)

ρ_{f3} – coolant density above the downcomer (kg/m³)

ρ_{f4} – coolant density in the downcomer (kg/m³)

Since $\rho_{f3} \approx \rho_{f4} \approx \rho_{f1}$, equation 3.107 can be simplified

$$2(h + H_1) \bar{\rho}_f \frac{dU}{dt} = gH(\rho_{f1} - \bar{\rho}_f) + gH_1(\rho_{f1} - \rho_{f2}) - \left(\frac{fH}{2D_e} + \frac{\wp}{2} \right) \bar{\rho}_f U^2 \tag{3.109}$$

Where

$$f = \frac{64}{\text{Re}}, \quad \rho_{f1} \text{ – coolant density at the inlet of core (kg/m}^3\text{)}$$

If the reactor power $Q_u(t)$ and the inlet coolant temperature $T_1(t)$ are known, Equations 3.102, 3.104, 3.106 and 3.109 are simultaneously solved, and we obtain $T_c(t)$, $\bar{T}_f(t)$, $T_2(t)$ and $U(t)$. However, the inlet coolant temperature $T_1(t)$ is unknown during the

reactor start-up. In order to calculate $T_1(t)$, it is necessary to supply some energy balance equations in upper part of reactor tank, in annular downcomer and outside water pool.

Bounded by the elevation of the outlet of the reactor core, the water in the reactor tank is divided into upper and lower parts, their energy equations are as follows:

$$G_3 C_{pf} \frac{dT_3}{dt} = A_{up} C_{pf} U (\rho_{f2} T_2 - \rho_{f3} T_3) - Q_0 \quad (3.110)$$

$$G_4 C_{pf} \frac{dT_4}{dt} = A_{dow} C_{pf} U (\rho_{f3} T_3 - \rho_{f4} T_4) - Q_4 + Q_B \quad (3.111)$$

$$G_0 C_{pf} \frac{dT_0}{dt} = Q_0 + Q_4 \quad (3.112)$$

Where Q_0 and Q_4 – heat transferred to pool, calculated with natural convection correlation; Q_B – heat transferred from beryllium to downcomer.

Experiments show that the temperature at downcomer does not change much, hence $T_4 = T_1$. Thus Equation 3.111 is rewritten as

$$G_4 C_{pf} \frac{dT_4}{dt} = A_{dow} C_{pf} U (\rho_{f3} T_3 - \rho_{f1} T_1) - Q_4 + Q_B \quad (3.113)$$

Equations 3.110, 3.112 and 3.113 include three unknown temperatures T_0 , T_1 and T_3 . The pool water, which weighs G_0 , has a large heat capacity and may be considered as isothermal to the ambient, in other words, the heat ($Q_0 + Q_4$) is all absorbed by water in the pool.

Solving equations 3.102, 3.104, 3.106, 3.109, 3.110 and 3.112, we can get the cladding temperature T_c , the average water temperature of the reactor core $\overline{T_f}$, the water temperature at the core inlet and outlet T_1 and T_2 , the water velocity in core U , the water

temperature in the upper part of the reactor tank T_3 and the water temperature in the pool, T_o .

Figures 3.7, 3.8 and 3.9 show the water temperature at core inlet, T_1 , water temperature difference between core inlet and outlet, and the water velocity in core U , they vary with time (minute), the reactor power Q_u as parameter.

During the early period of start-up, the temperature difference is small between primary water (water in reactor tank) and the pool water, therefore the heat is less transferred to the pool, and most is used to raise the temperature of the primary water and the fuel elements, thus the average and the inlet temperature of the reactor rise more quickly [55]. With the increasing of primary water temperature, the temperature difference for heat transfer increases, and more heat is transferred to the pool, so that the temperature increase of the primary water is reduced, and after three hours, the condition becomes steady.

In several minutes, the reactor power reaches the rated value and the temperature difference between outlet and inlet reaches maximum value as shown in Figure 3.11. After that, the temperature of the primary water increases continuously (Figure 3.10) and the buoyancy force increases and the water flow velocity in the reactor core increases slightly (Figure 3.12), thus the temperature difference between outlet and inlet decreases slightly (Figure 3.11).

Arranging the calculated results, the correlation between reactor power and inlet-outlet temperature difference is realized [55].

$$T_2 - T_2 = (5.725 + 147.6H_{in}^{-2.674})T_1^{-0.35}Q_u^{(0.59+0.0019T_1)} \quad (3.114)$$

Where H_{in} is the height of the inlet channel (mm), the size of H affects the form of resistance at the core inlet, and the form of resistance makes up the greater part of total resistance. So that, the H_{in} is smaller, the form resistance is larger, and the coolant velocity in the core is smaller. As a result, the inlet-outlet temperature difference increases.

During reactor operation, the temperature difference between core outlet and inlet can be measured, and the reactor power can be calculated with the correlation (29)

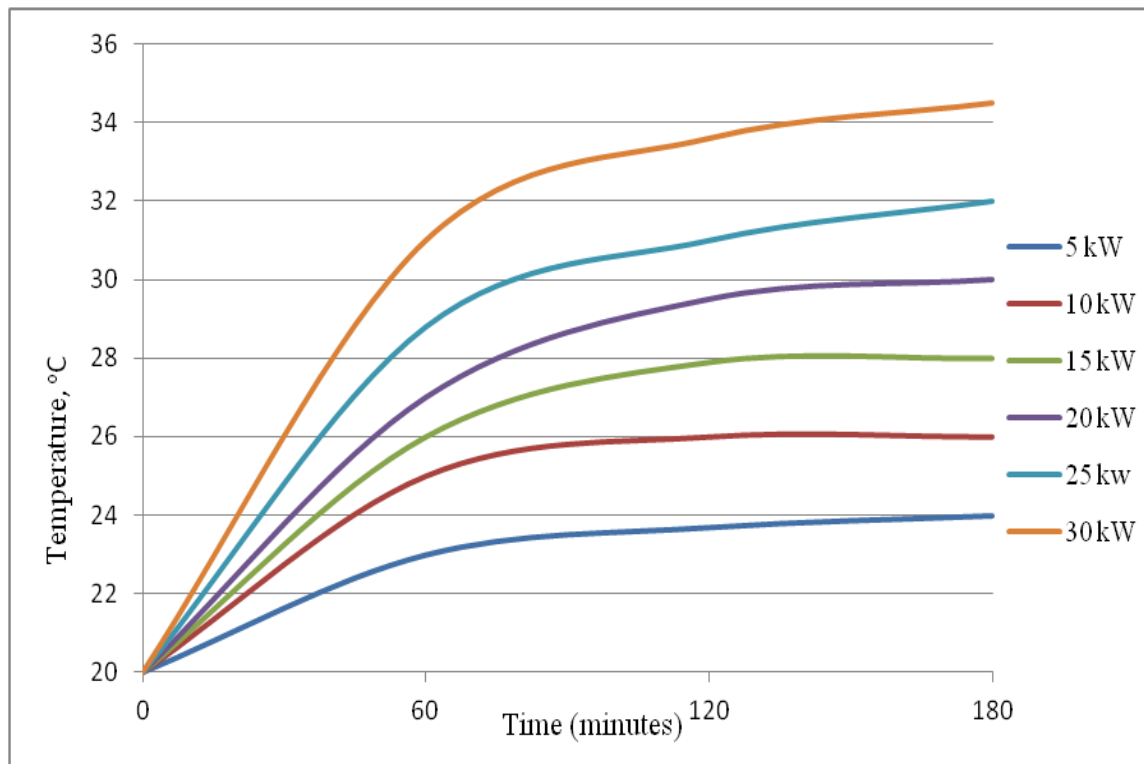


Figure 3.10: Water temperature variation at core inlet (T_1)

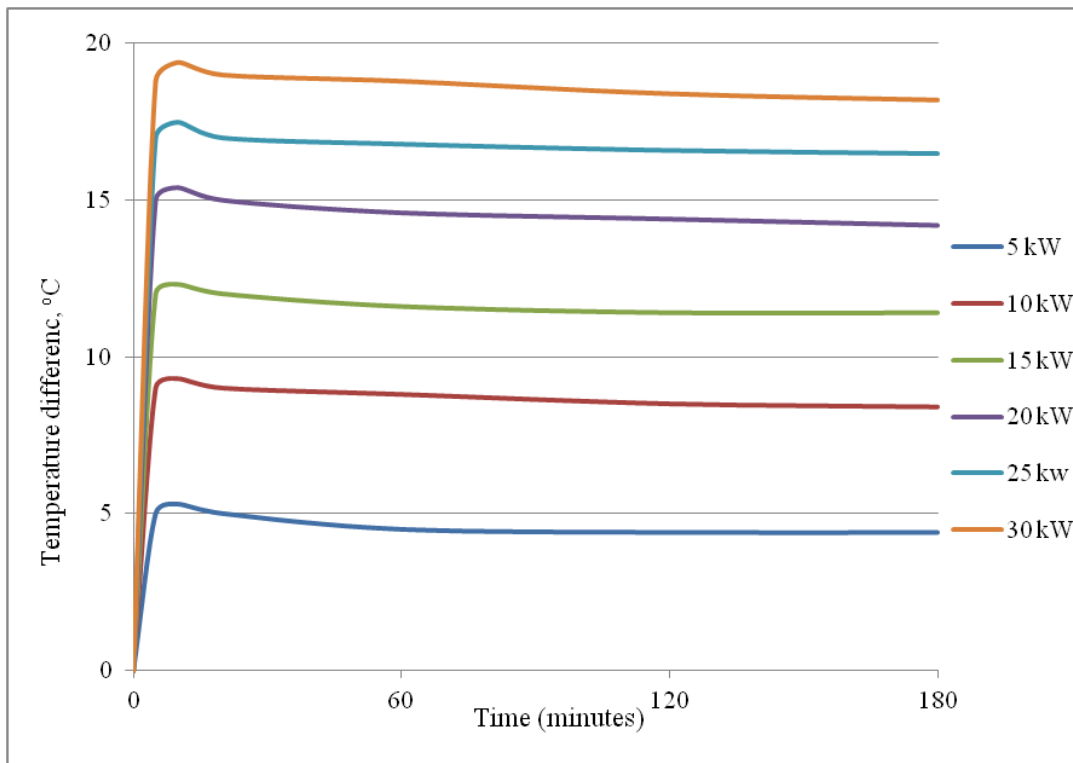


Figure 3.11: Variation of temperature difference between core inlet and outlet.

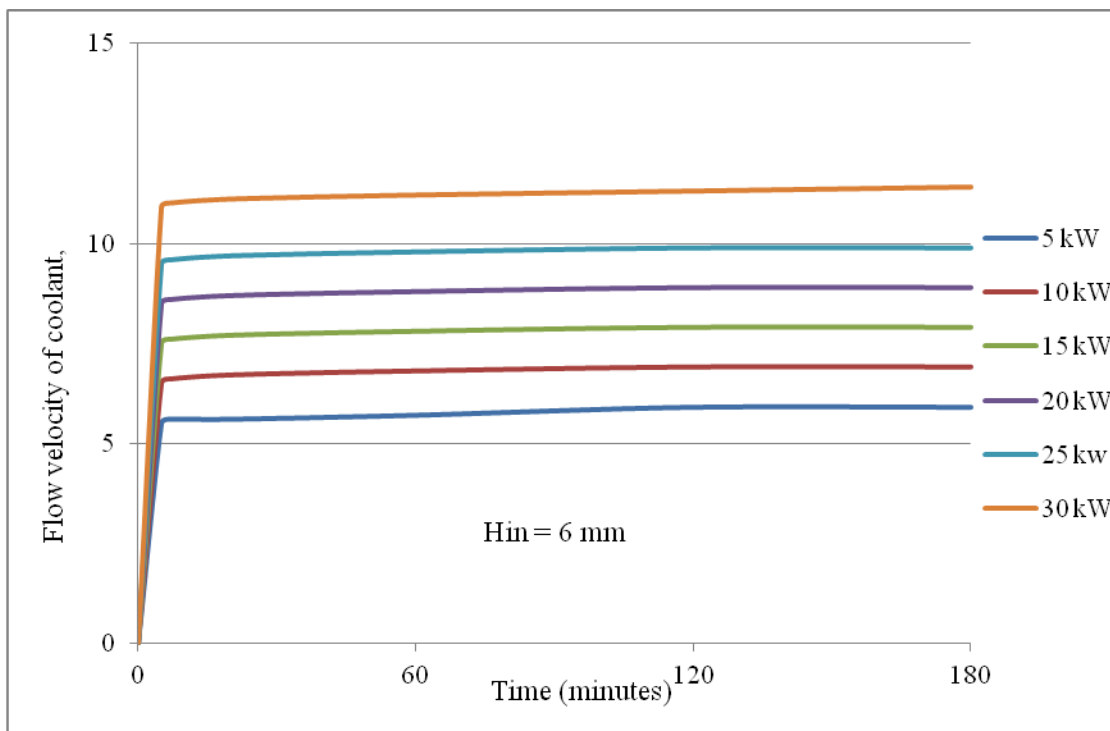


Figure 3.12: Variation of coolant velocity in reactor core.

The methodology engaged in undertaking the studies of this work is provided in Chapter Four. Firstly, the neutronics aspect including burnup is analysed using neutronics codes; the MCNP and the REBUS codes. Secondly, the thermal hydraulics analysis which comprises of the Steady State as well as the Transients is analysed using the PLTEMP and PARET codes.

CHAPTER FOUR

4 METHODOLOGY

MNSR reactors are simple in design and structure. As per all types of reactor, neutronics analysis of MNSRs can be done with reactor codes based on both deterministic and Monte Carlo approaches as described in Chapter 3. In the past, deterministic methods and codes have been employed for reactor analysis of the GHARR-1 [63].

In recent times, however, the Monte Carlo approach to reactor analysis has been included. In particular, multipurpose Monte Carlo particle transport codes generally have the capability to model and treat different complicated geometries in 3-D and also simulate the transport behavior of different particles and nuclear interaction processes. Good and accurate modeling of the different zones and diverse geometries of the MNSR reactor is important for realizing good neutronics, particle transport simulation, and physics analysis. For these reasons, the versatile and widely utilized MCNP code particle transport code was employed to develop a 3-D Monte Carlo model for MNSR for particle transport simulation and neutronic analysis of MNSR reactors [25].

In this Chapter, the 3-D Monte Carlo developed for MNSR reactors using the versatile MCNP transport code and upon which this work is derived is described. The methodology adopted in the modeling and neutronic simulation relevant to this work is also presented.

4.1 Monte Carlo Model for GHARR-1

The Monte Carlo method has been in use for almost sixty years to solve radiation transport problems in high energy physics, nuclear reactor analysis, radiation shielding, medical imaging, etc [64]. Individual particles histories are simulated using random numbers, highly accurate representations of particle interaction probabilities, and exact models of three dimensional problem geometry. Monte Carlo methods are sometimes the only viably methods for analyzing complex, demanding particle transport problems.

This work is based on the Monte Carlo model for MNSR reactors modified at Argonne National Laboratory in the USA using the MCNP transport code. The model was developed following the approaches used in the 3-D combinatorial, generalized geometry and continuous energy methods applied in MCNP. Thus different geometries in planar, conical, spherical and cylindrical configurations of the various zones, sections and materials such as the fuel assembly, control systems, reflectors, experimental channels, shim tray, reactor vessel, reactor pool and other structural components were modeled accordingly using available design data. The centre of the GHARR-1 core assembly which has a cylindrical configuration with 10 fuel lattices concentrically arranged about the central control rod guide was chosen as the geometrical centre of the Monte Carlo model.

Typically, MNSR reactors are designed to have different core loadings. This means that the fuel loading of a typical MNSR facility could vary or differ from other operating MNSR facilities. Taking cognizance of this variation, the GHARR-1 Monte

Carlo model provided for the modeling and simulation of MNSR reactors with varying core configurations ranging from 342 – 350 fuel lattices.

The MCNP5 [27] transport code was used to perform the Monte Carlo calculations. Nuclear data for fissile and non-fissile isotopes associated with materials (fuel and clad, coolant, moderator, control rod and clad, reflectors, 5 structural components) of the physical model was chosen from ENDF/B-VI nuclear data libraries. The special $S(\alpha, \beta)$ scattering feature was applied in the nuclear model to treat thermal scattering in beryllium and hydrogen in light water for the reflector material and water regions respectively of the GHARR-1 Monte Carlo model. Neutronics analyses were performed using a condensed 3-group neutron energy structure: up 0.625eV for thermal neutrons, < 8.21 eV for epithermal neutrons and up to 20 MeV for fast neutrons.

All this were done to establish the deck for the HEU core and after it been ascertained that results compare very well with experimental data, the necessary modifications were made to acquire the LEU model for the core conversion exercise.

MCNP5 permits a very general, detailed representation of 3D geometry. Volumes in space called cells are defined in terms of their bounding surfaces. Surface types include planes, quadrics, and tori (aligned with a major axis). Alternatively, users may specify macro-bodies (e.g., sphere, finite cylinder, ellipsoid, etc.), which are converted internally into individual surfaces. Boolean operators (union, intersection) and surface-senses (inside, outside) may be used with the surface specifications to precisely define the volume enclosed by a cell. Cells may also include the complement of another cell and may be composed of non-convex or disjoint volumes. The MCNP input file

describes the problem geometry, specifies the materials and source, and defines the results you desire from the calculation. The geometry is constructed by defining cells that are bounded by one or more surfaces. Cells can be filled with a material or be void.

An MCNP input file has three major sections: cell cards, surface cards, and data cards. A one-line title card precedes the cell card section and MCNP uses a blank line delimiter to denote separation between the three different sections. The word “card” describes a single line of input of up to 80 characters. A section consists of one or more cards.

The MCNP plots of the GHARR-1 core configuration and the vertical cross-section are shown in Figure 4.1 and Figure 4.2 respectively.

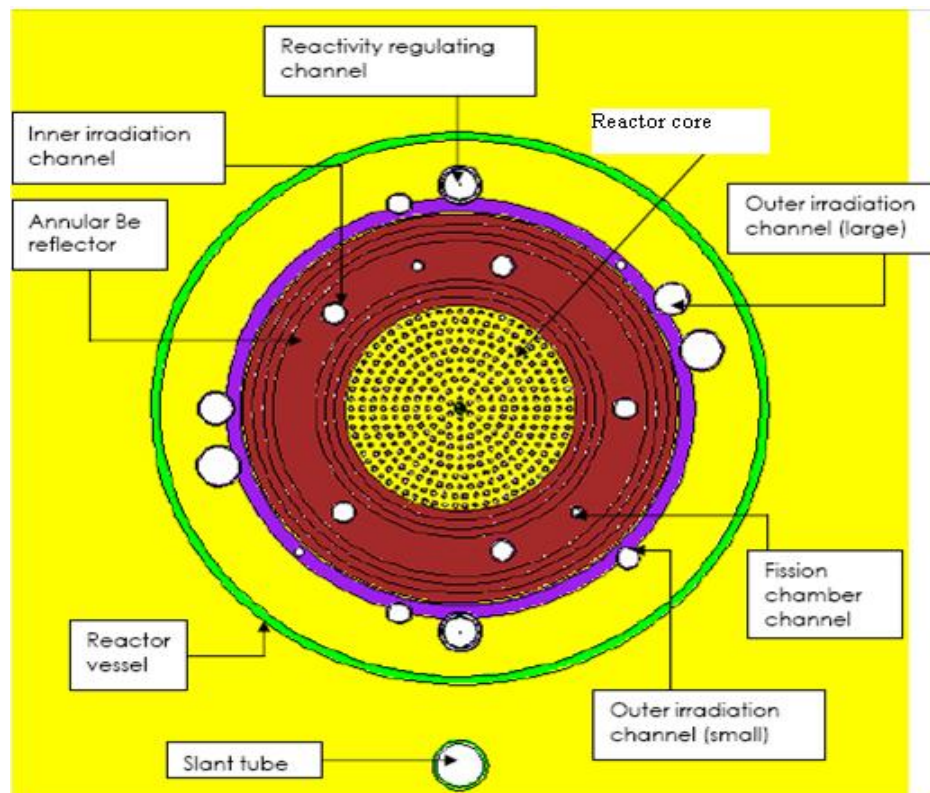


Figure 4.1: MCNP plot of the core configuration and associated experimental channels

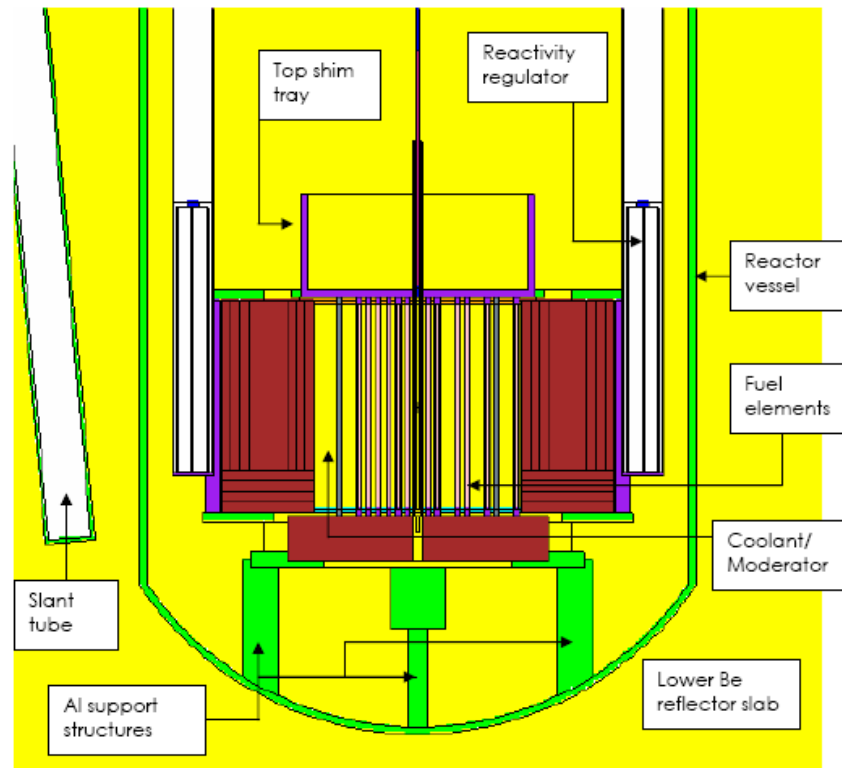


Figure 4.2: MCNP plot of vertical cross-section of GHARR-1 reactor (in full power mode).

4.1.1 Auxiliary shutdown system

As stated earlier, the auxiliary shutdown system is a completely independent method of shutting down the reactor in the event of a failure of the control system. This system is not automatically actuated at the onset of an abnormal condition. Auxiliary shutdown is accomplished by the manual insertion of cadmium capsules into the inner irradiation sites. A safer means of inserting the cadmium needs to be designed, as per the objective of this study. Furthermore, the shutdown margin for the CR of the LEU core is below that of the HEU, and an introduction of an auxiliary rod can increase the shutdown margin of the LEU core. To achieve this, the constituents of the cadmium capsules were studied and their reactivity worth measured using the MCNP code. In the course of this, it appeared as though the surface area exposed to the neutrons were a factor to the

reactivity worth of the cadmium. Hence further studies were carried out to ascertain this fact. Results of this analysis are shown in chapter five. The figures below depict the nature and dimension of the cadmium and capsule.



Figure 4.3: Cadmium Capsule

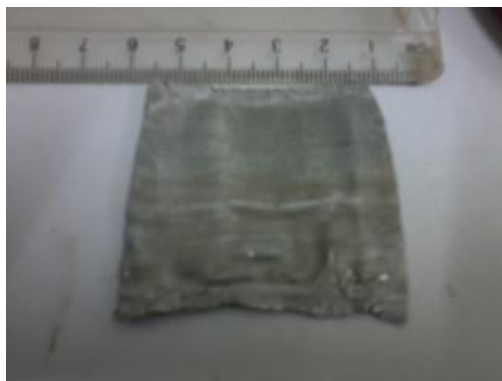


Figure 4.4: Cadmium foil



Figure 4.5: Measurement of Cadmium (Side)



Figure 4.6: Measurement of Thickness (a)



Figure 4.7: Measurement of Thickness (b)

Table 4.1 Dimension of cadmium in capsule (average along each side)

Parameter	Dimension (cm)
Length	~ 4.60
Width	~ 4.54
Thickness	~ 0.05

First of all, the cadmium capsules which are sent into the reactor core during control rod failure were analyzed. The cadmium capsule is made up flat cadmium piece with dimensions shown in Table 4.1. The width of each cadmium piece was translated into the circumference and the length became the height of a cylinder in the MCNP modeling for this analysis. The depth of the irradiation site in the beryllium reflector is

18.75 cm which accommodates the cadmium capsules. This is depicted by the MCNP visual editor as shown in Figure 4.8 below:

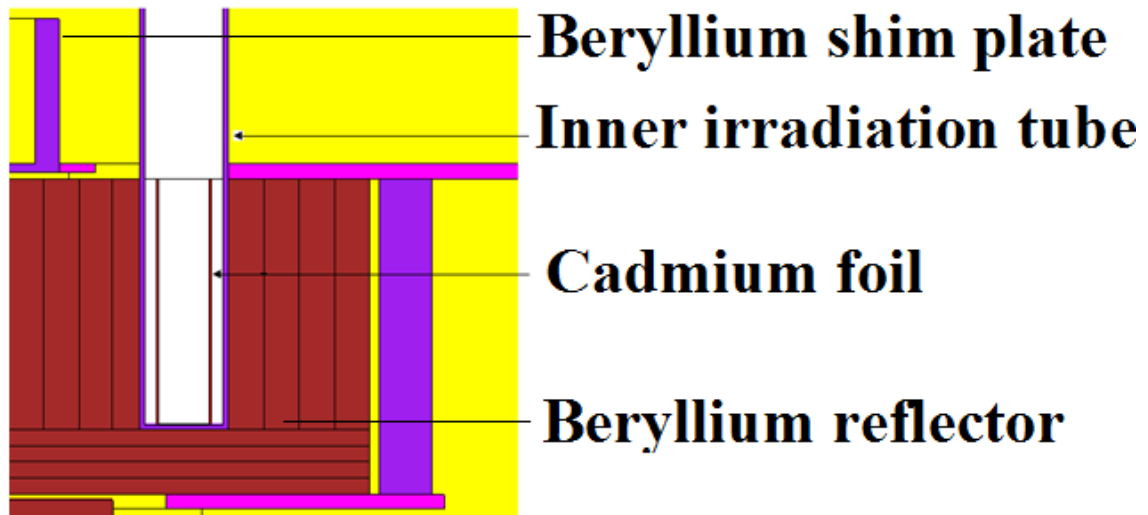


Figure 4.8: Cadmium foil in irradiation channel (Visual editor of MCNP)

For this analysis, six various shapes of cadmium were designed with the MCNP code. Three of these designs are such that the irradiation site had to be gouged further down by 4.475 cm. This is to make the rod longer for a better reactivity worth of the auxiliary rod. The hollow foil is investigated first, followed by a three layer foil arranged in concentric circles and then finally a solid rod. Results for auxiliary rod analysis are presented in section 5.2. Images from the MCNP visual editor are shown in Figure 4.9 to Figure 4.13 below for the arrangements considered with the dimensions for the various safety rods are shown in Table 4.2.

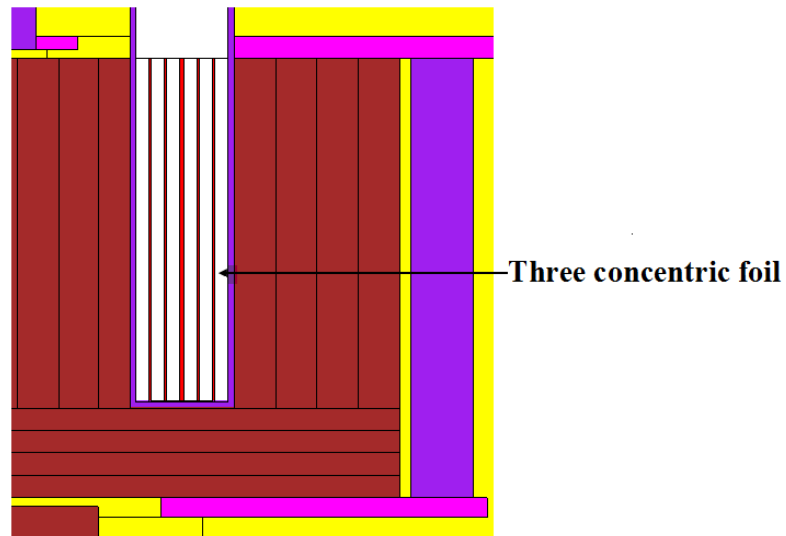


Figure 4.9 Three concentric foils in unmodified irradiation site (CFU)

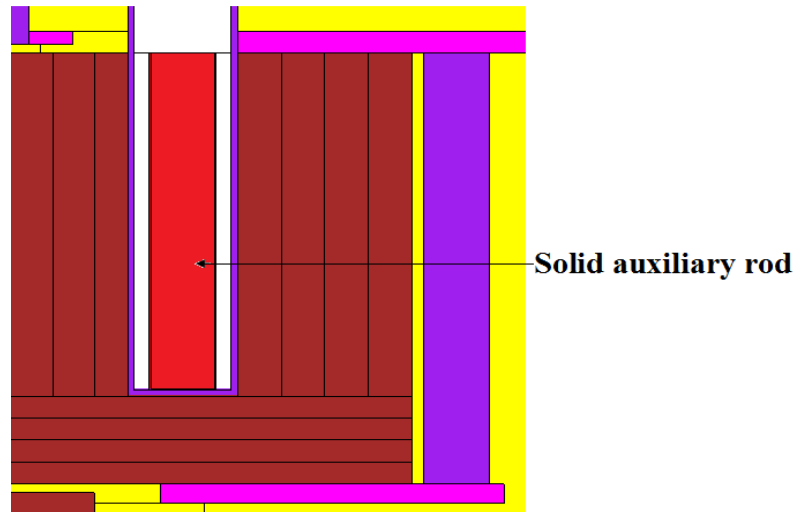


Figure 4.10. Solid auxiliary rod (SR)

Table 4.2 Dimensions of various safety rods

Safety Rod	Thickness (cm)	Height (cm)	Radius (cm)
F1	0.50	18.70	0.78
CFU	0.50	18.70	0.78
SR	--	18.70	0.78
F2	0.50	23.12	0.78
CFM	0.50	23.12	0.78
SR2	--	23.12	0.78

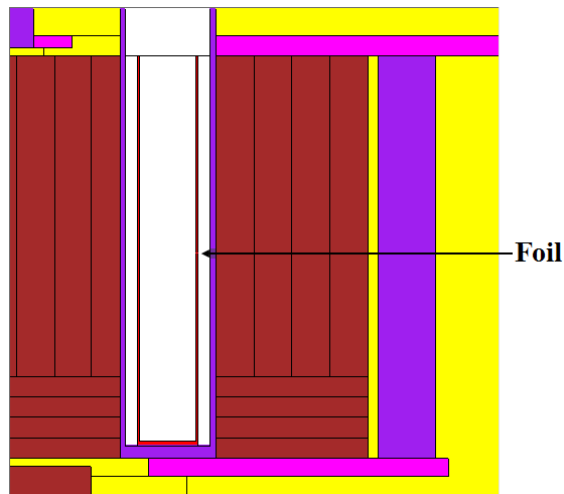


Figure 4.11 Foil with a similar arrangement to the cadmium capsule (F2)

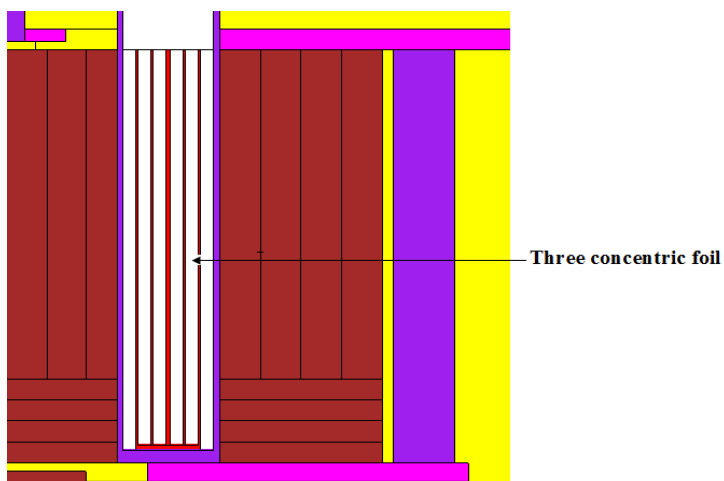


Figure 4.12 Three concentric foils in modified irradiation site (CFM)

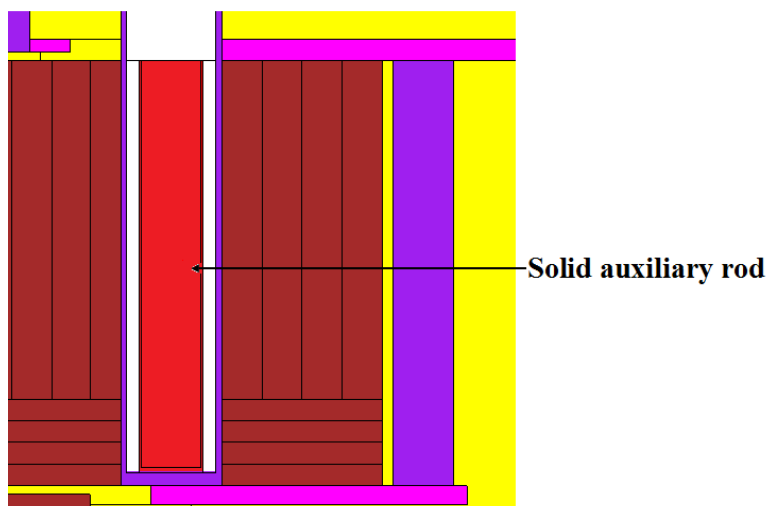


Figure 4.13 Solid auxiliary rod (SR2)

4.2 REBUS Model for GHARR-1

An R-Z diffusion theory model using the REBUS-3 code was developed to understand the basic fuel depletion characteristics of the GHARR-1 core. Important fuel cycle parameters such as core excess reactivity, xenon worth, rate of fuel depletion, and fuel cycle length can be obtained by performing simple reactivity rundown calculations. In these calculations, a newly loaded fresh core with control rod fully withdrawn is depleted at a fixed power level for a given length of time. Because the REBUS-3 RZ-model can run very fast, key core parameters can be calculated at many small time steps to capture the details of temporal variations during fuel depletion. These details are important to help understand the basic fuel depletion characteristics of the GHARR-1 core under different operational schemes. Using RZ model, the core region is homogenized. The control rod is positioned at the centre of the core, followed by its clad. This is followed by the first ring of fuel which is homogenized as one entity. Subsequently, the moderator /coolant between the first and second ring modeled. The other set of fuel elements in each ring and adjoining moderator are all placed in a concentric pattern. This results in a ten concentric ring of fuel elements as depicted in Figure 4. 14.

In addition to this, the beryllium reflector is placed around the core. Furthermore, the reactor vessel is placed at the centre of the pool in the REBUS model (not shown in figure).

The REBUS input deck allows for specification of the various regions. The dimensions of the various radii of the components of the reactor are specified and the dimensions of

the height (Z axis) are also specified. The components are divided into subsections for the sake of analyses. The more nodes you desire, the more the axial sections (e.g. the beryllium reflector was divided into 5 sub sections). Mesh intervals are specified in the deck. The mesh intervals were chosen with respect to the stability of the regions. In areas where there are many variations, a finer mesh is used in order to capture every detail. The homogenization of every fuel ring is very important. The constituents of the reactor components are specified. The code allows for the user to end the run after the neutronic calculation or continue doing burnup calculation. In reactors where fuel management is practiced, you are able to assign the homogenized fuel to a particular fuel management path. The input also contains the number of days the reactor is operated, the power at which the reactor is operated, the beginning of a particular stage of operation and the end of that particular stage of operation. The deck also specifies when the neutronic calculation should be done. In other words, it divides the number of hours for which the reactor runs into sub intervals based on the run time of the reactor.

The total reactor burn cycle time is divided into subintervals depending on the analysis. An explicit burnup is performed in each region of the reactor over each of these subintervals using the average reaction rates over the subinterval. These average reaction rates are based on fluxes obtained from an explicit 3-dimensional diffusion theory neutronics solution computed at both the beginning and end of the subinterval. The transmutation equations are solved by the matrix exponential technique. The isotopes considered in the burnup equations, as well as their transmutation reactions, were specified.

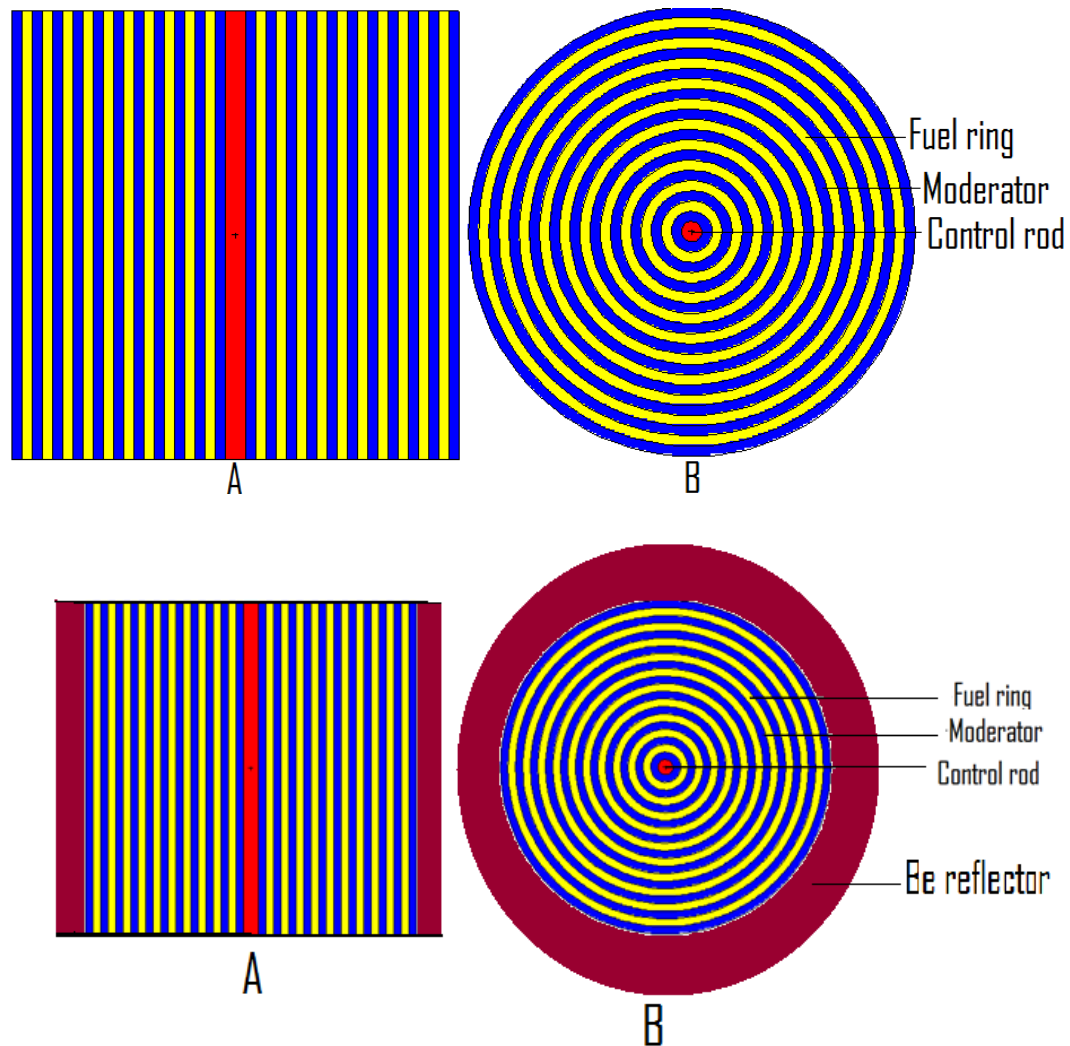


Figure 4.14 RZ model of the reactor core (figure is not drawn to scale);
A – Vertical cross section; **B** – Horizontal cross section

4.3 Thermal Hydraulic Analyses

Both the steady state and transients were analyzed for the two cores under the thermal hydraulics. PLTEMP/ANL and PARET code were used for the steady state and transient analyses respectively. Some of values obtained were compared with those stated in current HEU SAR.

4.3.1 Steady State

Four input data files were used in the PLTEMP/ANL V4.1 code to calculate the safety margins in the steady-state operation of GHARR-1 with HEU core. In addition, an input file giving the axial power shape of the fuel pin modeled (the average power pin or the peak power pin in the HEU core) was also used with the four input data files. Another set of four similar input data files were used to calculate steady-state safety margins of GHARR-1 with LEU core at both 30 kW and 34 kW. In addition, an input file giving the axial power shape of the fuel pin modeled (the average power pin or the peak power pin in the LEU core) was also used with each set of the four input data files; this is required by the PLTEMP/ANL V4.1.

One set of input models one (average fuel pin) of the 344 or 348 fuel pins in the HEU or LEU core respectively with a reactor power of 15 kW and a coolant inlet temperature of 24.5 °C. The pin is modeled as a solid rod of radius 2.15 mm in a 0.6 mm thick cladding, without any gap resistance in the case of HEU core. This input data file was used to calibrate the hydraulic resistance in the PLTEMP/ANL model to reproduce an experimentally measured coolant temperature rise of 13 °C (from 24.5 °C to 37.5 °C).

Another input data file uses the above determined value of the hydraulic resistance coefficient, and models one (average fuel pin) of the pins in the HEU and LEU cores respectively when the reactor is operating at the nominal reactor power of 30 kW. The purpose of this input data file is to raise and adjust the coolant channel inlet temperature so that the coolant exit temperature is 70 °C. The next input data file uses the above adjusted values of the hydraulic resistance coefficient and the channel inlet

temperature, and models the peak power pin of the core, with six hot channel factors (HCF). The purpose of this input data file is to determine the maximum allowed operating reactor power with all hot channel factors applied.

The final set of input data files is identical to the third set of input data files except that five of the hot channel factors have been set to 1.0 in order to calculate the maximum allowed reactor power without hot channel factors. The hot channel factor for power was kept unchanged at its actual value because the ratio of the peak pin to the average pin power is certain. Using this input data file, the pin power was raised and adjusted so that the minimum ONBR on the cladding outer surface is exactly 1.0. The minimum ONBR occurs in axial node 10. When this minimum ONBR is 1.0, the pin power multiplied by number of pins gives the maximum allowed operating reactor power of the core without hot channel factors.

Six hot channel factors (defined below) are used in the PLTEMP/ANL V4.1 code to calculate research reactor safety margins. These factors are different in natural circulation flow from those in forced flow. The basic reason for this is that in natural circulation the coolant flow is induced by the power produced in the pin (thus softening the effect of pin power on inlet-to-outlet coolant temperature rise) whereas it is not so in forced flow. In forced flow, the pressure drop induces the coolant flow [65]. The hot channel factors for forced flow over research reactor fuel plates have been formulated earlier [66]. The equations relating these factors to manufacturing tolerances and other uncertainties for natural circulation over fuel pins are derived in Section 2. Table 4.3 shows the type of uncertainties included in each of the six hot channel factors. The uncertainties of pool water level and pin heated length are not included.

Table 4.3 Uncertainties Included in the Six Hot Channel Factors

No.	Uncertainty Type	FPOWER	FFLOW	FNUSLT	FBULK	FFILM	FFLUX
1	Neutronics calculation of power density in a pin, u_1				X	X	X
2	U-235 mass per pin, u_2				X	X	X
3	UO ₂ pellet radius, u_3					X	X
4	U enrichment in a pellet, u_{10}					X	X
5	Fuel pin radius, u_{12}				X	X	X
6	Fuel pin pitch, u_{13}				X	X	
7	Flow redistribution among channels, u_6				X		
8	Reactor power measurement uncertainty, u_7	X					
9	Flow uncertainty due to uncertainty in friction factor, u_8		X				
10	Heat transfer coefficient uncertainty due to uncertainty in Nu number correlation, u_9			X			

*1 – 8 are for local or random uncertainties while 9 – 11 represent system-wide uncertainties

System-wide or Global Hot Channel Factors:

FFLOW = a factor to account for the uncertainty in total reactor flow

FPOWER = a factor to account for the uncertainty in total reactor power

FNUSLT = a factor to account for the uncertainty in Nusselt number correlation

Local Hot Channel Factors:

FBULK = a hot channel factor for local bulk coolant temperature rise

FFILM = a hot channel factor for local temperature rise across the coolant film

FFLUX = a hot channel factor for local heat flux from cladding surface

4.3.2 Transients Analysis

PARET: “Program for the Analysis of REactor Transients” code was developed for testing methods and models and for subsequent applications in the analysis of transient behaviour in research reactors [67]. The code was originally developed for the analysis of the SPERT-III experiments for temperatures and pressures typical of power reactors [68]. Subsequently, the code has been modified to address some reactor thermal–hydraulic analysis including a selection of flow instability, departure from nucleate boiling, single and two-phase heat transfer correlations, and flow rates encountered in research reactors. Essentially, the code provides a coupled thermal–hydraulic and point kinetics capability with continuous reactivity feedback, and an optional voiding model which estimates the voiding produced by subcooled boiling [69]. For PARET applications, the reactor core can be represented by one to four regions. Each region may have different power generation, coolant mass flow rate, and hydraulic parameters as represented in a single fuel pin with its associated coolant channel. The heat transfer in each fuel element is computed on the basis of one-dimensional conduction solution, providing for a maximum of 21 axial segments. The hydrodynamics solution is also one-dimensional for each of the two channels at each time node [70]. The heat transfer could take place by natural or forced convection, nucleate, transition, or stable film boiling, and the coolant could range from subcooled liquid through the two-phase regime, and up to and including super-heated steam and

allows for coolant flow reversal. The code has been used for transient analysis of GHARR-1 [71].

4.3.2.1 PARET Thermal Hydraulic Model

MNSRs transients have been studied by the RERTR program for quite some time now [72]. The methodology for thermal-hydraulic investigation has been enhanced to account for the transient characteristics of these reactors. MNSR transient analyses based upon extensions to modeling capabilities of the PARET/ANL code have been addressed [73]. The PARET/ANL version 7.3 is intended for the analyses of research and test reactors using plate-type (flat) or pin-type fuel elements. The code has been used for many research reactor conversion studies in support of reactor licensing. It is essential, when simulating many-hour transients, to account for the primary coolant heatup and temperature feedback effects. Results will be shown for transient analysis against experiment, obtained in Ghana MNSR.

The water volume that is actively in the natural convection cooling in the core tank (primary loop) is treated as passing through an inlet pipe section, the core, an outlet pipe section and a lump volume. The pipe sections are assumed to be 10 % of the active primary loop volume each, and are subdivided into 40 nodes. Coolant is tracked through these nodes and the lump based upon volumetric flow rate discharged from the core. By “tracking”, it is meant that the coolant in each node is subjected to heat and mass balance equations which are integrated over a time step typically much longer than that needed for the reactor kinetics calculations. A one second step size was used in this work. Heat is exchanged through a tank surface area between the primary loop and the pool, using a specified heat-transfer coefficient. This heat transfer coefficient can be

obtained by other means, such as from a RELAP model, or simply fitted to the experimental results described below. The pool acts as a secondary loop. Pool heat up is modeled as a lump receiving heat from the primary loop through the tank surface, and at the same time being cooled by air flow over the pool surface causing evaporation. The pool air temperature, humidity and velocity control the evaporation rate of the water at the pool surface and affect its bulk temperature. These parameters can be specified along with the pool surface area, volume and initial temperature. Since the pool temperature changes only a few degrees over many hours, it is not necessary to model it in greater detail.

Evaporative cooling from the pool surface is computed using an ASHARE model [74]. The evaporation rate is

$$w_p \text{ (kg / s)} = A(p_w - p_a)(0.089 + 0.0782V/Y) \quad (4.1)$$

where

A = area of pool surface, m^2

p_w = saturation vapour pressure taken at surface water temperature, kPa

p_a = saturation vapour pressure taken at surface air temperature, kPa

V = air velocity over surface water, m/s

Y = latent heat required to change liquid to vapour at surface water temperature, kJ/Kg

The original PARET model for natural convection was based on fitting SPERT III transient tests in the “E-core” under no forced flow conditions [75]. These tests used

pin-type fuel clad in stainless steel. The coolant passed up through the core components and then reversed direction to flow downward through the thermal shields surrounding the core. This flow path is quite similar to the GHARR-1. But the active height of the SPERT III E-core fuel was 97.3 cm, which is substantially longer than the 23 cm active height of GHARR-1 fuel. In addition, the coolant passages were partially isolated in a square lattice, with a hydraulic diameter of about 11.9 mm, compared to an open rod lattice of 2.25 for a typical MNSR. The pitch/diameter ratios were 1.258 and 2.0 for the E-core and MNSR respectively. These differences have large impacts on the development of the natural convection flow during reactor operation as they affect the driving head, the heat transfer coefficient and the friction losses.

CHAPTER FIVE

5 Results and Discussion

The results show that throughout the lifetime of the proposed LEU core:

1. The shutdown margin meets Operational Limits and Conditions (also referred to as Technical Specification Limits).
2. Reactivity coefficients meet required limits and are comparable to the existing HEU core.
3. Fuel integrity is maintained under all operating conditions.
4. There will be no tradeoff in the thermal neutron fluxes in the experimental channels. This will be achieved by increasing the power of the LEU core by 13 %.

5.1 Criticality Results

The core excess reactivity calculated for the LEU UO₂ fuel with 344 fuel pins was below the 3 mk which is insufficient for the design of MNSR core. An insufficient excess reactivity implies the core will become subcritical after relatively short operation. Hence the number of pins was increased to 348 to achieve the design reactivity of MNSR which is between 3.5 mk and 4.0 mk. Results are presented in Table 5.1.

Table 5.1 Comparison of Reactivities for various cores

Fuel / No. of Pins	Multiplication factor, k_{eff}	Reactivity, mk
HEU; 344 pins	1.00375 ± 0.00005	3.74 ± 0.05
LEU; 344 pins	1.00289 ± 0.00006	2.88 ± 0.05
LEU; 348 pins	1.00385 ± 0.00004	3.84 ± 0.04

A comparison of the criticality data for the HEU and LEU cores are shown in

Table 5.2. The Multiplication factors, k_{eff} , and of course the reactivities are quite comparable and also compare well with values stated in the HEU SAR. The delayed neutron fractions for the two cores as estimated by Monte Carlo N Particle Code are 3.3 % and 3.9 % higher than MNSR manufacturer's quoted value of 0.00808 [20] respectively. Nevertheless, the two compares well with the delay neutron fraction of 0.00837 reported for NIRR-1 [76].

Table 5.2: Comparison of Criticality Results for HEU and LEU

Criticality Result	HEU SAR	HEU	Sigma	LEU	Sigma
Keff – Control rod completely withdrawn	-	1.00375	0.00005	1.00385	0.00004
Keff - Control rod fully inserted	-	0.99680	0.00004	0.99714	0.00004
Core excess reactivity, mk	4.0	3.74	0.05	3.84	0.04
Delayed neutron fraction (β_{eff}), 10^3	8.5	8.347	0.0641	8.395	0.0566
Prompt Neutron lifetime (Λ), s	8.52×10^{-5}	8.46×10^{-5}	0.06×10^{-5}	7.39×10^{-5}	0.06×10^{-5}
Control rod worth, mk	6.80	6.95	0.018	6.74	0.017
Shutdown margin, mk	3.0	3.21	0.012	2.87	0.011

The design control rod worth of the reactor is 6.8 mk and the shutdown margin is 3.0 mk for maintaining the reactor in safe shutdown conditions. The total cold excess reactivity to be compensated is about 4.0 mk by the control rod [2]. The Monte Carlo

calculation of the control rod worth is about 10.5 % more for the HEU core. Both the HEU and LEU cores have shutdown margin close to 3 mk.

5.1.1 Integral and Differential Control Rod Worth

The exact effect of control rods on reactivity can be determined experimentally. For example, a control rod can be withdrawn in small increments, such as 1 cm, and the change in reactivity can be determined following each increment of withdrawal. By plotting the resulting reactivity versus the rod position, a graph obtained for both cores are shown in Figure 5.1. The graph depicts integral control rod worth over the full range of withdrawal. The integral control rod worth is the total reactivity worth of the rod at that particular degree of withdrawal and is usually defined to be the greatest when the rod is fully withdrawn.

Differential control rod worth is the reactivity change per unit movement of a rod and is normally expressed as ρ/cm or $\Delta K/K$ per cm. The graph for the Differential control rod worth is shown in Table 5.3 for both HEU and LEU cores. The integral rod worth at a given withdrawal is merely the summation of the entire differential rod worth up to that point of withdrawal. It is also the area under the differential rod worth curve at any given withdrawal position. The highest differential control rod worth occurred below the centre of the core.

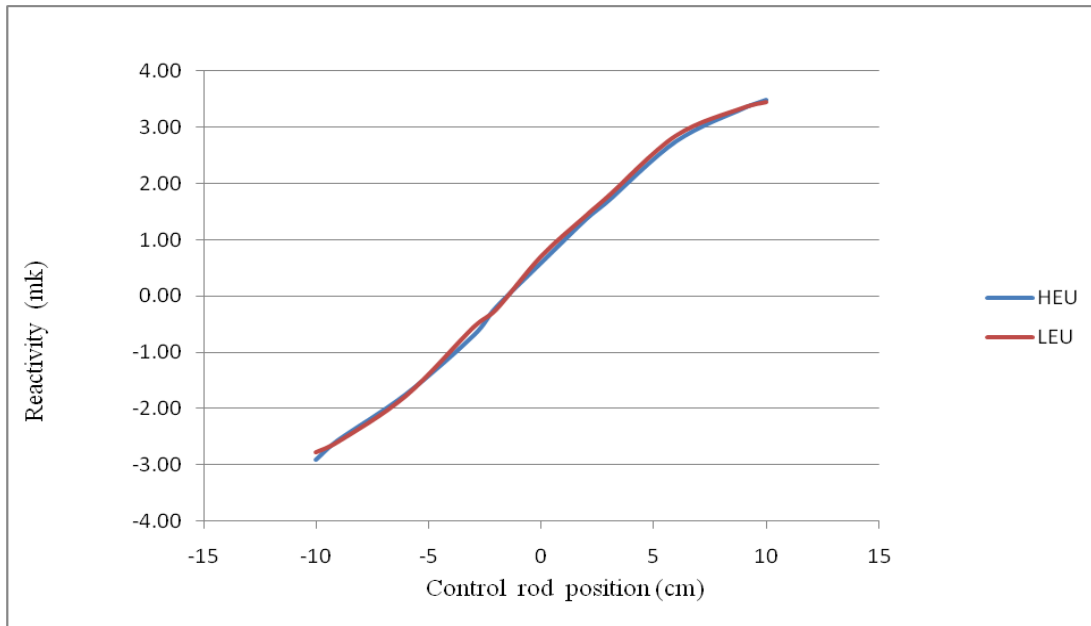


Figure 5.1: The Integral Control Rod Curve.

Table 5.3: Differential Reactivity, mk

Rod Position, cm	HEU	LEU
-10	0.3220	0.8754
-9	0.3519	0.0804
-6	0.8135	0.8135
-3	1.0425	1.2228
-2	0.5005	0.3403
0	0.7897	0.9195
2	0.8383	0.7583
3	0.2692	0.3190
6	1.0056	1.07499
9	0.7553	0.49689
10	0.1291	0.20855
12.4	0.4664	0.47635

The midpoint of the control rod's position is designated as 0 cm which happens to be the arbitrary geometric centre of the MCNP input deck for the core.

5.1.2 Flux Distributions

Measurement of neutron flux and neutron energy spectrum parameters in the inner irradiation sites can be utilised to determine linearity, repeatability and stability of the neutron measurement system, which includes detectors and secondary instrument. The LB1120 miniature fission chamber is employed as a neutron detector for the reactor. It has a small size and can be put into the side annulus. In the linear range of this detector the absolute neutron flux over 4-5 decades could be measured with both gold and manganese foils [2].

The average flux distributions in the inner irradiation channels, outer irradiation channels and that of the fission chambers are shown in Figure 5.2, Figure 5.3 and Figure 5.4 respectively. The centre of the core is equidistant from the inner irradiation channels and the fission chamber which houses the device used in measuring the neutron flux experimentally. The various graphs follow the same pattern and also depict the reduction in the thermal neutron flux of the LEU core at 30 kW. Both at the inner and outer irradiation channels it was observed that the HEU and LEU epithermal fluxes are comparable at all points on the graph and the same is observed for the fast fluxes of both cores. But as stated earlier, the thermal flux of the LEU core is about thirteen per cent less than that of the HEU at the various points.

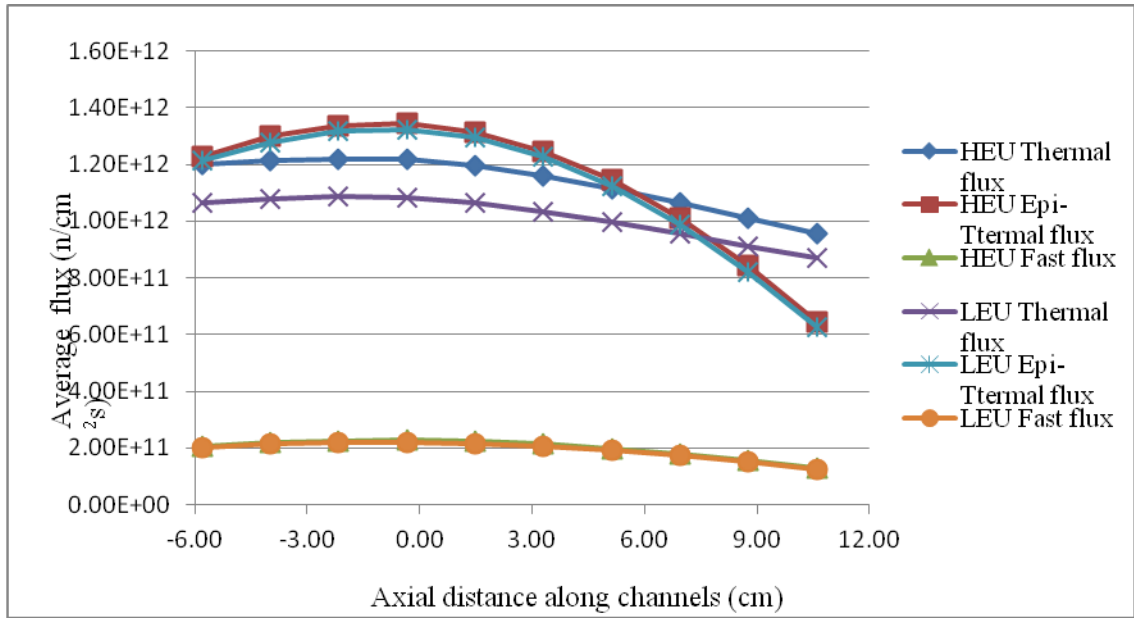


Figure 5.2: Comparison of average flux distribution in inner irradiation channel at 30 kW.

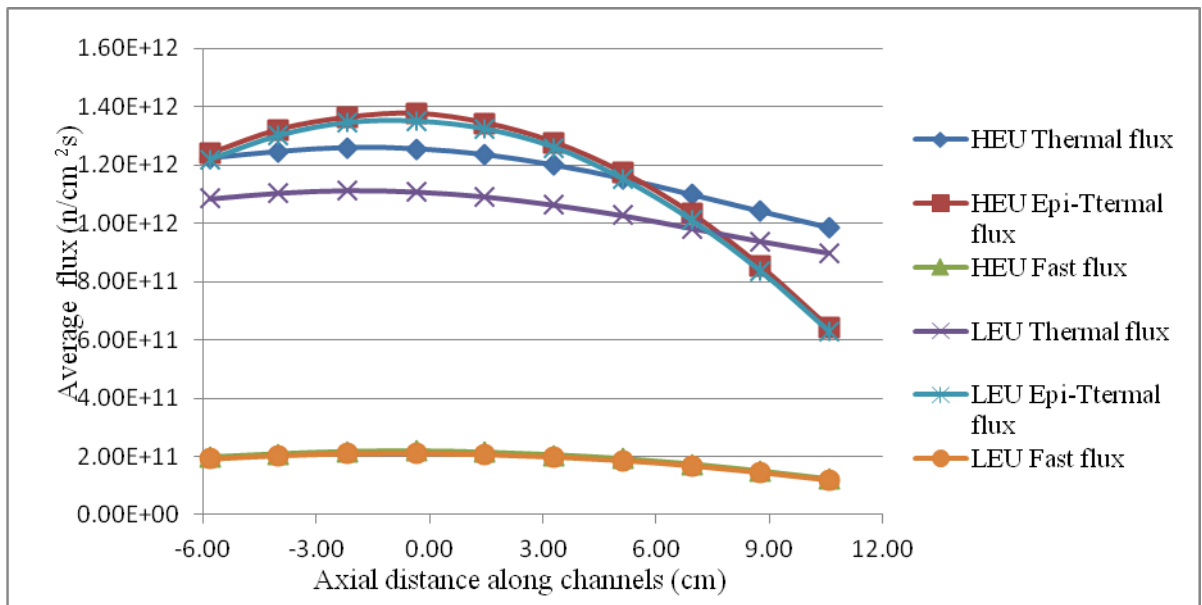


Figure 5.3: Comparison of Flux Distribution in Fission Chamber at 30 kW.

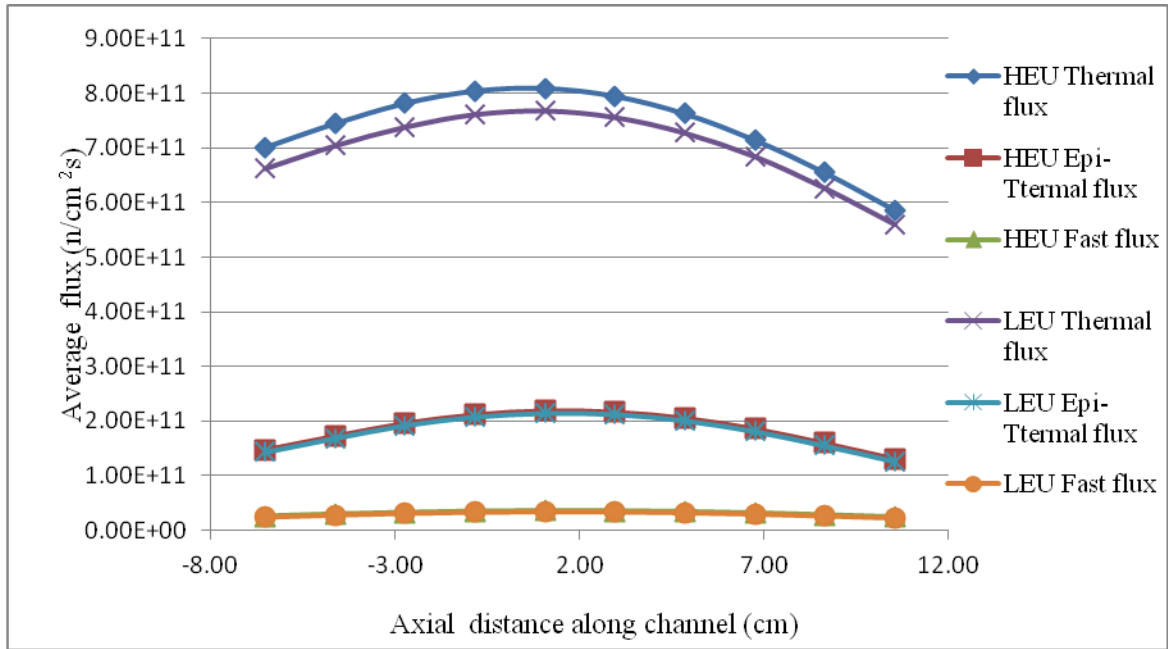


Figure 5.4: Comparison of average flux distribution in outer irradiation channel at 30 kW.

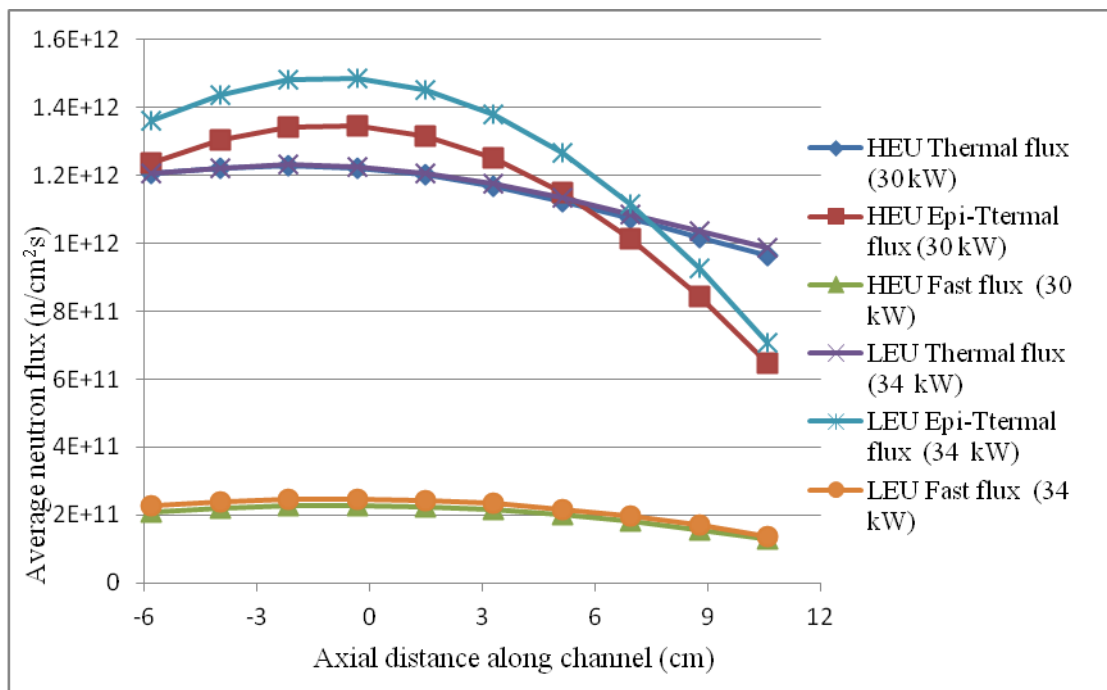


Figure 5.5: Comparison of average flux distribution in inner irradiation channel at nominal powers.

In order not to compromise the thermal neutron flux especially in the inner irradiation channel, the power of the LEU core is increased by 13 % to compensate for the fall in flux at 30 kW. The power for LEU core was increased to 34 kW based on the average ratio of the thermal neutron flux in the inner irradiation channel at 30 kW of the LEU core to that of the HEU core. This is to normalize the thermal neutron flux ratio in the inner irradiation channels to unity. So the two profiles of the thermal flux are almost completely superimposed on the other as observed in Figure 5.5 above. The effects of the increase in power of the LEU core on the neutron fluxes in the other locations are shown in Figure 5.6 and Figure 5.7.

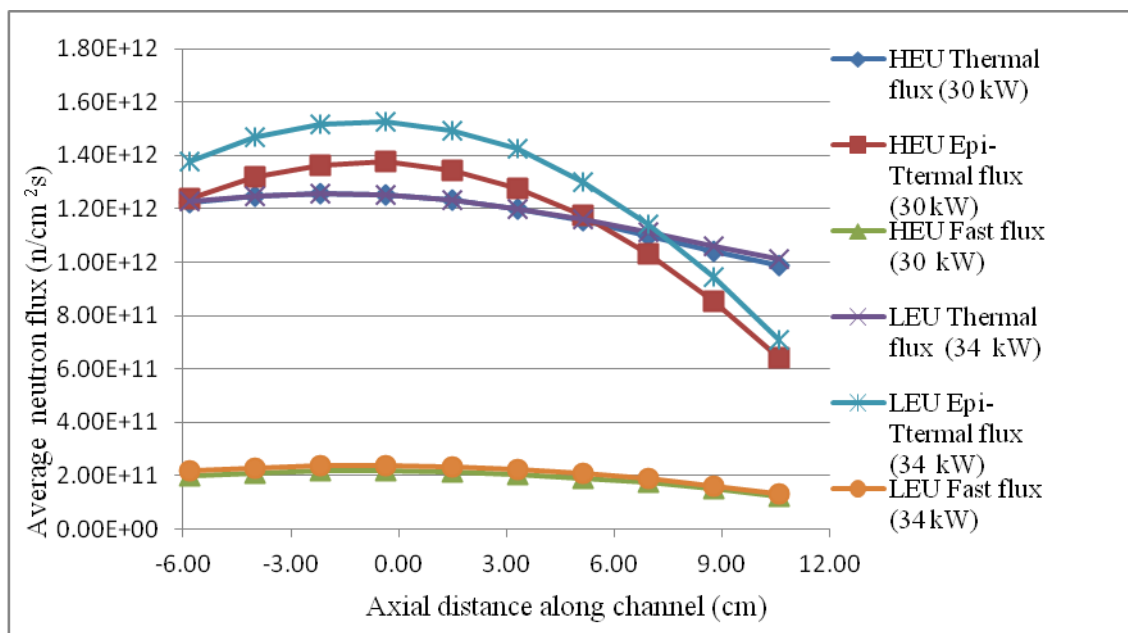


Figure 5.6: Comparison of average flux distribution in fission chamber at nominal powers.

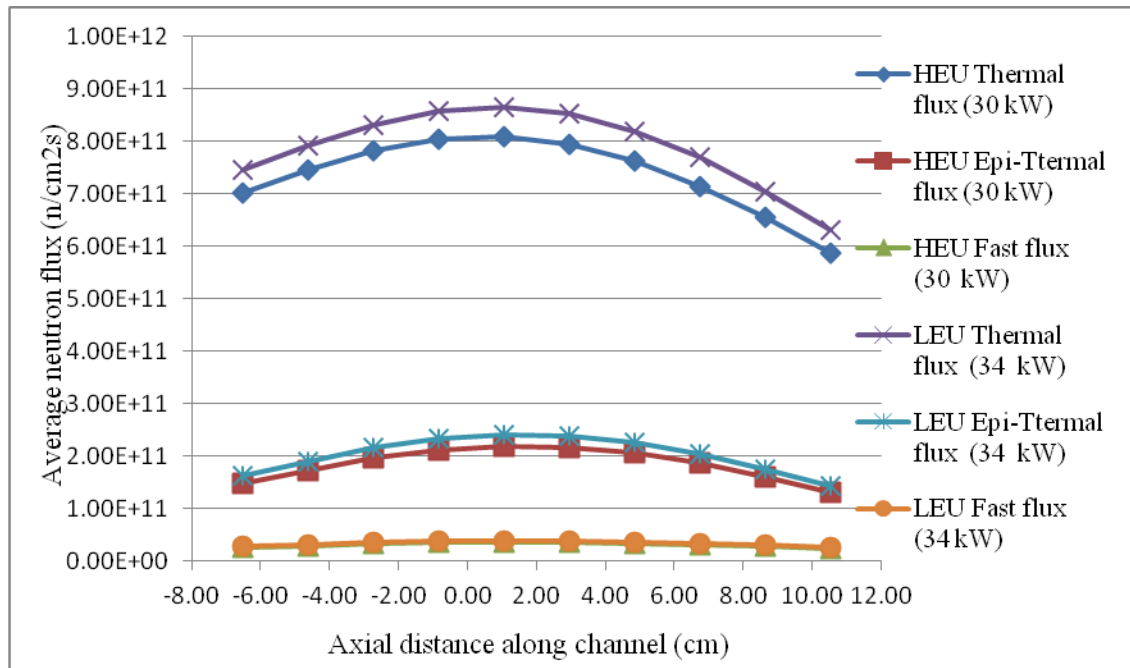


Figure 5.7: Comparison of average flux distribution in outer irradiation channel at nominal powers.

The peak fluxes in the inner irradiation channels are shown in Table 5.4. The decreases in the peak fluxes as a result of the core conversion are in the range of 10 % to 13 % with an average of about 11 %. This supports the increase in power of the LEU core by about 13 % to compensate for the decrease in neutron flux estimated.

Table 5.4: Peak Flux in the Inner Irradiation Channels ($\text{n/cm}^2\text{s}$)

Channels (MCNP)	HEU 30 kW ($\text{n/cm}^2\text{s}$)	LEU 30 kW ($\text{n/cm}^2\text{s}$)	LEU 34 kW ($\text{n/cm}^2\text{s}$)
Cell 971	(1.220±0.0018)E+12	(1.087± 0.0017)E+12	(1.223± 0.0017)E+12
Cell 933	(1.231± 0.0018)E+12	(1.091± 0.0018)E+12	(1.228± 0.0017)E+12
Cell 935	(1.217± 0.0018)E+12	(1.100± 0.0018)E+12	(1.238± 0.0018)E+12
Cell 937	(1.253± 0.0018)E+12	(1.098± 0.0018)E+12	(1.236± 0.0018)E+12
Cell 939	(1.221± 0.0018)E+12	(1.097± 0.0018)E+12	(1.235± 0.0018)E+12
Average	(1.228± 0.0006)E+12	(1.095± 0.0018)E+12	(1.232± 0.0018)E+12

The MCNP5/MCNPX code is capable of computing the axial power profiles of the fuel pins in the core. Comparison of peak power profile for the two cores is shown in Figure 5.8; the axial power profile of the LEU core at 34 kW is also included. The axial power profiles are important for thermal hydraulic analyses, and thermal hydraulic codes such as PARET and PLTEMP require both peak and average power profile for computation of safety margins, transients, etc.

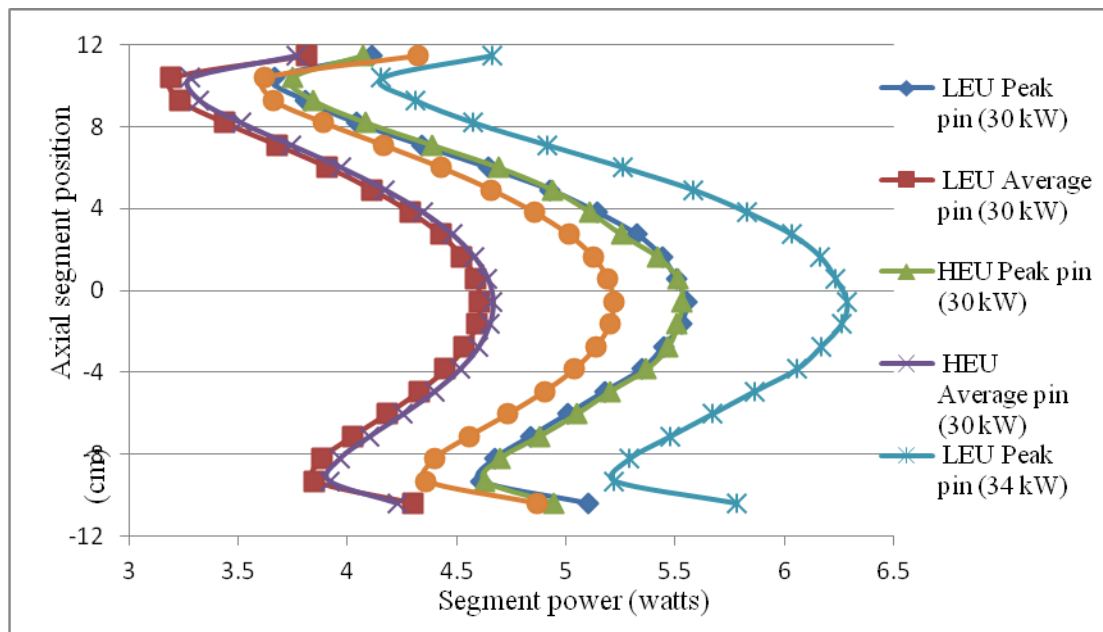


Figure 5.8: Peak Power Pin Axial Profile (21 Segments)

5.1.3 Reactivity Coefficients

Reactivity changes are due to changes in the physical properties of the materials in the reactor. Reactivity coefficients are useful in quantifying the reactivity change that will occur due to the change in a physical property such as the temperature of the moderator [77]. The temperature coefficient can conveniently be considered to consist of three partial contributions: nuclear temperature coefficient, density temperature

coefficient and volume temperature coefficient [78]. Some reactivity coefficients evaluated for the core conversion are discussed next.

The fuel temperature coefficient for both cores at various temperatures is shown in

Table 5.5. That for the LEU fuel is consistent since the coefficients computed are all negative and hence makes the core more inherently stable than the HEU core.

Table 5.5: Fuel Temperature Coefficient

Temperature (°C)	HEU (mk/°C)	LEU (mk/°C)
20	-	-
126.85	$(1.02 \pm 0.001) * 10^{-3}$	$(-6.69 \pm 0.005) * 10^{-3}$
226.85	$(4.80 \pm 0.020) * 10^{-4}$	$(-9.57 \pm 0.004) * 10^{-3}$
326.85	$(-9.71 \pm 0.002) * 10^{-5}$	$(-10.2 \pm 0.003) * 10^{-3}$
526.85	$(-9.79 \pm 0.002) * 10^{-5}$	$(-9.92 \pm 0.002) * 10^{-3}$
Average	0.000326682	$(-9.08 \pm 0.002) * 10^{-3}$

The moderator (water) temperature coefficient was computed in three ways. First, only the temperature card was varied and the results are shown in Table 5.6.

Secondly, the density of the moderator changes by the introduction of void in reactor moderator. As such the density of the water in the coolant cell is changed accordingly without the change in temperature. The density was decreased from 0.99825 g/cm³ to 0.95838 g/cm³ corresponds to temperature increase in the range of 20 °C to 100 °C respectively, and the void coefficient of reactivity for the HEU and LEU cores in this range are show in Table 5.7

Table 5.6: Moderator temperature coefficient (partial)

Temperature (°C)	HEU (mk/ °C)	LEU (mk/°C)
20	-	-
30	$(-6.75 \pm 0.049) * 10^{-2}$	$(-3.37 \pm 0.026) * 10^{-2}$
32	$(-4.96 \pm 0.030) * 10^{-2}$	$(-3.89 \pm 0.025) * 10^{-2}$
40	$(-6.10 \pm 0.052) * 10^{-2}$	$(-3.77 \pm 0.015) * 10^{-2}$
50	$(-1.88 \pm 0.008) * 10^{-2}$	$(-3.74 \pm 0.010) * 10^{-2}$
60	$(-6.14 \pm 0.017) * 10^{-2}$	$(-3.48 \pm 0.007) * 10^{-2}$
70	$(-5.99 \pm 0.013) * 10^{-2}$	$(-3.64 \pm 0.006) * 10^{-2}$
100	$(-6.35 \pm 0.007) * 10^{-2}$	$(-3.95 \pm 0.004) * 10^{-2}$
Average	$(-5.45 \pm 0.020) * 10^{-2}$	$(-3.69 \pm 0.008) * 10^{-2}$

Table 5.7: Moderator void coefficient

Temperature (°C)	HEU (mk/ °C)	LEU (mk/°C)
20	0	0
25	$(-1.27 \pm 0.021) * 10^{-1}$	$(-1.03 \pm 0.017) * 10^{-1}$
30	$(-1.01 \pm 0.009) * 10^{-1}$	$(-0.88 \pm 0.007) * 10^{-1}$
50	$(-1.15 \pm 0.003) * 10^{-1}$	$(-1.22 \pm 0.003) * 10^{-1}$
60	$(-1.28 \pm 0.003) * 10^{-1}$	$(-1.34 \pm 0.003) * 10^{-1}$
100	$(-1.77 \pm 0.002) * 10^{-1}$	$(-1.86 \pm 0.002) * 10^{-1}$
Average	$(-1.30 \pm 0.008) * 10^{-1}$	$(-1.27 \pm 0.007) * 10^{-1}$

Finally, the temperature and density were both varied simultaneously, as shown in the

Table 5.8. This is the most viable result amongst the three.

Table 5.8: Moderator Temperature coefficient

Temperature (°C)	HEU (mk/°C)	LEU (mk/°C)
32	0	0
50	-0.15883	-0.18768
60	-0.18148	-0.20405
70	-0.39561	-0.40581
100	-0.24293	-0.25832
Average	-0.24471	-0.26397

The three means of computing moderator coefficient for both the HEU and LEU show comparable results. Water was used as moderator in all cases.

5.1.4 Worth of the top beryllium reflector

The purpose of calculating the worths of beryllium shims was to determine the reactivity increase by adding different thickness of shim pieces that will compensate the reactivity losses due to the burn-up of U-235 and Sm-149 poisoning. The total thickness available is 109.5 mm, which corresponds to a total reactivity worth of about 18 mk. Figure 5.9 and Figure 5.10 shows the comparison of experimental and calculated shim worth of HEU with that of calculated LEU. The differential reactivity inserted by the shim decreases with the increasing thickness of Be shim.

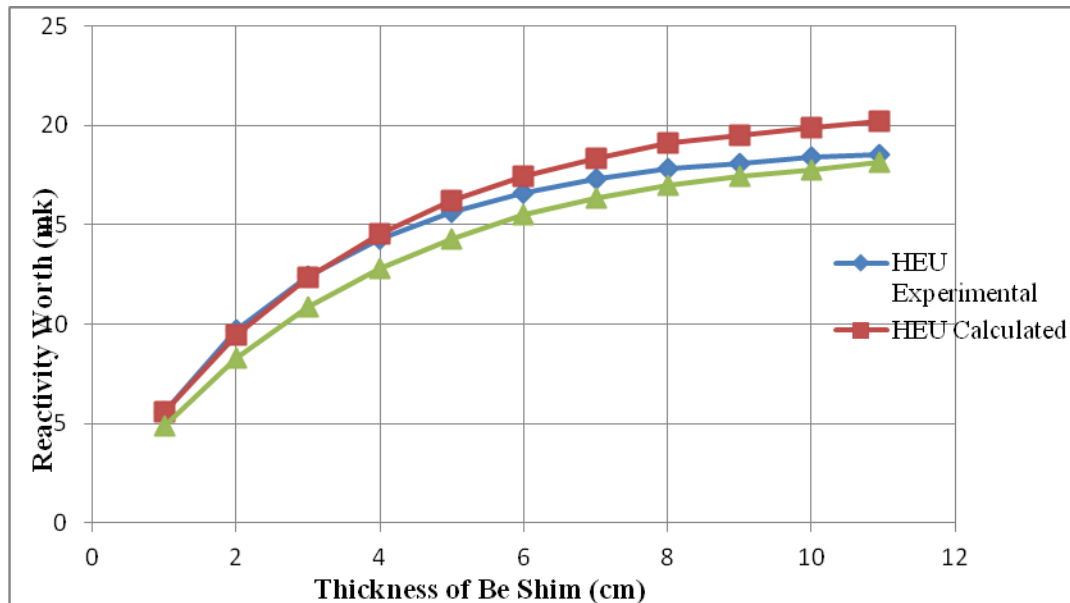


Figure 5.9: Reactivity worths of top Be shims for HEU and LEU cores

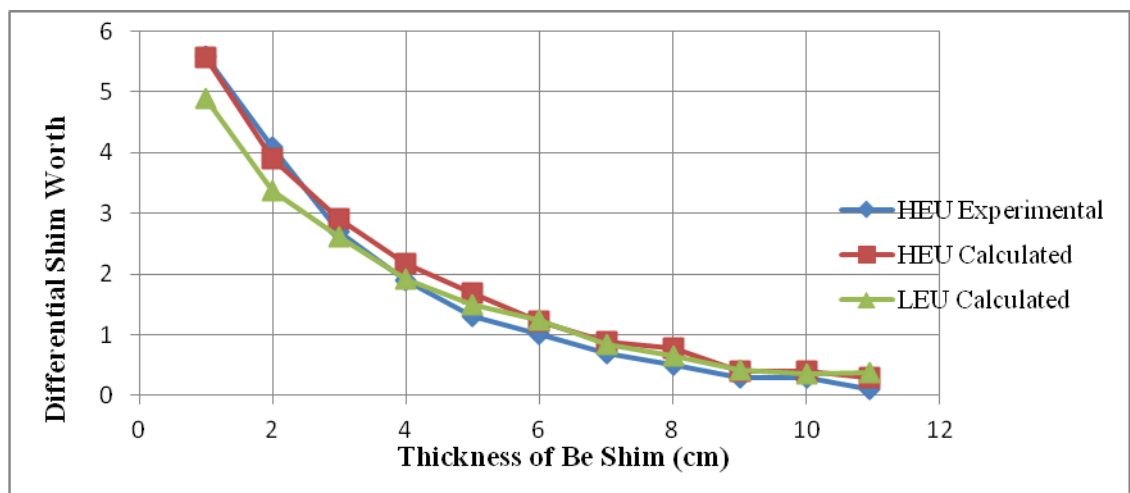


Figure 5.10: Differential Reactivity worths of top Be shims for HEU and LEU cores

5.2 ANALYSIS FOR AUXILIARY SAFETY ROD FOR LEU CORE

A similar work has been done for the GHARR-1 HEU Core [79]. The worth of the central control rod for the LEU is 6.74 mk (Table 5.2). The control rod worth value is achieved because it is placed at the centre of the core. It is impractical to get a similar result for a cadmium safety rod placed anywhere else in the surroundings of the core. After a couple of trials, the best results for cadmium in a single irradiation channel are shown in Table 5.9 and Table 5.10.

Table 5.9. Auxiliary rod worth, mk for unmodified irradiation site (inner)

Rod design	Multiplication Factor	Worth of cadmium capsule
Reference deck	1.00385	0
Single layer foil	1.00099	2.85
Three concentric foil	1.00098	2.86
Solid rod	1.00092	2.92

The single layer foil is tantamount to the set of cadmium capsules sent into the outer irradiation channel when it is necessary. The concentric foil and the solid rod with the same height do not give any better worth. Hence the designs with modified irradiation sites are more considerable.

Table 5.10. Auxiliary rod worth, mk for modified irradiation site (inner)

Rod design	Multiplication Factor	Worth of cadmium capsule
Reference deck	1.00385	0
Single layer foil	1.00042	3.42
Three concentric foil	1.00031	3.53
Solid rod	1.00027	3.57

The results in Table 5.10 give cadmium worth higher than that of the cadmium capsules, with the best scenario given by the solid cadmium rod. This auxiliary safety rod, when fixed in one of the inner irradiation channels, can also be used to increase the shutdown margin of the reactor core when not in operation; this is due to the reduction in the shutdown margin of the LEU core.

5.3 CORE LIFETIME ANALYSIS

R-Z diffusion theory model using the REBUS-3 code was developed to identify the basic fuel depletion characteristics of the GHARR-1 core. Various parts of the core were homogenized. Xenon worth, rate of fuel depletion and fuel cycle length were obtained by performing simple reactivity rundown calculations. Newly loaded fresh core with control rod fully withdrawn is depleted at a fixed power level for a given length of time. Cross-sections were generated using WIMS/ANL code. Results of burn-up analyses are shown in the Table 5.11.

The GHARR-1 core has a very small window of excess reactivity (only ~ 1.7 mk) for operation (between 4.0 mk and 2.3 mk). Based on the above reactivity rundown study, it is found that the equilibrium xenon worth is high as compared to the allowed excess reactivity window for typical reactor operation. Consequently, GHARR-1 cannot be operated continuously to allow the xenon build up to its equilibrium level. As per the

Table 5.11: Xenon Worth and Reactivity Change Rates

Parameters	HEU		LEU	
	15 kW	30 kW	17kW	34 kW
Equilibrium Xe Worth (mk)	2.013	3.827	1.617	3.099
Fuel depletion (mk/day)	0.0250	0.0489	0.0198	0.0389
Hours to operate before adding shim	1631.8	835.1	2059.5	1049.9
Core Lifetime (years)	46		57	

design, GHARR-1 can only operate for a very short operational time, no more than ~ 4.5 hours per day at half power or no more than ~ 2.5 hours per day at full power to avoid excessive xenon buildup.

5.4 THERMAL HYDRAULICS ANALYSES

5.4.1 Steady State

The ANL/PLTEMP Code was employed in the Steady State analysis of the two cores. The reactor power at minimum onset of nucleate boiling ratio, ONBR=1 without hot channel factors is 65.72 kW for the HEU and 67.75 kW for the LEU, furthermore the reactor power at ONBR=1 with all six hot channel factors are 51.6 kW and 53 kW for the HEU and LEU core respectively. The minimum departure from nucleate boiling ratio with all six hot channel factors is 8.9 for the HEU and 8.5 for the LEU core.

The onset of nucleate boiling ratio (ONBR) and departure from nucleate boiling ratio (DNBR) computed so far indicate there is no boiling in both cores. And these indicate the limits of operating power for both the HEU and LEU cores. This is the true allowed power in the sense that there is no allowance in it for any error in the power measuring instrument. This maximum allowed operating power assumes that the power measuring instrument is perfect without any measuring error. The results also indicated good safety margins so far as the boiling point of the coolant and the melting points of both the fuel and clad are concerned.

Thermal hydraulic parameters obtained from further studies undertaken on both the HEU and LEU cores at nominal reactor powers are show in Table 5.12 and Table

5.13. The results of the calculations for the clad surface and coolant temperatures using an inlet temperature of 30 °C and a coolant pressure of 1 bar are also shown.

Table 5.12: Comparison of HEU and LEU steady-state parameters using PLTEMP/ANL

Parameter	HEU – 344 rods	LEU – 348 rods	LEU – 348 rods
Power (kW)	30.0	30.0	34.0
Core Flow Rate (Kg/S)	1.1E-3	1.1E-3	1.2E-3
Peak Fuel Temp. (°C)	104	135	142
Max. Clad Surface Temp. (°C)	77.3	95.0	98.3
Max. Coolant Temp. (°C)	53.1	53.4	57.1

For the LEU core the nominal power is raised to 34 kW in order to meet the flux level of 1×10^{12} n/cm².s. Hence the computations, using PLTEMP, were done for the LEU core at this power and the steady-state parameters were also compared with those of HEU and LEU at 30 kW in table 2.12.

The melting point of UAl₄ and UO₂ fuels are 650 and 2800 °C respectively, and that of Al and Zirc-4 clad are 600 and 1850 °C respectively. The peak fuel temperature for the LEU core is higher than that of the HEU by a factor of 1.37; similarly, the factor by which the melting points of the respective fuels are increased is 4.3. The peak clad surface temperature is increased by a factor of 1.272 but the melting point of Zirc-4 for the LEU is higher than that of Al for the HEU core by a factor of 3.08. These give wider

safety margins. Besides, the core is located at a depth of 6 m thus increasing the boiling point of water at that pressure to about 113 °C.

The computer code was used to calculate the thermal-hydraulics parameters of the HEU reactor core, which consists of 344 fuel elements generating a total power of 30 kW. This was repeated for the LEU reactor core with 348 fuel elements. Computed outlet temperatures using inlet temperatures at different operating power levels were checked against measured values. It can be seen in Table 5.13 that the results measured and calculated for HEU compare favourably well. More inlet temperatures were computed for the HEU and LEU cores which are also comparable.

Table 5.13: Comparison of computed coolant outlet temperatures at various powers and inlet temperatures

Power (kW)	Inlet Temp. (°C)	HEU Outlet Temp. (°C)		LEU Outlet Temp.(°C)
		Measured	Calculated	
0.3	32.0	32.6	33.2	33.2
	35.0	-	36.1	36.1
3	32.0	35.9	37.0	37.0
	37.0	-	41.7	41.7
	39.0	42.0	43.6	43.6
15	30.0	-	43.9	44.0
	37.0	48.5	50.0	50.2
	42.0	-	54.6	54.7
30	30.0	-	51.4	51.7
	34.0	53.0	54.7	55.4
	37.0	-	57.3	57.5
	42.0	-	61.6	61.9

The safety settings of the reactor ensure that protective action will correct an abnormal situation before a safety limit is exceeded [2]. For the HEU, the safety system settings for reactor thermal power, P , height of water above the top of the core, H , and ΔT are as follows:

$$P(\text{max}) = 36 \text{ kW}$$

$$H(\text{min}) = 465 \text{ cm}$$

$$\Delta T(\text{max}) = 21 \text{ }^\circ\text{C}$$

The effect of inlet temperature on temperature difference, as computed by PLTEMP, for both HEU and LEU are shown in Table 5.14.

Table 5.14: Effect of Inlet Temperature on Temperature Difference at Nominal Operating Power for the HEU and LEU Cores

T_{IN} ($^\circ\text{C}$)	30 kW		36 kW	
	HEU – ΔT ($^\circ\text{C}$)	LEU – ΔT ($^\circ\text{C}$)	HEU – ΔT ($^\circ\text{C}$)	LEU – ΔT ($^\circ\text{C}$)
10	24.10	29.15	27.00	32.28
15	21.63	27.16	24.20	30.20
20	20.20	25.59	22.66	28.54
30	18.60	23.26	20.97	26.03
35	18.30	22.37	20.63	25.07
40	18.03	21.61	20.54	24.24

5.4.2 Transient

PARET code was utilized for the Transient Analysis in order to compare the reactor power, fuel temperature and clad temperature for the two cores. Results are

shown in Figure 5.11, Figure 5.12 and Figure 5.13 for reactivity insertion of 3.8 mk respectively.

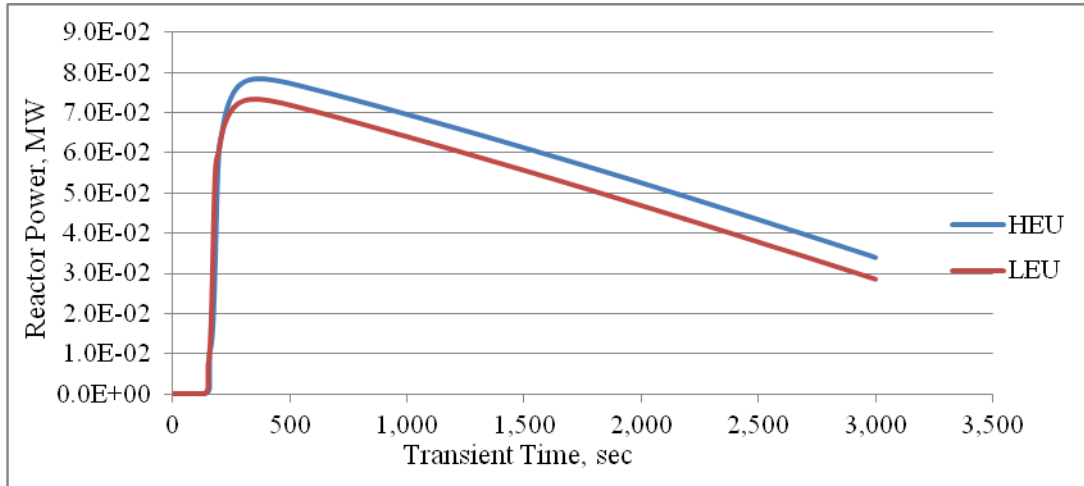


Figure 5.11: Time vs. Power for a 3.8 mk Reactivity Insertion with HEU and LEU Fuel

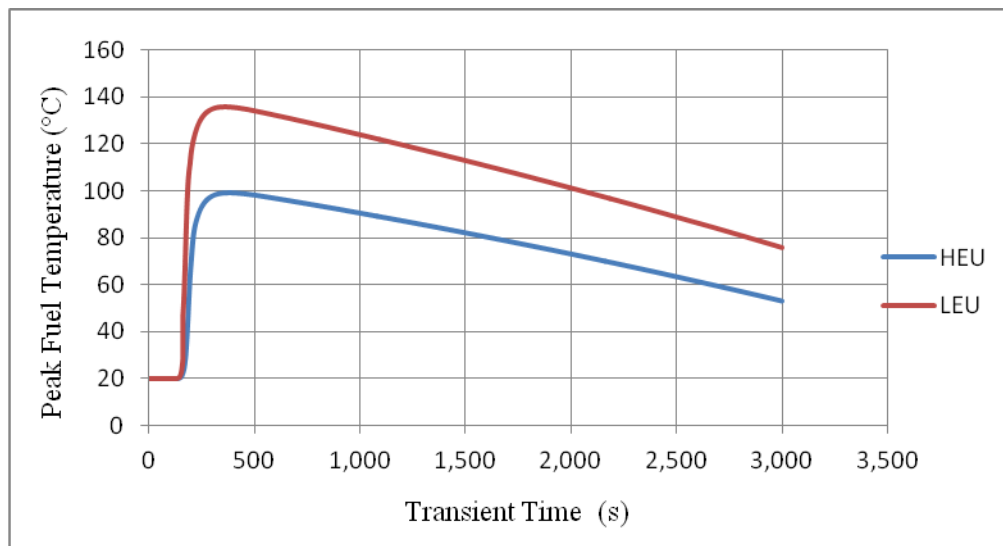


Figure 5.12: Fuel Temperature comparison of HEU and LEU cores for 3.8 mk reactivity transient.

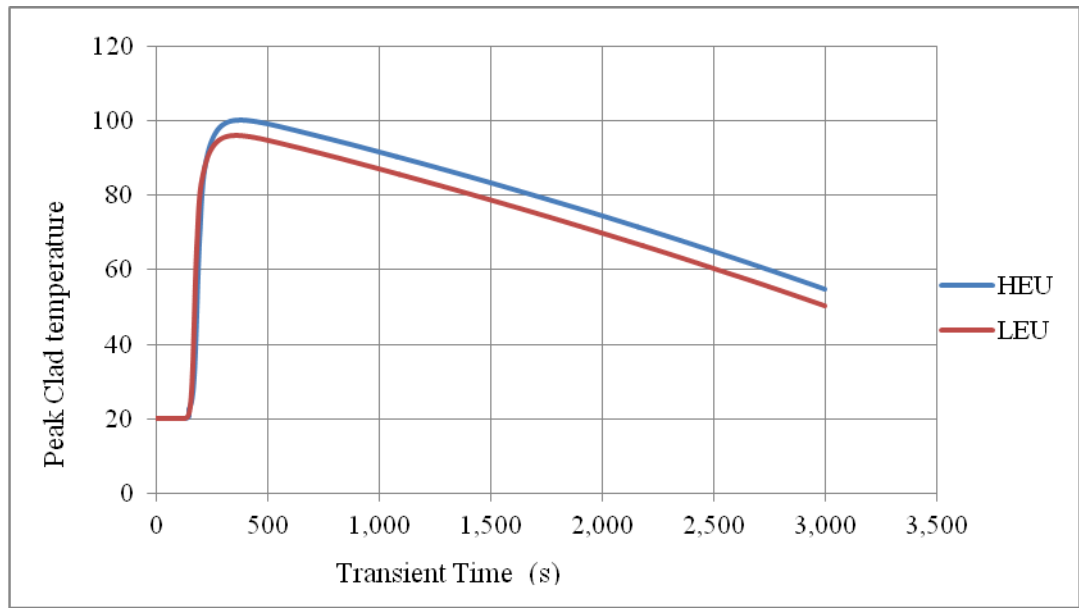


Figure 5.13: Clad Surface Temperature comparison of HEU and LEU cores for 3.8 mk reactivity transient.

Hypothetical reactivity insertions for 6 mk and 8 mk were also done to show the inherent safety margin of the LEU core. The results are shown in the Figure 5.14, Figure 5.15 and Figure 5.16 for the reactor power, fuel temperature and clad temperature respectively.

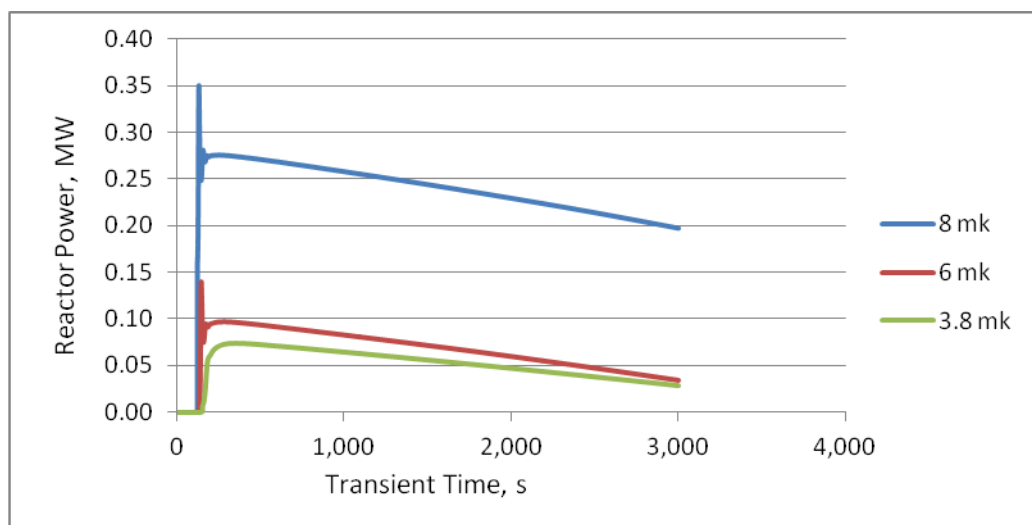


Figure 5.14: Reactor power for reactivity insertions of 3.8 mk, 6 mk and 8 mk for LEU.

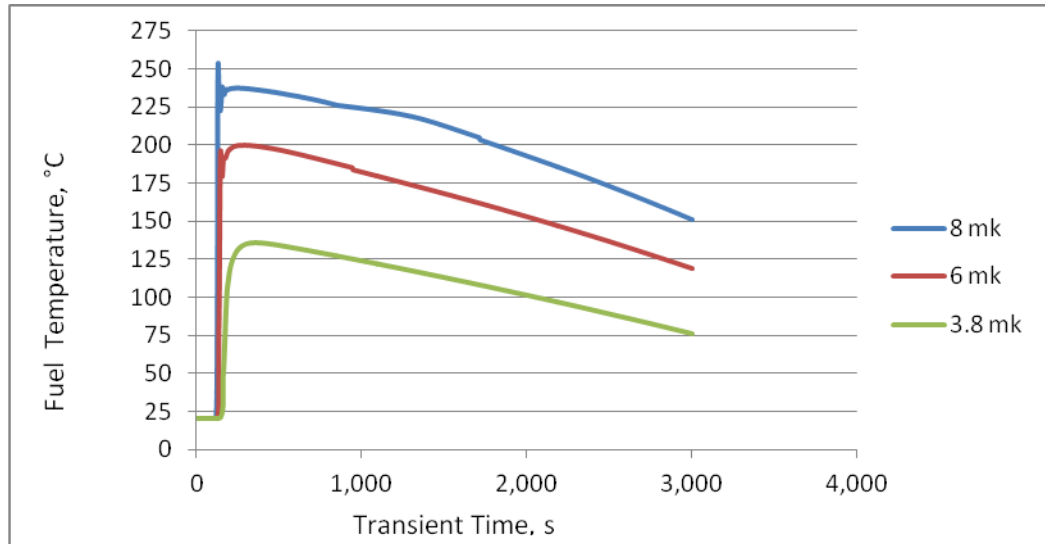


Figure 5.15: Fuel Temperature for reactivity insertions of 3.8 mk, 6 mk and 8 mk for LEU

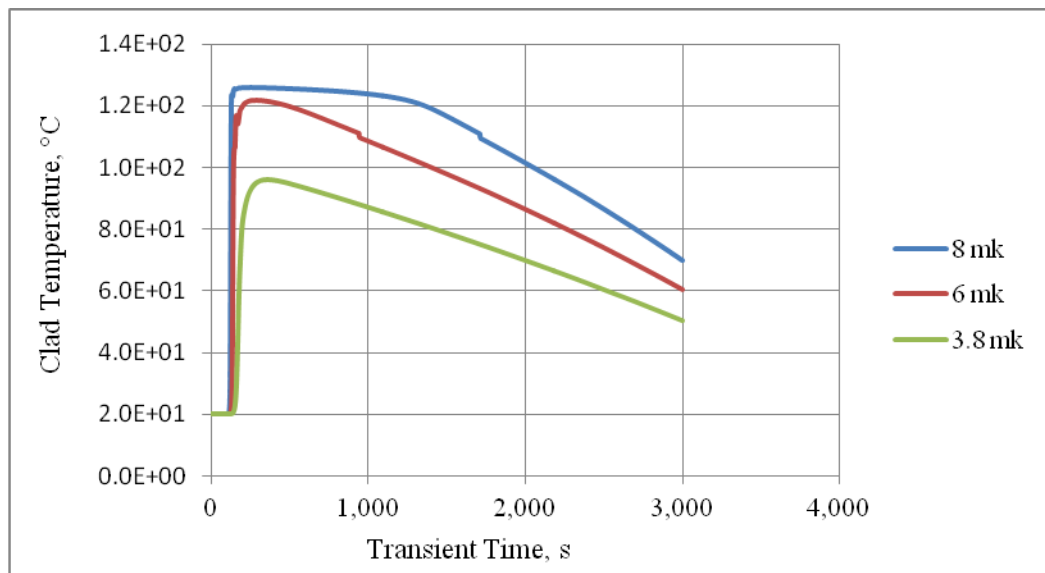


Figure 5.16: Clad Temperature for reactivity insertions of 3.8 mk, 6 mk and 8 mk for LEU

The peak temperature for the fuel as shown in

Table 5.15 is far below its melting point of 2800 °C and that of the clad is also far below its melting point of 1850 °C, indicating good safety margins.

Table 5.15: Peak power, peak fuel temperature and peak clad temperature for various reactivity insertions

Reactivity Insertion, mk	Peak power, kW	Peak Fuel Temp, °C	Peak Clad Temp, °C
3.8	73.5	136	96.1
6.0	140	200	122
8.0	350	254	126

CHAPTER SIX

6 CONCLUSION AND RECOMMENDATION

6.1 Conclusion

Ghana is committed to ensuring the success of the IAEA-RERTR HEU-LEU conversion program and 12.5 % enriched UO_2 has been chosen as fuel for LEU Core on the basis of feasibility studies performed. To achieve a core excess reactivity of 3.5 – 4.0 mk, 348 fuel pins would be appropriate for the GHARR-1 LEU core. Results indicate that flux distribution in the inner irradiation channels will not be compromised if the power of LEU core is increased to 34 kW. The properties of UO_2 and Zirc-4 will increase the safety of the LEU core due to their higher melting points, relative to the HEU core. Zirc-4 will increase core lifetime because it is less corrosive. The GHARR-1 core using LEU- UO_2 -12.5% fuel can be operated for 23 shim cycles, with cycle length 2.5 years, for over 57 years at the 17 kW power level. All 23 LEU cycles meet the ~ 4.0 mk excess reactivity required at the beginning of cycle. For comparison, the MNSR HEU reference core can also be operated for 23 shim cycles, but with a cycle length of 2.0 years for just over 46 years at the 15.0 kW power level. It is concluded that the GHARR-1 core with LEU UO_2 fuel enriched to 12.5% and a power level of 34 kW can be operated ~25% longer than the current HEU core operated at 30 kW. Both cores will have the same value of thermal neutron flux in their experimental positions.

On the various designs for the auxiliary safety rod, the solid cadmium rod placed in the modified inner irradiation channel gives the highest negative reactivity worth.

This makes it more suitable for the intended purpose. This could also be used alongside the original control rod to increase the shut down margin.

The onset of nucleate boiling ratio (ONBR) and departure from nucleate boiling ratio (DNBR) computed so far indicated there is no boiling in both cores. And these indicate the limits of operating power for both the HEU and LEU cores. This is the true allowed power in the sense that there is no allowance in it for any error in the power measuring instrument. The results also indicated good safety margins so far as the boiling point of the coolant as well as the melting points of both the fuel and clad are concerned.

6.2 Recommendation

It is recommended that the NNRI gets its staff acquainted with the reactor core conversion steps by sending staffs to the manufacturer in China during the conversion of the MNSR prototype. This should include the performance of the Zero Power Test for the LEU core. And thereafter the Institute comes up with the steps specifically for GHARR-1 for approval by the Regulatory Board.

Even though it is not likely that the control rod for the LEU will pose any challenges, there is the need for further work to ascertain the velocity of the control rod's upward and downward movements both under normal operations and during emergency prior to the substitution by one with new dimension.

After the conversion from HEU to LEU, a number of experiments are recommended to ascertain parameters which can be measured experimentally. The auxiliary safety rod needs be installed during this period.

The core lifetime is over forty years and therefore recommended that the water purification activity undertaken weekly at the reactor site should be taken seriously since corrosion of reactor components have the potential of determining the actual lifetime of the reactor system.

References

- [1] Y. W. Yan, "Reactor complex of Miniature Neutron Source Reactor Training Document," China Institute of Atomic Energy, China, 1993.
- [2] E. H. K. Akaho, S. Anim-Sampong, G. Emi-Reynolds, D. N. A. Dodoo-Amoo and T. B. Maaku, "Safety Analysis Report for Ghana Research Reactor -1," *GEAC-NNRI-RT-26*, March 1995..
- [3] International Atomic Energy Agency Information Circular , "Project and Supply Agreement," INCIRC/468, April, 1995.
- [4] E. H. K. Akaho, B. T. Maaku, S. Anim-Sampong, L. Yizheng and Z. Wuqin, "On-Site Critical and Zero Power Experiments for Start-up of GHARR-1," *GAEC-NNRI-RT-22*, Kwabenya - Ghana, 1995.
- [5] International Atomic Energy Agency, "Research Reactors Database," May, 2013. <http://nucleus.iaea.org/RRDB/RR/ReactorSearch.aspx?filter=0>.
- [6] P. Beeley, L. Bennet, W. Lewis, W. Andrews and J. Edward, "Medication and Utilisation of SLOWPOKE-2 Facility at the Royal Military College of Canada," *Proc. of Int. Symp. on Res. Reactor Safety, Operation and Modification, CRNL, London IAEA-SN-310 (5P)*, 1989.
- [7] International Atomic Energy Agency, "Follow-up Integrated Safety Assessment for Research Reactors (INSARR) Mission Report," *Report for Ghana Research Reactor - I*, May 2009.
- [8] H. Abou Yehia, "INSARR: Integrated Safety Assessment for Research Reactors," in *Research Reactors Safety Section, Division of Nuclear Installation Safety*; http://www-ns.iaea.org/downloads/ni/training/rr-presentations-pdf/insarr_methodology.pdf.
- [9] E. Bradley, P. Adelfang and G. I. N., in *International Atomic Energy Agency Support of Research Reactor Highly Enriched Uranium to Low Enriched Uranium Fuel Conversion Projects*, Research Reactor Unit, International Atomic Energy Agency Support of Research Reactor Highly Enriched Uranium to Low Enriched Uranium Fuel Conversion Projects; Division of Nuclear Fuel Cycle and Waste Technology, www.iaea.org/.../documents/.../20070709-INMMPaper-IAEA Conversion.doc.
- [10] International Atomic Energy Agency Safety Standards, "CRP on Conversion of

- Miniature Neutron Source Research Reactors (MNSR) to Low Enriched Uranium (LEU)," IAEA - Research Reactor Section,
<http://www.iaea.org/OurWork/ST/NE/NEFW/Technical-Areas/RRS/mnsr.html>.
- [11] L. Yiguo, X. Pu, Z. Shuyun and Z. Yongbao, "The Physics Experimental Study for In-Hospital Neutron Irradiator," in *Reduced Enrichment for Research and Test Reactors*, Prague, Czech Republic, 2007.
- [12] G. Kennedy, J. St. Pierre, L. G. .. Bennett and K. S. Nielsen, "LEU-Fuelled SLOWPOKE-2 Research Reactors: Operational Experience and Utilisation," in *International Meeting on Reduced Enrichment for Research and Test Reactors*, Bariloche, Argentina, 2002, November 3-8.
- [13] Ecole Polytechnique, Montreal; Institute of Nuclear Engineering,
<http://www.polymtl.ca/nucleaire/en/LTN/SLP.php>.
- [14] "Reactor Restart Ceremony for RPI Core Conversion," pp. <http://www-tc.iaea.org/tcweb/regionalsites/europe/news/newsstory/default.asp?newsid=281>, November 2007.
- [15] University Research Reactor Institute, "Operational Experience of Kyoto University Research Reactor (KUR) with LEU Fuel," in *RERTR 2011 — 33rd INTERNATIONAL MEETING ON REDUCED ENRICHMENT FOR RESEARCH AND TEST REACTORS*.
- [16] Ole Reistad and Stykkaar Hustveit, "HEU Fuel Cycle Inventories and Progress on Global Minimization, The Nonproliferation Review," Vol. 15, No. 2, pp. 266-287, http://cns.miis.edu/npr/pdfs/152_reistad_appendix2.pdf, July 2008.
- [17] National Nuclear Security Administration, "Press release," <http://www.nnsa.energy.gov/mediaroom/pressreleases/research-reactor-university-florida-has-been-converted>, October 2006.
- [18] Idaho National Laboratory, "Global Threat Reduction Initiative Convert Program," 09-50787 R2-12, pp. <http://www.inl.gov/research/global-threat-reduction-initiative-convert-program/d/global-threat-reduction-initiative-convert-program.pdf>.
- [19] G. Chenzhan, "Experimental of Adding Top Beryllium Shims for MNSR," *MNSR Training Materials, CIAE Technical Report*, 1993.
- [20] G. Chenzhan, "The Effect of Xenon Poisoning on MNSR Operation," MNSR

- Training Materials, CIAE Technical Report, 1991.
- [21] L. Yizheng, "The Start-up and Parameter Measurement of Pakistan MNSR," Atomic Energy Science and Technology, Volume 24 No. 6, 1990.
- [22] W. Deliang, "Maintenance of MNSR Control Rod Drive Mechanism, MNSR Training Materials - CIAE Technical Report," 1992.
- [23] L. Yizheng, Z. Wuqin, Z. Guosheng and Z. Xianfa, "Testing Protocol - Zero Power Testing of Ghana Equipment," *China Institute of Atomic Energy; Report Code MNSR GN-7*, August, 1993.
- [24] J. R. Lamarsh and A. J. Baratta, Introduction to Nuclear Engineering, New Jersey 07458: Prentice-Hall, Inc., 2001.
- [25] H. C. Odoi, "Nuclear Criticality Studies of Effects of Reflector Thickness on Neutronic Performance of Low Enriched Uranium Fueled MNSR using MCNP Code," Master of Philosophy - Thesis, School of Nuclear and Allied Sciences, University of Ghana , Accra - Ghana, 2008.
- [26] J. J. Duderstadt and L. J. Hamilton, Nuclear Reactor Analysis, MIT Press, ISBN04712236, 1976.
- [27] J. F. Briesmeister, "MCNP - A General Monte Carlo N- Particle Transport Code," Los Alamos National Laboratory, USA, Los Alamos, 2000.
- [28] P. F. Rose, "ENDF - 201, ENDF/B-VI Summary Documentation," Brookhaven National Laboratory, BNL-NCS-17541, 1991.
- [29] R. E. MacFarlane, D. W. Muir and R. M. Boicourt, "The NJOY Nuclear Data Processing System, Volume I: User's Manual," LA-9303-M," Los Alamos National Laboratory, 1982.
- [30] S. C. Frankle, R. C. Reedy and P. G. Young, "ACTI: An MCNP Data Library for Prompt Gamma-ray Spectroscopy," in *12th Biennial Radiation Protection and Shielding Topical Meeting*, Santa Fe, NM, 2002.
- [31] R. J. Howerton, D. E. Cullen, R. C. Haight and M. H. MacGregor, "The Evaluated Nuclear Data Library (ENDL): Evaluation Techniques, Reaction Index, and Descriptions of Individual Reactions," Lawrence Livermore National Laboratory report UCRL-50400, Vol. 15 Part A, 1975.

- [32] D. E. Cullen, M. H. Chen, J. H. Hubbell, S. T. Perkins, E. F. Plechaty, J. A. Rathkopf and J. Scofield, "Tables and Graphs of Photon Interaction Cross Sections from 10 eV to 100 GeV Derived from the LLNL Evaluated Photon Data Library," Lawrence Livermore National Laboratory Report UCRL - 504000 Volume 6, Rev. 4, Part A:Z= 1 to 50 and B:Z= 51 to 100, 1989.
- [33] M. A. Gardner and R. J. Howerton, "Evaluated Neutron Activation Cross-Section Library - Evaluation Techniques and Reaction Index," Lawrence Livermore National Laboratory report UCRL-50400, Vol. 18., 1978.
- [34] E. D. Arthur and P. G. Young, "Evaluated Neutron-Induced Cross-Sections for 54, 54 Fe to 40 MeV," Los Alamos Scientific Laboratory Report LA-8626-MS, Los Alamos, 1980.
- [35] D. G. J. Foster and E. D. Arthur, "Average Neutronic Properties of "Prompt" Fission Products," Los Alamos National Laboratory LA-9168-MS, Los Alamos, 1982.
- [36] A. E. D., P. G. Young, A. B. Smith and C. A. Philis, "New Tungsten Isotope Evaluations for Neutron Energies between 0.1 and 20 MeV," Trans. American Nuclear Society 39, pp. 793. , 1981.
- [37] J. F. Breismeister, "MCNP - A General Monte Carlo N-Particle Transport Code," Los Alamos National Laboratory, USA, Los Alamos, Version 4B Manual LA - 12625-M.
- [38] N. N. Madras, "Lectures on Monte Carlo Methods Library Cataloging," Publication Data - American Mathematical Society, USA, 1957.
- [39] D. E. Knuth, "The Art of Computer Programming," *Addison Wesley Longman, 2nd Edition*, vol. 2, no. Semi numerical Algorithms, 1981.
- [40] P. L'Ecuyer, "Handbook on Simulation," *John Wiley and Sons, New York*, 1998.
- [41] J. H. Halton, "A Restrospective and Perspective Survey of the Monte Carlo Method," *Society for Industrial and Applied Mathematics Review*, vol. 12, pp. 1 - 63, 1970.
- [42] M. Marseguerra, "Nuclear Reaction Data and Nuclear Reactor Physics, Design and Safety," *The Abdus Salam ICTP; Scientific Publisher*, pp. 512 - 535, 1999.
- [43] F. B. Brown and T. M. Sutton, "Monte Carlo Fundermentals," Lockheed Martin

Company Ltd, 1996.

- [44] X-5 Monte Carlo Team, "MCNP—A General Monte Carlo N-Particle Transport Code,," Los Alamos National Laboratory, USA, Los Alamos, 2005 - Version 5 Edition.
- [45] E. Roger, "Stan Ulam, John Von Neumann and the Monte Carlo Method," Argonne, USA, 1987.
- [46] I. Lux and L. Koblinger, "Monte Carlo Particle Transport Methods: Neutron and Photon Calculations," CRC Press, USA., 1991.
- [47] L. Devroye, "Non-Uniform Random Variate Number Generation," New York Inc., USA, NY, Springer-Verlag 1986.
- [48] F. B. Brown and T. M. Sutton, "Monte Carlo Methods for Radiation Transport Analysis on Vector Computers.," *Progress in Nuclear Energy*, vol. 14, no. 3, pp. 269 - 299, 1984.
- [49] R. C. Gast and N. R. Candelore, "Monte Carlo Eigenfunction Strategies and Uncertainties,," *Argonne National Laboratory, USA.*, pp. ANL-75-2, , 1974.
- [50] M. R. Mendelson, "Monte Carlo Criticality Calculations for Thermal Reactors," *Nuclear Science Engineering* , p. pp. 319, 1968.
- [51] S. M. Weston, "Fuel Reprocessing and Recycling," in *Nuclear Reactor Physics*, Weinheim, Wiley-VCH Verlag GmbH & Co., 2007, p. 223.
- [52] J. Carlson, J. Bardsley, V. Bragin and J. Hill, "Plutonium Isotopics - Non-Proliferation and Safeguards Issues," Australian Safeguards Office, Canberra ACT Australia , IAEA-SM-351/64.
- [53] H. W. J. Graves, "Nuclear Fuel Management," Wiley, New York, 1979.
- [54] R. B. M. Sogbadji, R. Abrefah and E. Ampomah-Amoako, "Neutron Energy Spectrum Flux in Ghana's Miniature Neutron Source Reactor Core," *Ann. Nucl. Energy*,, vol. doi:10.1016/j.anucene., 2011.
- [55] L. Hao, "MNSR Thermal Hydraulics, MNSR Training Material," China Instituted of Atomic Energy.
- [56] E. H. K. Akaho and B. T. Maakuu, "Simulations of Reactivity Transients in a Miniature Neutron Source Reactor Core," *Nuclear Engineering and Design*,

www.elsevier.com/locate/nucengdes, pp. 31 - 42, 2002.

- [57] D. Butterworth and G. F. Hewitt, Two Phase Flow and Heat Transfer, Harwel Series: Oxford University Press, 1978.
- [58] J.-M. L. Corre and e. al, "Two-phase flow regimes and mechanisms of critical heat flux under subcooled flow boiling conditions," *Nuclear Engineering and Design*, vol. 240, no. Science Direct. doi:10.1016/j.nucengdes. 2008.12.008, pp. 245 - 251, 2009.
- [59] International Atomic Energy Agency, "U.S. Generic Enrichment Reduction Calculations for Plate-Type and Rodded-Type Reactors," *Reduced Enrichment for Research and Test Reactors (RERTR) Program*, vol. IAEA_233.pdf, no. Appendix A.
- [60] S. A. Jonah, "Heat Transfer in MNSR," Fellowship (Tutorial Document), Zaria, Nigeria, 2008.
- [61] F. P. Incropera, D. P. Dewitt, T. L. Bergman and A. S. Lavine, Fundamentals of Heat and Mass Transfer, River Street, Hoboken: John Wiley & Sons, Inc., 2007.
- [62] J. P. Hartnett, Mass Transfer Cooling - Handbook of Heat Transfer, New York: McGraw-Hill, 1973.
- [63] S. Anim-Sampong, "Minimization of Highly Enriched Uranium in the Civilian Nuclear Sector," in *International Symposium*, Oslo, June 17 - 19, 2006.
- [64] W. Gudowski, "Monte Carlo Methods for Accelerator-Driven Systems (SMR/1326-8)," in *Workshop on Hybrid Nuclear Systems for Energy Production, Utilization of Actinides and Transmutation of Long-Lived Radioactive Waste*, Miramare - Trieste, Italy, 3 - 7 September, 2001.
- [65] A. P. Olson and M. Kalimullah, "A Users Guide to the PLTEMP/ANL V4.1," *Global Threat Reduction Initiative (GTRI)*, pp. Nuclear Engineering Division, Argonne National Laboratory - Chicago, USA, 5 April 2011.
- [66] W. L. Woodruff, "Evaluation and Selection of Hot Channel (Peaking) Factors for Research Reactors Application," in *CONF-8709189-2, Intl Mtg. on Reduced Enrichment for Research and Test Reactors (RERTR)*, Buenos Aires, Argentina, Sept., 1987.
- [67] W. L. Woodruff, "The Paret Code and the analysis of the SPERT I transients,"

Argonne National Laboratory, RERTR/TM-4, Argonne, USA, 1982.

- [68] C. F. Obenchain, "A Program for Analysis of Reactor Transients," IDO-17282.
- [69] A. P. Olson and S. A. Jonah, "MNSR Transient Analysis and Thermal-Hydraulic Safety Margins for HEU and LEU Cores using PARET," in *Intl. Mtg. on Reduced Enrichment for Research and Test Reactors*, Prague, Czech Republic, Sep. 23-27, 2007.
- [70] B. E. Clancy, J. W. Connolly and B. V. Harrington, "Transients in Aluminium plate-type Reactors initiated at ambient temperatures," *An analysis of power transients observed in SPERT I reactors. AAEC, E345*, 1975.
- [71] E. Ampomah-Amoako, E. K. K. Akaho and B. J. B. Nyarko, "Transient analysis of Ghana Research Reactor -1 using PARET/ANL thermal-hydraulic code," *Nuclear Engineering and Design* 239, pp. 2479 - 2483, 2009.
- [72] S. A. Jonah, J. R. Liaw, A. Olson and J. E. Matos, "Criticality Calculations and Transient Analysis of MNSR," in *Reduced Enrichment for Reduced and Test Reactors*, Cape Town, SA, 2006.
- [73] F. E. Dunn, J. Thomas and J. E. Matos, "Transient Analysis for MNSR HEU and LEU Cores," in *Reduced Enrichment for Research and Test Reactors*, Prague - Czech Republic, 2007.
- [74] ASHARE Application Handbook (SI), American Society of Heating, Refrigeration and Air-conditioning Engineers, 1995.
- [75] J. Dugone, "SPERT III Reactor Facility: E-Core Revision, AEC Research and Development Report IDO-17036," Philips Petroleum Company, 1965.
- [76] S. A. Jonah et al, "Monte Carlo simulation of core physics parameters of the Nigeria Research Reactor-1," *Annals of Nuclear Energy*, vol. 34, pp. 953-957, 2007.
- [77] U. S. Department of Energy, Washington, D. C. 20585, "DOE Fundamental Handbook," *Nuclear Physics and Reactor Theory Volume 1 and 2*, p. , DOE-HDBK-1019/1-93; FSC-6910 January 1993.
- [78] S. E. Liverhant, Elementary Introduction to Nuclear Physics, John Wiley and Sons Inc., 1960.

- [79] J. Boffie, H. C. Odoi, E. H. K. Akaho, B. J. B. Nyarko and K. Tuffour-Achampong, "Design of an Additional Safety Rod for Ghana Research Reactor-1 using MCNP5 Code," *Nuclear Engineering and Design*, vol. 245, no. www.elsevier.com/locate/nucengdes, pp. 13 - 18, 2012.